

Lecture Notes on Surface Science

Philip Hofmann

October 5, 2005

Århus University, Fall 2005

Version 2.5

Contents

1	Introduction and Ultra High Vacuum (UHV)	6
1.1	Format of this lecture series	6
1.2	Introduction	7
1.3	Some Surface Science books and www-links	9
1.4	Ultra High Vacuum (UHV)	10
1.4.1	Vacuum requirements	10
1.4.2	Pumping and bakeout[7]	11
1.4.3	Pressure measurement[7]	13
1.4.4	Materials and construction[7]	14
1.4.5	Chemical analysis of the rest gas[7]	16
1.5	Further reading	17
2	From Solids to Surfaces	18
2.1	Introduction	18
2.2	Lattice and reciprocal lattice	19
2.2.1	Lattice	19
2.2.2	Reciprocal lattice	20
2.2.3	Lattice and reciprocal lattice at surfaces	22
2.3	Electronic states	23
2.3.1	The Drude model of metals	23
2.3.2	A quantum mechanical treatment of free and independent electrons	24
2.3.3	Electrons in a periodic potential	25
2.3.4	Nearly free electrons: metals	26
2.3.5	Tightly bound electrons: semiconductors	26
2.3.6	Electronic structure of surfaces	27
2.4	Lattice vibrations	30
2.4.1	Lattice vibrations in the harmonic crystal: phonons	30
2.4.2	Vibrations at surfaces	31
2.5	Further reading	31

3	Electron spectroscopy	32
3.1	Introduction	32
3.2	Why electrons: The mean free path	33
3.3	Electron sources and analysers	34
3.4	Electrons in solids: elastic and inelastic scattering	36
3.4.1	The dielectric function	37
3.4.2	Phonons	38
3.4.3	Excitons	38
3.4.4	Interband transitions	39
3.4.5	Bulk and surface plasmons	39
3.4.6	Core levels	42
3.5	Concluding remarks	42
3.6	Further reading	42
4	Surface cleaning and chemical analysis	43
4.1	Surface cleaning	43
4.2	Surface chemical analysis	44
4.3	X-ray photoelectron spectroscopy (XPS)	45
4.3.1	X-ray sources	45
4.3.2	XPS cross sections	48
4.3.3	Qualitative analysis: typical spectra	50
4.3.4	XPS binding energies	51
4.4	Auger electron spectroscopy (AES)	55
4.4.1	Auger nomenclature	56
4.4.2	Experimental	56
4.4.3	Qualitative analysis: typical spectra	56
4.4.4	Quantitative analysis	56
4.5	Further reading	57
5	Adsorption, Desorption and Chemical Reactions	58
5.1	Introduction	58
5.2	Physisorption	59
5.3	Chemisorption	60
5.4	Interaction between adsorbates	65
5.5	Kinetics	66
5.5.1	Adsorption	67
5.5.2	Desorption	69
5.5.3	Adsorption-desorption equilibrium	71
5.6	Single-crystal adsorption calorimetry	71
5.7	Chemical reactions and catalysis	72
5.8	Further reading	75

6	Surface Structure	76
6.1	Surface Thermodynamics and general crystal shape	76
6.2	Surface geometry: truncated bulk, relaxation, reconstruction, defects and super-structures	79
6.2.1	General phenomena	79
6.2.2	Lattice and reciprocal lattice	82
6.3	Low energy electron diffraction (LEED), LEED patterns and quantitative structure determination	85
6.3.1	Instrumentation	86
6.3.2	Diffraction pattern and their analysis	87
6.3.3	Interpretation of LEED patterns	92
6.3.4	Quantitative structure determination	94
6.4	Some examples from LEED structure determination	95
6.4.1	Metal surfaces	95
6.4.2	Semiconductor surfaces	98
6.4.3	Insulator surfaces	100
6.5	Other scattering techniques	101
6.5.1	Extended X-ray Absorption Fine Structure (EXAFS and Surface EXAFS (SEXAFS)	102
6.5.2	EXAFS	102
6.5.3	SEXAFS	105
6.6	Photoelectron diffraction (PhD, PED)	106
6.6.1	Introduction	106
6.6.2	Simple Theory	108
6.6.3	Structure determination: experimental results	111
6.6.4	Suggested reading	114
6.7	Scanning Tunnelling Microscopy	114
6.7.1	Basic principle and experimental setup	115
6.7.2	Theory of operation	117
6.7.3	Clean metal surfaces	119
6.7.4	Adsorbates on metal surfaces	121
6.7.5	Adsorbate induced reconstruction of metal surfaces	123
6.7.6	Semiconductor surfaces	123
6.7.7	Insulator surfaces	124
6.7.8	Other applications and further instrumental development	126
6.8	Further reading	128
7	The electronic structure of surfaces	129
7.1	Work function	129
7.2	Electronic surface states: basic ideas	132

7.3	Measuring the electronic structure of surfaces with angle-resolved photoemission	135
7.3.1	Introduction	135
7.3.2	The photoemission process	136
7.3.3	Instrumentation	140
7.3.4	The three step model	140
7.3.5	Band mapping: 2d bands and 3d bands	141
7.3.6	Some surface states investigated by ARPES	144
7.4	Scanning Tunnelling Spectroscopy	157
7.5	Further Reading	160
8	Optical properties of surfaces	162
8.1	Reflection of Light at a Surface	163
8.2	Polaritons	164
8.3	Reflection Anisotropy Spectroscopy (RAS)	166
8.4	Second Harmonic Generation	168
9	Vibrational properties of surfaces	170
9.1	Introduction	170
9.2	Electron scattering: EELS	172
9.3	Optical spectroscopy: IRAS	178
9.4	He Atom scattering	181
9.5	Vibrational spectroscopy with the STM	181
9.6	Further reading	183

Chapter 1

Introduction and Ultra High Vacuum (UHV)

1.1 Format of this lecture series

This course consists of about 14 lectures on the subject of surface science. The scope of the series is to give a brief introduction into some important concepts in the physics and chemistry of solid surfaces. It is probably appropriate to start with a few warnings / disclaimers:

- This is NOT a theory course. Theoretical concepts are only very briefly introduced when they are needed to understand some essential part of the science presented. The main focus of the course lies on the phenomena and their experimental investigation. The reasons for this are two-fold: (1) treating the theory as well would not fit into the time-frame for this course and (2) the theory is going to be presented (much better than I could ever do it) in the Surface Science Theory course by Bjørk Hammer.
- The course covers only a small fraction of the field. The choice is rather subjective. I present what I think is important and fun. Some areas are only touched very briefly. Experimental surface science consists of a combination of a large variety of techniques. In this course, however, I discuss only a few. If you want to learn about the techniques not described here you have to look them up in a book or on the www.
- These lecture notes are NOT a textbook. They are just a rough draft to let you know what is going on in the lectures and to give you the possibility to (ideally) prepare for the lecture or (realistically) look up

things after the lecture. I also still revise them quite a lot. If you find errors in the notes (which is very likely) or if you have any suggestions please let me know.

I gratefully acknowledge the help from my colleagues David Adams and Flemming Besenbacher. I have used a lot of electronic pictures and lecture notes from David in this document. Many of the other images are made by Erik Holst Mortensen. I am very grateful for this professional help.

1.2 Introduction

This course deals with some aspects of the physics and chemistry of surfaces and interfaces. Surfaces and interfaces are everywhere and many related phenomena are common in daily life (texture, friction, surface-tension, corrosion, heterogeneous catalysis). We are here concerned with understanding the microscopic properties of surfaces, asking questions like: what is the atomic structure of the surface compared to that of the bulk? What happens to the electronic properties and vibrational properties upon creating a surface? What happens in detail when we adsorb an atom or a molecule on a surface? In some cases, establishing a connection to the macroscopic surface phenomena is possible in others the microscopic origin of these phenomena is still completely unclear. We will mostly concentrate on simple model systems like the clean and defect-free surface of a single-crystal substrate. Such things do of course only exist in theory but the technological progress in the last 30 years (see below) has made it possible to get close to this ideal. This together with the progress in surface science theory makes it meaningful to compare experimental results to first-principles calculations. Why does one want to study surfaces and interfaces in the first place? Here are some motivating aspects.

One of the most important motivations in surface science is the understanding of heterogeneous catalysis. The fact that the presence of a solid could accelerate a chemical reaction without modifying the solid was first discovered in the early 19th century. Knowledge about catalysis has then rapidly grown and been the basis of the developing chemical industry. In the beginning, the microscopic mechanism of the catalytic process was, of course, unknown. Much was tried and “good” catalysts were made from experience. A typical surface science experiment on an “ideal” single crystal surface in ultra-high vacuum (UHV) is rather far away from the conditions a real catalyst is working in: the catalyst may be made of small metal particles dispersed on an inert substrate in a high pressure of gas at elevated

temperature. Nevertheless, the surface science approach can give important information about many fundamental processes in catalysis. But there are of course situations where this is not enough. Therefore one tries to move into a direction where one is closer to the real catalyst but still very controlled. One can, for example, study the catalytic properties of well-defined metal clusters on a well-defined surface. The ultimate goal is of course to really understand the catalytic reaction in all steps and to improve the catalyst (make it cheaper or more efficient).

Closely related to this is the issue of corrosion. Questions are: What are the chemical reactions leading to corrosion? How do they take place on the surface and what can we do to prevent them?

Another reason for the growing interest in surfaces is related to the semiconductor industry. There is a strong need to build smaller and smaller structures to get higher integration on computer chips. One consequence of small structures is that the relative importance of the surfaces is increasing. Another, more practical, consequence is the need to build these structures with high precision and to have flat interfaces between them. This is also an issue in the growth of thin and ultra-thin films and multilayers needed for semiconductors, magnetic storage, coatings and so on. One wishes to learn how to grow thin and uniform films of material A on material B. Even if such a film growth is not possible (for example because A forms drops and clusters on B) one might still find a way to grow the film adding by using so-called “surfactants”. Surface Science research on semiconductor surfaces is much closer to the real technological world than the research in heterogeneous catalysis. Most semiconductor devices are made of Si, grown on the surface of a single-crystal wafer.

Related to the increased importance of surfaces in connection to smaller semiconductor structures is the field of nano technology . The importance of surface (or even edge and kink) effects is obvious. In addition to this, the surface is the ideal starting point for building very small structures. A promising current research field is for example the study of structural formation by self-organization.

A more fundamental issue is that surfaces and interfaces provide a unique opportunity to study (nearly) two-dimensional electronic systems. The most famous examples for this are the integer and the fractional quantum hall effect where a two-dimensional electron gas is generated in a semiconductor heterostructure (we will later see how) and studied at very low temperature and in high magnetic fields. Another example might be the electronic structure of the new high T_C superconductors and related compounds where much of the interesting physics goes on in the two-dimensional copper oxide planes. Yet another example are quasi two-dimensional electronic states on

surfaces which can be used to study a lot of interesting many-body effects.

Historically, the interest in surfaces is an old one [6]. People were always fascinated by the more macroscopic phenomena of surface colour and texture. It was also realized early that very little oil spreads over enormous areas on the surface of water. Catalysis was discovered, as mentioned above, in the first half of the 19th century. In the 1870ies the theory of surface thermodynamics was essentially completed by J.W. Gibbs. Systematic experimental studies were pioneered in the beginning of last century by I. Langmuir. His studies of gas-surface interactions were even closely related to technical progress in electrical lamps. Around the same time, the basis of two other very important surface science experimental techniques was discovered: Einstein developed the theory of the photoelectric effect and Davisson and Germer showed that electrons behave like “matter waves” and can be diffracted from a crystal. We will come back to these two types of experiments later. In the 30s and 40s of last century tremendous theoretical progress about the surface and interface electronic structure was made (electronic surface states and semiconductor junctions) and the transistor was invented. Well-controlled experimental work first took off in the 60s when it became possible to generate vacuum conditions which were so good that surfaces could be cleaned and kept clean for a time long enough to do some useful experiments with them. Many experimental techniques were introduced, in particular the use of electron spectroscopy turned out to be essential for the progress in surface science. In the 80s the scanning tunnelling microscope was invented. It led to a wide range of real-space studies on a truly atomic scale.

1.3 Some Surface Science books and www-links

Here is a short list of some books on surface science. When you compare the contents of certain books to these notes, you will find striking similarities because I have stolen a lot of the material I liked.

- Surfaces and Interfaces of Solid Materials (Springer Study edition) by H. Lüth. An excellent book, mostly focused on the surfaces of semiconductors.
- Modern Techniques of Surface Science (Cambridge Solid State Science Series) by T. A. Delchar, and D. P. Woodruff. A very good book which is mainly concerned with technique (as the title indicates). If you work in the field this book is a “must”.

- Physics at Surfaces (Cambridge Univ. Press) by A. Zangwill. This book is complementary to the first. It is more about theory and concepts than about technique. It is rather old but I think it is one of the best books one can buy.
- Oberflächenphysik des Festkörpers (Teubner) by Martin Henzler and Wolfgang Göpel. The book covers a broad range. In German and inexpensive.
- Concepts in Surface Physics (Springer Series in Surface Sciences) by M. C. Desjonqueres, D. Spanjaard. A modern and theory-focused book.

A lot of very interesting teaching material can be found on the www. A very good link site is [this](#).

1.4 Ultra High Vacuum (UHV)

The key-ingredient to surface science experiments is ultra-high vacuum. This means pressures in the 10^{-9} mbar range and below. Only such a low pressure will assure that a surface stays clean for a time long enough to do some experiments (we will see later how to obtain a clean surface). In the following, some important parts of UHV technology are described. To get a feel for it we will go down to the lab during the exercise and look at the hardware!

1.4.1 Vacuum requirements

We can quickly estimate the vacuum requirements for surface science. Let's imagine a surface in the vacuum. The number of gas molecules impinging on the surface is

$$R = \frac{dN}{dt} = \frac{P}{\sqrt{2\pi mkT}} = \frac{2.635 \times 10^{22} P_{\text{mbar}}}{\sqrt{MT}} \text{cm}^{-2}\text{s}^{-1}. \quad (1.1)$$

where m is the molecular mass in kg and M is the molecular mass in units of the atomic mass constant. The usual units for the pressure in vacuum technology are torr or mbar (1 torr = 1.3332 mbar = 133.32 Pascal). For a pressure of 10^{-6} mbar and a temperature of 300K we find

molecule	M	R(cm ⁻² s ⁻¹)
H ₂	2	1.1x10 ¹⁵
H ₂ O	18	3.6x10 ¹⁴
CO	28	2.9x10 ¹⁴
O ₂	32	2.7x10 ¹⁴
CO ₂	44	2.3x10 ¹⁴

As an order of magnitude value a surface has 10^{15} atoms per square centimetre. This means that if every rest-gas molecule at the above conditions sticks to the surface the latter will only stay clean for a second or so. If we are not willing to tolerate more than, say, a percent of contaminating rest-gas molecules on the surface then the pressure has to be in the UHV region.

It is also interesting to calculate the mean free path of the molecules at a given pressure, i.e. the mean distance before hitting another molecule. It is

$$\lambda = \frac{kT}{\sqrt{2}\pi\xi^2P} \quad (1.2)$$

where ξ is the molecular diameter. For typical UHV pressures the mean free path of the molecules is many meters. This means that it is much more likely that the molecule hits the walls of the vacuum vessel than another molecule. We come back to this later.

1.4.2 Pumping and bakeout[7]

In order to achieve UHV conditions two stages of pumping are needed (see Fig 1.1).

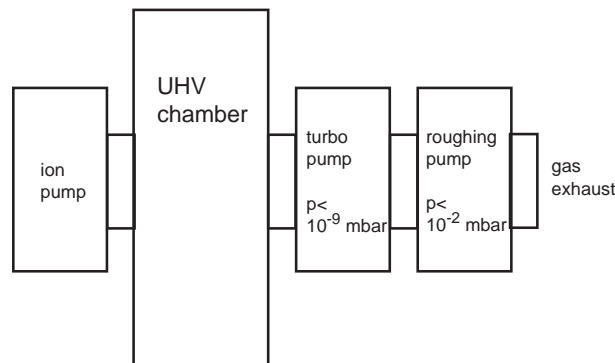


Figure 1.1: Pumping of a UHV system.

A roughing pump is used to pump the system down in the 10^{-3} mbar region. A typical pump is an oil-sealed rotary vane pump as shown in Fig. 1.2. The operation principle of this pump makes it obvious why there are two stages on the vacuum system: the rotary vane pump will work fine when the pressure is high enough to ensure a gas flow through the pump but hopeless when the mean free path of the molecules is very long.

The pump of choice for the second stage is a so-called turbomolecular pump (see Fig. 1.3). The rotor of the pump is build such that the gas

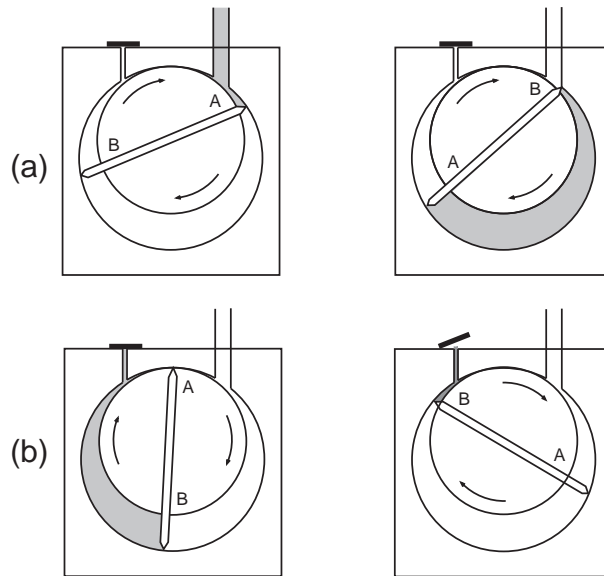


Figure 1.2: A oil-sealed rotary vane pump. Principle of operation: (a) gas from the vacuum system is expanded into the pump and (b) the gas is pushed through the pump exhaust.

molecules collide with the fast moving rotor and thereby attain an impulse in the direction of the roughing pump. In order to achieve efficient pumping the speed of the rotor has to be very high. Typical values are up to 80 krpm.

Once the low pressure has been achieved it can also be maintained by another type of pump, the so-called ion pump shown in Fig. 1.4. The rest gas in that pump is ionized by a plasma discharge due to the high voltage between anode and cathode. The ionization probability is increased by the presence of the magnetic field which makes the electrons travel on spiral trajectories. When the ions hit the Titanium cathode they can be buried in it or react with it. Additionally, Ti is sputtered off the cathodes and deposited on other parts of the pump. This Ti can react with the rest gas and increases the pumping effect. The ion pump does not remove the rest gas from the system. It just binds it such that it can not contribute to the pressure any more. The current provided by the high-voltage power supply is proportional to the pressure in the system. Ion pumps can therefore be used to estimate the pressure. The ion pump can be operated at pressures between 10^{-3} and 10^{-11} mbar.

In order to reach a low pressure in a short time it is necessary to perform a so-called bakeout of the whole vacuum system. During the bakeout the system is heated to at least 100-200°C for an extended period of time (24h or

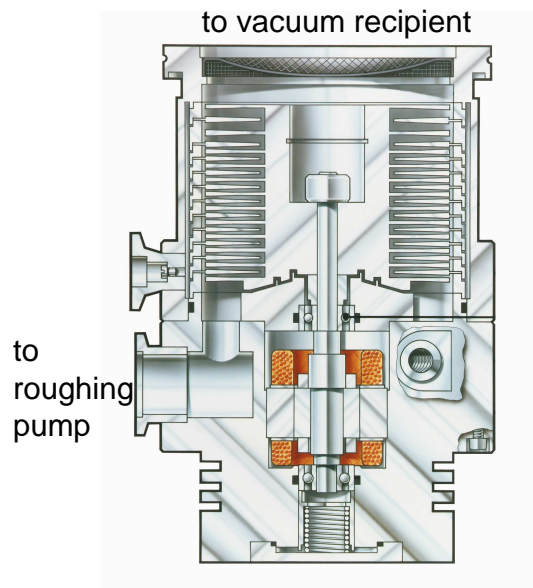


Figure 1.3: A turbomolecular pump. Picture: Leybold Vacuum GmbH, used with permission.

so). The heating causes a fast removal of the impurities adsorbed on the walls of the vacuum system (mostly water). The need for baking systems renders working with UHV chambers rather time-consuming. It also requires that the system is build only of components which can withstand high temperatures for a long period of time.

1.4.3 Pressure measurement [7]

For the roughing pump stage one can use a so-called Pirani gauge to measure the pressure. The idea of this instrument is to measure the resistance of a heated wire placed into the vacuum system. The resistance depends on the temperature of the wire. At high pressures the wire will be cooled by collisions with the rest gas molecules, i.e. by warming up the rest gas. As the pressure is reduced this cooling mechanism gets less effective and the temperature of the wire rises. The resistance of the wire can be calibrated as function of the pressure. Pirani gauges work from ambient pressure down to about 10^{-3} mbar.

For lower pressures, a so-called ion gauge can be used. It is shown in Fig. 1.5. The filament emits electrons which are accelerated inside the cylindrical cage. In the cage the electrons hit rest gas molecules and ionize them. The

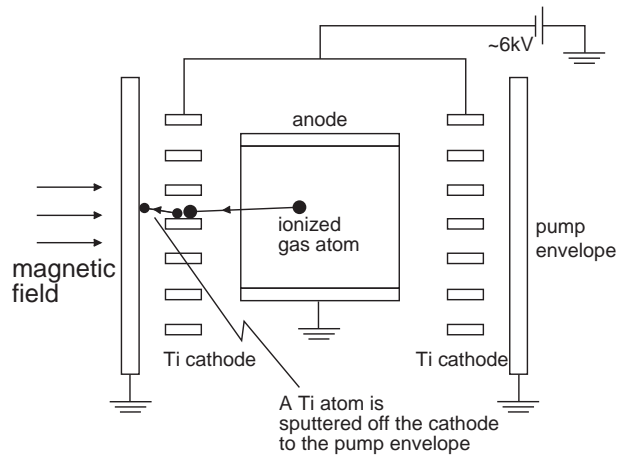


Figure 1.4: An ion pump.

ions are collected at the wire in the middle of the cage and the current from that wire is a measure for the pressure. A problem is that the sensitivity of the gauge depends on the chemical identity of the rest gas. The ion gauge can be used in for pressures between 10^{-4} and 10^{-11} mbar. The low pressure limit is given by an unwanted effect: when an electron hits the cage it produces a photon which then can cause the emission of an electron from the centre wire. While this effect sounds extremely unlikely it becomes the dominant contribution to the current at very low pressures.

1.4.4 Materials and construction[7]

We have already seen above that all materials in the vacuum system have to be able to withstand high temperatures during the bakeout. Another important criterion is that the vapour pressure of the materials has to be very low at the normal operating temperature of the vacuum system. The following table gives the temperatures in K to generate a certain vapour pressure.

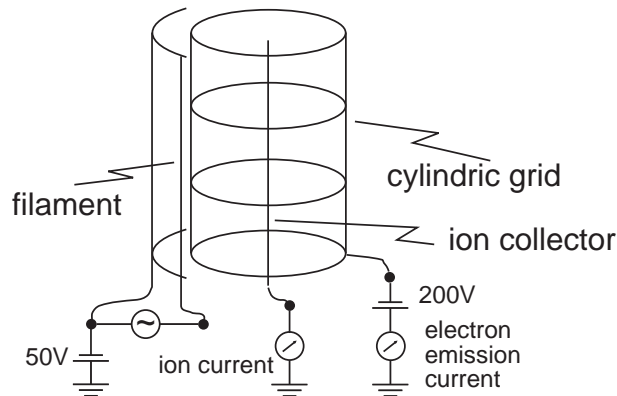


Figure 1.5: An ion gauge.

	10^{-10} mbar	10^{-6} mbar
Na	310K	400K
Zn	355K	450K
Cd	310K	390K
Hg	150K	230K
Mg	405K	505K
Al	860K	1100K
Fe	1000K	1300K
W	2160K	2680K

Obviously, the first materials in the table are very undesirable in a vacuum chamber! The last two are important for the actual construction: most chambers are made of stainless steel and almost all the filaments (for example in the ion gauges) are made of W. Electrical insulators are made of ceramics with a low vapour pressure.

A vacuum vessel has many circular flanges where windows or equipment with the same flange type can be bolted on. These flanges have sharp knife-edges profiled on their operating sides. A leak-tight seal between the two flanges is achieved by placing a copper gasket between the knife edges and pressing it until it is tight. It is necessary to use copper (instead of simply “rubber”) because of the bakeout.

When putting the pumps on the chamber one has to consider the concept of conductance. Keep in mind that in the low pressure region the mean free path of the molecules is much longer than the dimensions of the vacuum system. It is therefore clear that it does not make sense to connect a very powerful pump to the vacuum system via a small diameter tube with many right angles. The rest-gas molecules will never find their way to the pump.

Another important requirement is to linearly move items inside the vacuum or to rotate them. Most of the motions are transferred from outside via stainless steel bellows. We will look at some linear and rotational feedthroughs in the lab.

1.4.5 Chemical analysis of the rest gas[7]

Finally, it is desirable to measure the chemical compositions of the rest gas in the system. This can be used to see if there is a leak in the vacuum chamber, to check the purity of gases used for the experiment and to leak-test the system. To do this, one directs a stream of He gas on the suspected leak from outside the system. If one observes a increase in the partial pressure of He inside, the leak has been found.

A so-called quadrupole mass spectrometer is shown in Fig. 1.6. It consists of three sections. In the first, rest-gas atoms are ionized just as in the ion gauge. These ions are then accelerated and focused into the second section, the actual mass filter. It consists of four bars which set up an electrical quadrupole field, driven by the superposition of a DC and a radio frequency AC voltage. The filter works such that only ions with the same m/e can pass it. The last element of the spectrometer is the ion detector which contains an electron multiplier leading to an amplification of the signal by a factor 10^4 - 10^6 . The lower limit of the partial pressures which can be detected with such a spectrometer is about 10^{-14} mbar.

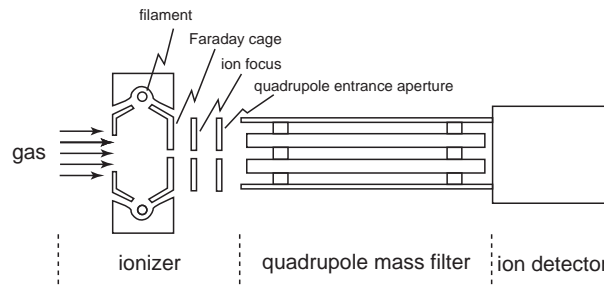


Figure 1.6: A quadrupole mass spectrometer

A typical mass spectrum is shown in Fig. 1.7. The main residual gases in the vacuum are hydrogen, water, carbon monoxide and some carbon dioxide. It is important to note that the criterion is m/e and not simply m ! It means that doubly charged ions appear as particles with half the mass in the spectrum. CO does for example not only give a peak at $m=28$ but also one at $m=14$ due to double ionization. The gases are also dissociated in the

spectrometer such that one does not only find one peak for single-ionized water at $m=18$ but also peaks at $m=16$, 17 and 2 for the fragments.

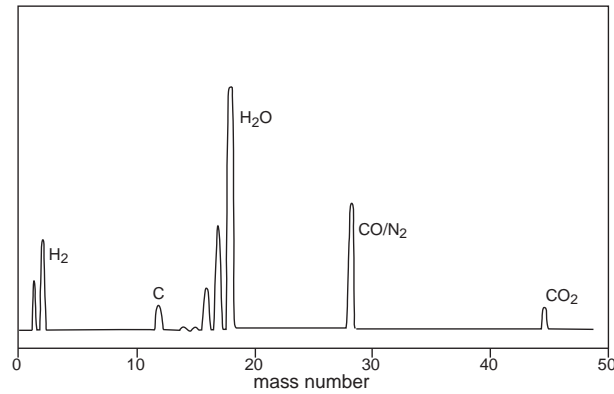


Figure 1.7: A typical mass spectrum.

After the bakeout of the system, the partial pressure of water will be strongly reduced and the total pressure will be determined by CO and atomic hydrogen. If there is an air leak in the system this would show up as peaks of 28 and 32.

1.5 Further reading

An excellent book on vacuum technology in surface science is

- Experimental Innovations in Surface Science (AIP Press / Springer 1998) by John T. Yates, Jr.

Chapter 2

From Solids to Surfaces

2.1 Introduction

The idea of this lecture is to remind you about the basic ideas of solid state physics and to establish a link to our actual subject, the physics and chemistry of solid surfaces. I assume that you have already followed a basic course on solid state physics. Hence, any detailed mathematical treatment is omitted and I just focus on some highlights.

When trying to learn something about solids the biggest problem one encounters is that a macroscopic solid contains very many (10^{23}) atoms. It is therefore impossible to solve any equations of motion, classical or quantum, in a direct way. On surfaces the situation is better (10^{15} atoms or so) but still absolutely hopeless. From the beginning on, physicists have therefore treated the electrons in a solid in a statistical way, first by applying kinetic gas theory (Drude) and later by using the correct Fermi-Dirac statistics (Sommerfeld).

The key-concept to a quantitative description of the electronic and vibrational properties of solids is the fact that most solids are crystals. One can use periodic boundary conditions and solve the problem in reciprocal space. The first section reminds the reader you about the description of crystals and about reciprocal space.

In the following two sections we divide the properties of a solid into electronic contributions and lattice vibrations. This division is not without problems: In principle one would have to solve the Schrödinger equation for the whole system, with the co-ordinates of all the electrons and all the atoms. The reason why it works anyway is that the atoms are so much heavier and slower than the electrons. When the atoms move out of their equilibrium-position the electrons follow quickly but they stay in their ground state. They just move to another ground-state with higher energy. When the atoms are

moved back the electrons follow to their initial ground state. This is called *adiabatic* or *Born-Oppenheimer* approximation.

The mass difference is also reflected in the different energy scales in electron and ion motion: typical kinetic energies of electrons are in the region of several eV while the phonon energies are several meV. The strategy to follow is therefore to solve the electronic structure assuming a rigid crystal. Then the vibrational properties can be calculated from the known electronic properties. Finally, the influence of the vibrational states on the electronic system can be considered: it is usually just a very small (but potentially important!) change.

2.2 Lattice and reciprocal lattice

2.2.1 Lattice

Many solids exist in a crystalline form. Not only the ones which appear as crystals in nature (like diamond, many minerals and salts) but also metals grow as crystals. In solid state physics one can idealize the crystal structure and use the perfect periodicity to facilitate many of the problems.

The most fundamental definition is that of a *Bravais lattice*. It is defined as a lattice of points with position vectors

$$\vec{R} = n_1\vec{a}_1 + n_2\vec{a}_2 + n_3\vec{a}_3. \quad (2.1)$$

Examples for a Bravais lattice are the body centred cubic lattice and the face centred cubic lattice, like shown in Fig. 2.1.

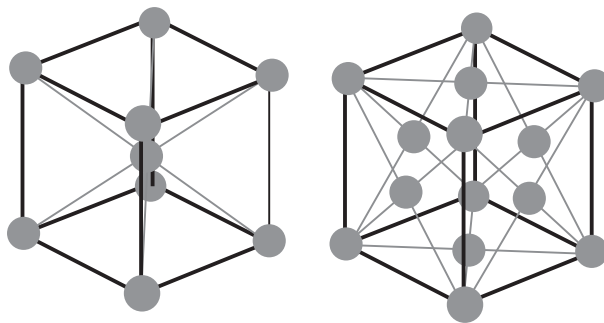


Figure 2.1: The body-centred cubic (bcc) and the face-centred cubic (fcc) Bravais lattice.

Given the Bravais lattice the *primitive unit cell* can be defined: it is any volume of space which when translated through all the vectors of the

Bravais lattice fills all of space without either overlapping itself or leaving voids. There are of course many possible choices for this primitive unit cell.

One very common choice is the *Wigner-Seitz* cell. This cell has the full symmetry of the lattice and is defined as the region of points closer to any given lattice point than to any of the other lattice points. The Wigner-Seitz cells of the bcc and fcc lattice are given in Fig. 2.2.

Sometimes it is also convenient to think in terms of non-primitive unit cells, e.g. in case of the two above cubic structures. When the unit cell is thought of as a cube then the bcc cell contains two atoms and the fcc cell contains four.

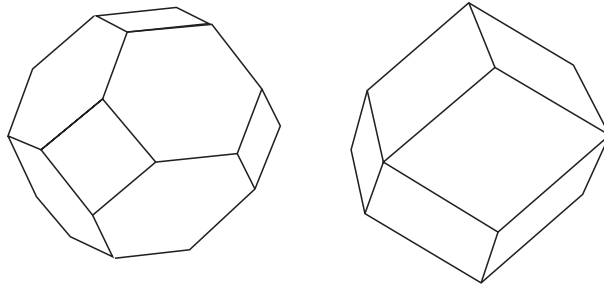


Figure 2.2: The Wigner-Seitz cells for the body-centred cubic (bcc) and the face-centred cubic (fcc) Bravais lattice.

Finally, a real crystal can be described by a Bravais lattice and a so-called *basis*. The basis is a fixed arrangement of atoms or molecules which is sitting on each point of the Bravais lattice. It can just be one atom or it can be a whole protein in biological crystals.

2.2.2 Reciprocal lattice

A central concept in solid state physics is the *reciprocal lattice*. It is defined as the set of all wave vectors \vec{G} that yield plane waves with the periodicity of a given Bravais lattice. This means that if \vec{G} belongs to the reciprocal lattice of a Bravais lattice with points \vec{R} then the relation

$$e^{i\vec{G}(\vec{r}+\vec{R})} = e^{i\vec{G}\vec{r}} \quad (2.2)$$

or

$$e^{i\vec{G}\vec{R}} = 1 \quad (2.3)$$

must hold. In other words: let $\vec{a}_1, \vec{a}_2, \vec{a}_3$ be the vectors defining the primitive direct lattice. Then the reciprocal lattice vectors $\vec{g}_1, \vec{g}_2, \vec{g}_3$ are defined by

$$\vec{G} = n_1\vec{g}_1 + n_2\vec{g}_2 + n_3\vec{g}_3. \quad (2.4)$$

where

$$\vec{a}_i\vec{g}_j = 2\pi\delta_{ij}. \quad (2.5)$$

Note that the reciprocal lattice is also a Bravais lattice. The fcc lattice, for example, has a bcc lattice as its reciprocal lattice and vice versa.

The concept of the reciprocal lattice allows to re-write many solid state problems in Fourier space and this is the way to solve them because of their periodic nature. Take for example a periodic one dimensional function

$$\rho(x) = \rho(x + na) \quad n = 0, \pm 1, \pm 2, \pm 3 \dots \quad (2.6)$$

Then ρ can be written in a Fourier series

$$\rho(x) = \sum_n \rho_n e^{i(n2\pi/a)x}. \quad (2.7)$$

In the three dimensional case the sum is taken over the reciprocal lattice vectors \vec{G}

$$\rho(\vec{r}) = \sum_{\vec{G}} \rho_{\vec{G}} e^{i\vec{G}\vec{r}}. \quad (2.8)$$

ρ could be anything with the periodicity of the lattice. An important example is the charge density in the solid. In reciprocal space ρ can be described by a few Fourier coefficients whereas it has to be defined at by its value for every point in real space.

In the reciprocal lattice it is of course also possible to define a primitive unit cell. Of special importance in the theory of electronic and vibrational states is the Wigner-Seitz cell in the reciprocal lattice. It is called the *first Brillouin zone*. The first Brillouin zones for the bcc and fcc lattice look like the Wigner-Seitz cells for the fcc and bcc lattice in Fig. 2.2, respectively.

Another point worth mentioning in connection with our actual subject, the surface physics, is the definition of the Miller indices. These indices are used to define a lattice plane or a surface orientation. A plane can be conveniently defined by a vector perpendicular to the plane and the Miller indices use the reciprocal lattice vectors: the lattice plane with the Miller indices h, k, l is the plane perpendicular to the reciprocal lattice vector $h\vec{g}_1 + k\vec{g}_2 + l\vec{g}_3$. In a simple cubic lattice the reciprocal lattice is also simple cubic and the orientation of the reciprocal lattice vector is obvious (see Fig. 2.3). For the definition of lattice planes the bcc and fcc lattice are treated as simple cubic.

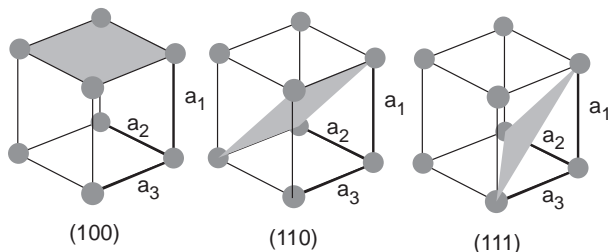


Figure 2.3: Three lattice planes and their Miller indices in the simple cubic lattice.

2.2.3 Lattice and reciprocal lattice at surfaces

A surface can be formed by cleaving a bulk crystal (two surfaces, actually). The first thing one could assume is that all the atoms stay at the same positions as before. This turns out not to be the case. Imagine the forces on an atom at the new surface. In the most simple picture it loses some of its nearest neighbours and an entirely new energetic situation arises. The first layer atoms could move further away from the remaining neighbours or closer towards them. Such a change of the first interlayer spacing is called a *relaxation*. On many surfaces, especially on semiconductors, the atoms try to find new “partners” for the broken bonds sticking into the vacuum. This can lead to a *reconstruction* of the surface where the periodicity parallel to the surface is not the same as in the bulk. For details see section 6.2.

If we now just consider the two-dimensional periodicity parallel to the surface then we can define a two dimensional Bravais lattice, a Wigner-Seitz cell and a basis for the lattice in exactly the same way as in three dimensions. The definition of the basis is somewhat open in that we can include more than one layer of atoms. We can also define a two-dimensional reciprocal lattice and a two-dimensional Brillouin zone, the surface Brillouin zone (SBZ). The high symmetry points in the SBZ have similar names as the points in the bulk Brillouin zone but they carry a bar over the letter. The centre of the zone, for example, is called Γ in the bulk and $\bar{\Gamma}$ on the surface.

An example illustrating the usefulness of reciprocal space again is given in Fig. 2.4. The Fig. shows a Scanning Tunnelling Microscopy (STM) image of a Pt(111) surface together with a Fourier transform of this image. Pt is an fcc metal and the (111) surface is a closed-packed surface with a hexagonal symmetry. In a very simple picture, the STM image corresponds to the charge density on this surface (at the Fermi level). A Fourier transform of the charge density should basically be an image of equ. 2.8 with the intensity at the

reciprocal lattice spots being equal to the Fourier coefficients of the charge density. This is indeed the case. We can see that the six spots around the origin are by far the most intense features. They alone give already a decent description of the image. Because of symmetry, it is basically one Fourier coefficient describing the whole STM image. This makes the usefulness of reciprocal space obvious. When looking closer, more weaker features at other reciprocal lattice points can be seen.

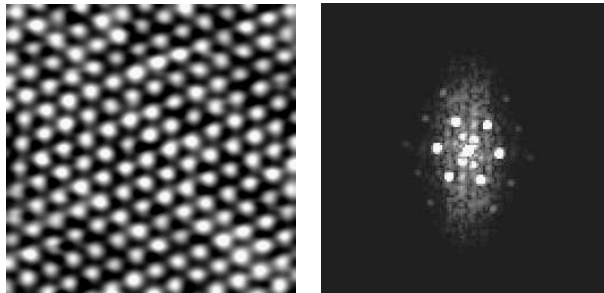


Figure 2.4: Scanning tunnelling microscopy image of Pt(111) (left) and the Fourier transform of this image (right) [10].

2.3 Electronic states

2.3.1 The Drude model of metals

The first theory for describing the properties of metals was given by Drude. Drude transferred the successful kinetic gas theory to the electrons in the metal. In this theory, the electrons are moving freely through the solid, not interacting with each other or with the rigidly fixed ion cores. The only interaction which takes place is an instantaneous scattering from the ion cores (but no scattering from other electrons). This theory was giving the right order of magnitude for the Hall coefficient of most metals and it seemed to explain the Wiedemann-Franz law that the ratio κ/σ of the thermal and electrical conductivity is proportional to the temperature. It gave the right proportionality constant (but for the wrong reasons). The Drude model totally failed to describe the properties like the heat capacity of a metal. In the kinetic gas theory the electronic contribution to the heat capacity would be very high, in the experiment it was not.

2.3.2 A quantum mechanical treatment of free and independent electrons

A quantum mechanical treatment of the electronic structure in a solid starts with considering free electrons in a box. First we calculate the possible states for one electron and then we fill them with electrons according to the right statistics. The electron-electron interaction is neglected. The Schrödinger equation is simply

$$-\frac{\hbar^2}{2m}\nabla^2\psi(\vec{r}) = E\psi(\vec{r}) \quad (2.9)$$

with the boundary conditions that the wave function must vanish at the border of the box. The solutions are

$$\psi(\vec{r}) \propto \sin k_x x \sin k_y y \sin k_z z, \quad (2.10)$$

with energies

$$E = \frac{\hbar^2 k^2}{2m} = \frac{\hbar^2}{2m}(k_x^2 + k_y^2 + k_z^2), \quad (2.11)$$

and with restrictions for the k vector

$$\begin{aligned} k_x &= \frac{\pi}{L}n_x; \quad n_x = 1, 2, 3, \dots \\ k_y &= \frac{\pi}{L}n_y; \quad n_y = 1, 2, 3, \dots \\ k_z &= \frac{\pi}{L}n_z; \quad n_z = 1, 2, 3, \dots \end{aligned} \quad (2.12)$$

where L is the length of the box. If we now go to periodic boundary conditions, i.e. to

$$\psi(x, y, z) = \psi(x + L, y + L, z + L), \quad (2.13)$$

the solutions of (2.9) are

$$\psi(\vec{r}) \propto e^{i\vec{r}\vec{k}} \quad (2.14)$$

and the k-points lie less dense in space:

$$\begin{aligned} k_x &= \frac{2\pi}{L}n_x; \quad n_x = 0, \pm 1, \pm 2, \pm 3, \dots \\ k_y &= \frac{2\pi}{L}n_y; \quad n_y = 0, \pm 1, \pm 2, \pm 3, \dots \\ k_z &= \frac{2\pi}{L}n_z; \quad n_z = 0, \pm 1, \pm 2, \pm 3, \dots \end{aligned} \quad (2.15)$$

If we consider the number of states inside a sphere in k -space it is

$$Z \propto k^3 \quad (2.16)$$

and with

$$E \propto k^2 \quad (2.17)$$

it is trivial to see that the density of states is

$$D(E) \propto E^{1/2}. \quad (2.18)$$

In the free and independent electron model the states in equation 2.10 are filled up with two electrons each (to account for spin) up to the Fermi level according to the Fermi-Dirac distribution

$$f(E, T) = \frac{1}{e^{\frac{E-\mu}{kT}} + 1} \quad (2.19)$$

where μ is the (temperature-dependent) chemical potential which is equal to the (temperature-independent) Fermi energy E_F at $T = 0$. Note that the important point with this distribution is that most of the electrons “sit” deep in the Fermi-sea and can not participate in any small excitations at all. This explains immediately why the Drude model gave a heat capacity which was much too large. For the heat capacity but also for transport by electrons only the electrons close (in the order of kT) to the Fermi energy are relevant.

Sommerfeld modified the Drude model such that the electrons have to obey the right statistics. This model then gives the correct prediction for the specific heat of the conduction electrons

$$c_v \approx \frac{\pi^2}{3} D(E_F) k^2 T \quad (2.20)$$

where $D(E_F)$ is the density of states at the Fermi level. In a classical gas the specific heat would be constant and $3nk_B/2$. The linear contribution of the electrons is very small and can only be measured at very low temperatures since the lattice contribution goes faster to zero $\propto T^3$.

2.3.3 Electrons in a periodic potential

In a real crystal the potential is not zero or constant. It has the same periodicity as the lattice. The Schrödinger equation is

$$\left(-\frac{\hbar^2}{2m} \nabla^2 + U(\vec{r})\right) \psi(\vec{r}) = E \psi(\vec{r}) \quad (2.21)$$

where $U(\vec{r}) = U(\vec{r} + \vec{R}) = \sum_{\vec{G}} U_{\vec{G}} e^{i\vec{G}\vec{r}}$ is the potential. The solutions of this equation are *Bloch waves* with the form

$$\psi_{\vec{k}}(\vec{r}) = u_{\vec{k}}(\vec{r}) e^{i\vec{k}\vec{r}} \quad (2.22)$$

where $u_{\vec{k}}(\vec{r}) = u_{\vec{k}}(\vec{r} + \vec{R})$ is a lattice periodic function. A general property of the Bloch waves is that

$$\psi_{\vec{k}}(\vec{r}) = \psi_{\vec{k}+\vec{G}}(\vec{r}) \quad (2.23)$$

where \vec{G} is a reciprocal lattice vector. This means that a Bloch wave does not change when it is shifted by a reciprocal lattice vector. Setting this into the Schrödinger equation gives that also

$$E_{\vec{k}} = E_{\vec{k}+\vec{G}} \quad (2.24)$$

Since both the wave-functions and the energies are periodic in reciprocal space it is sufficient to look at both in the first Brillouin zone.

2.3.4 Nearly free electrons: metals

For a very simple approach to the electronic structure of metals one can assume that the potential is very weak, i.e. that the electrons are nearly free. Formally this is done by taking only the first two coefficients in the Fourier series for the potential

$$U(\vec{r}) = \sum_{\vec{G}} U_{\vec{G}} e^{i\vec{G}\vec{r}} \quad (2.25)$$

The solution for this potential are similar to the free electron case. The only difference is that now *gaps* appear in the band structure because the bands split at the Brillouin zone boundaries. The size of the splitting is about twice the magnitude of the second Fourier coefficient in the potential.

2.3.5 Tightly bound electrons: semiconductors

The other limiting case is that the electrons are not free at all but rather bound almost as in the corresponding atoms with only a small overlap between the wave functions of neighbouring atoms. Let the Schrödinger equation for the atom

$$H_{at}\psi_{at} = E_n\psi_{at} \quad (2.26)$$

be solved. Then the Hamilton of the solid can be written as

$$H = H_{at} + \Delta U(\vec{r}), \quad (2.27)$$

where $\Delta U(\vec{r})$ describes the deviation of the potential from the superposition of the atomic potentials, i.e. $\Delta U(\vec{r})$ very small close to the atomic cores. This is known as the tight-binding approximation. The wave functions must be Bloch functions, of course, and can be written as

$$\Psi(\vec{r}) = \sum_{\vec{R}} \Phi(\vec{r} - \vec{R}) e^{i\vec{k}\vec{r}}, \quad (2.28)$$

where the Φ and the ψ_{at} wave functions are very similar. In the most simple case of an *s* state it leads to solutions of the form

$$E(\vec{k}) = E_n - \beta - \gamma \cos k, \quad (2.29)$$

i.e. to a band of width γ which is shifted from the atomic level position by the amount β . The band-width γ is given by the overlap of the atomic orbitals. Close to the bottom of the band this has again a nearly quadratic dispersion.

2.3.6 Electronic structure of surfaces

The local density approximation can be used to study some fundamental properties of surfaces. The most simple model for a surface is the so-called *jellium model*. Here, the ions are replaced by a uniform positive background charge. If each atom donates q electrons to the valence band then the charge of the ion is $e(Z - q)$. Smearing it out leads to a average charge of $\bar{n} = e(Z - q)/V = e/(\frac{4}{3}\pi r_s^3)$ where V is the volume of the Wigner-Seitz cell and the inverse-sphere radius r_s is just another way of expressing the electron density.

A surface in the jellium model is an abrupt change of the positive charge density at the surface

$$n_+(z) = \bar{n} \mid z \leq 0, n_+(z) = 0 \mid z > 0 \quad (2.30)$$

The charge density of the electrons does not follow n_+ exactly, of course. The result of a calculation is given in Fig. 2.5. One observes two things: the

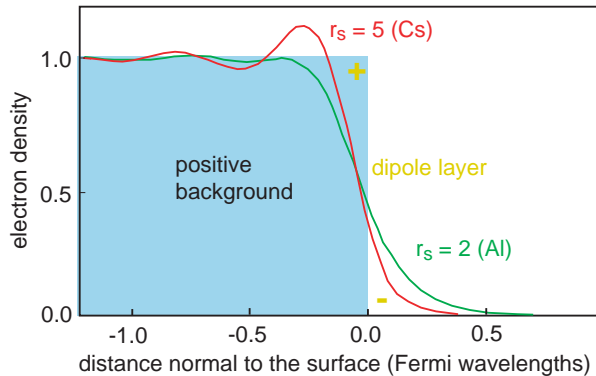


Figure 2.5: Electron density at the surface of jellium as a function of distance from the surface for two values of r_s (after Ref. [9]).

electron density spills out into the vacuum and, when approaching the density 1 inside the crystal, it shows small oscillations as a function of distance.

The spill out of the electrons into the vacuum happens because the electrons try to lower their kinetic energy. This energy gain is balanced by the loss of potential energy. The depletion of electrons just below the surface and the increase of density just above the surface sets up a dipole layer which leads to a change of electrostatic energy $\Delta\Phi$ when moving an electron across the surface.

The small oscillations of the charge density are Friedel oscillations. They have a periodicity of twice the Fermi wavelength (π/k_F) and arise because

the electron gas is not able to screen a perturbation with Fourier components larger than $2k_F$. The step is sharp and has high- k Fourier contributions and therefore it creates Friedel oscillations.

We can also be used to calculate the surface energy of jellium as a function of r_s (or electron density). Fig. 2.6 shows the result of such a calculation. At low densities the results are reasonable but at high density the result is completely inappropriate: the surface energy becomes negative. It might be reassuring to know that re-introducing the lattice solves this problem in the local-density approximation. While the surface energy is of fundamental importance in a total-energy calculation, it is very hard to measure. One can, for example, extrapolate the surface tension of liquid metals to 0 K but one can not measure the work done on a macroscopic crystal when cleaving it.

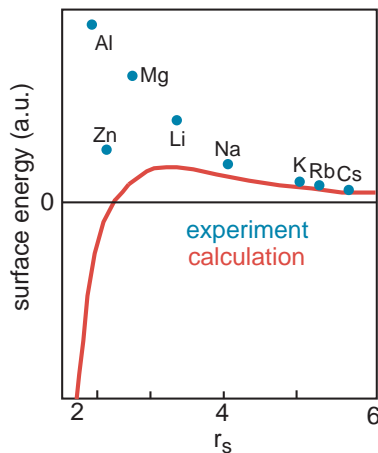


Figure 2.6: Experimental surface energies compared to the result of a jellium calculation (after Ref. [9]).

If we now go back to a crystal with a lattice we can discuss the fundamental properties of the electronic wave functions. The wave functions at the surface do, of course, have to obey the symmetry parallel to the surface but the translational invariance perpendicular to the surface is broken. This symmetry breaking can actually lead to new solutions of the Schrödinger equation, electronic states which reside only at the surface.

A simple qualitative picture is given in the following. Consider the Bloch wave functions in the solid:

$$\psi_{\vec{k}}(\vec{r}) = u_{\vec{k}}(\vec{r})e^{i\vec{k}\vec{r}} \quad (2.31)$$

Nothing in the derivation of the Bloch waves requires the \vec{k} -vector to be real. A \vec{k} with an imaginary part does, however, lead to problem in the bulk: it gives solutions which are growing without bound in the crystal. If however, only the component of \vec{k} perpendicular to the surface is non-real one can try to match the solution which is exponentially growing inside the crystal with an exponential decay outside the crystal. In this way a surface-state wave-function is created. Inside the crystal it can be written as

$$\psi_{\vec{k}}(\vec{r}) = u_{\vec{k}_{\parallel}}(\vec{r}_{\parallel}) e^{i\vec{k}_{\parallel}\vec{r}_{\parallel}} e^{-\kappa r_{\perp}}, \quad (2.32)$$

outside it is exponentially decaying. We write κ instead of k_{\perp} to make clear that we do not deal with a conventional k_{\perp} vector but with a complex one. Fig. 2.7 shows such a solution.

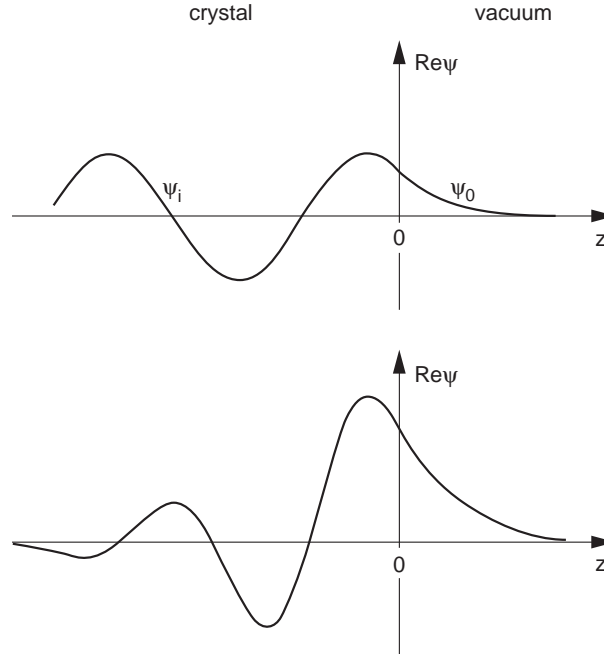


Figure 2.7: Sketch of a bulk and a surface state wave-function close to the surface (at $z=0$). Both are matched to an exponential decay into the vacuum. The surface state also decays exponentially into the bulk.

2.4 Lattice vibrations

2.4.1 Lattice vibrations in the harmonic crystal: phonons

We want to calculate the motion of the atoms in a solid in the so-called harmonic approximation. The interatomic potential is given by the ion-ion interaction and by the screening done by the electrons. We assume that we know this potential. Its precise form is of no importance for the following considerations. The interatomic potential is expanded around the equilibrium position. The constant term is irrelevant and the linear term is vanishing. We keep only the quadratic term. Then the equations of motion look like those for coupled harmonic oscillators (hence the name harmonic approximation):

$$M_\alpha \ddot{s}_{\vec{n}\alpha i} + \sum_{\vec{m}\beta j} \Phi_{\vec{n}\alpha i}^{\vec{m}\beta j} s_{\vec{m}\beta j} = 0. \quad (2.33)$$

This is confusing because of all the indices. $\vec{n} = (n_1, n_2, n_3)$ and $\vec{m} = (m_1, m_2, m_3)$ denote the unit cell. α and β are the numbers of the atoms in the unit cell. s is the displacement and i and j are the direction of the displacement. The term $\Phi_{\vec{n}\alpha i}^{\vec{m}\beta j} s_{\vec{m}\beta j}$ is the force on the α atom in the \vec{n} unit cell in direction i when the β atom in the \vec{m} unit cell is moved in direction j . Basically these are the second derivatives of the potential with respect to the displacements.

Now this complicated system of many coupled equations can be solved by a plane-wave ansatz:

$$s_{\vec{n}\alpha i} = \frac{1}{\sqrt{M_\alpha}} u_{i\alpha}(\vec{q}) e^{i(\vec{q}\vec{r}_n - \omega t)}. \quad (2.34)$$

This has the form of a plane wave which is only defined on the lattice points \vec{r} . Putting this back into the equations of motion leads to a simple system of equations:

$$-\omega^2 u_{\alpha i}(\vec{q}) + \sum_{\beta j} D_{\alpha i}^{\beta j}(\vec{q}) u_{\beta j}(\vec{q}) = 0. \quad (2.35)$$

The D is called dynamical matrix and contains mainly the force constants. The initial equation system with more equations than atoms in the crystal has been transformed into a system with $3r$ equations where r is the number of atoms in the unit cell. It has $3r$ solutions for each (\vec{q}) when the determinant vanishes.

The $3r$ solutions are called "branches". For one atom per unit cell there is only one branch, called the acoustic branch, which has a linear dispersion in the vicinity of $\vec{q} = 0$ and goes to 0 at $\vec{q} = 0$. This branch corresponds to the long-wavelength acoustic waves in the crystal. For each additional atom in the unit cell one gets more so-called optical branches which have a non-zero energy at $\vec{q} = 0$.

The excitations can be viewed as quasiparticles with a momentum \vec{q} and an energy $\hbar\omega$. They are called phonons. Note that these phonons only exist in an harmonic solid.

2.4.2 Vibrations at surfaces

For vibrations at surfaces we can make exactly the same argument as for electronic states at surfaces. Breaking the translational symmetry makes room for new solutions because we can have \vec{q} s which are imaginary perpendicular to the surface. It is easy to imagine that the forces between the atoms in the first layers are different from the forces in the bulk and hence the vibrational frequencies are also different. A genuine surface vibration exists if the frequency at the surface does not show up in the frequency spectrum of the bulk (at the same \vec{q}_{\parallel} , strictly spoken).

Surface-located vibrations (and electronic states) can of course also be created by adsorbing something on the surface. If we put, for example, CO molecules on the surface then the stretch frequency between the oxygen and the carbon is, by definition, a surface vibration .

2.5 Further reading

Most of the contents of this lecture is explained in much more detail in standard solid state physics books. I can particularly recommend those by Ashcroft and Mermin [11] and by Ibach and Lüth [12]. More detailed information about the electronic structure at surfaces can be found in [5] and is also worth considering the original article by Lang and Kohn [9].

Chapter 3

Electron spectroscopy

3.1 Introduction

If we want to learn something about a system, a general experimental approach is a scattering technique: we shoot some particles in a well-prepared state on the target and look at particles coming out of the target (which do not have to be the same). In surface science the most basic questions we want to solve with this approach are for example: Is the surface clean? Which elements are on the surface? And in which chemical compound? What is the exact geometric structure of the surface?

The most common particles to scatter from surfaces are electrons, ions, atoms and photons both as probe and response particles. An important issue is the *surface sensitivity* of an experiment. In general, it is high if we choose particles which have a small mean free path in the solid because this means that the detected particles must originate near the surface. The opposite is true, for example, when the scattering of light by a surface is investigated (reflectivity and change of polarization). The photons will penetrate relatively deeply into the crystal. The amount of photons scattered at or near the surface will be very small. Hence, light scattering is not a good tool to study surfaces. In some cases we can increase the surface sensitivity by choosing an experimental set-up where we use a very grazing angle of incidence or emission. In this way the particles travel a long way close to the surface, even if their mean free path is relatively long.

Very many surface science techniques are based on electrons as a probe. Electrons have very useful properties: they are, at certain energies, very surface sensitive. Electrons in this energy range carry also enough momentum to explore the whole surface Brillouin zone of a material (in contrast to light), they also carry a spin and they are easy to generate and to handle. The

extensive use of electrons in surface sciences justifies a lecture explaining the physics of electron-solid interaction in some more detail. Along with this, we will start to learn about some electron-based analytical techniques.

A technique which is of particular interest in this lecture is Electron Energy Loss Spectroscopy (EELS) where a beam of monochromatic electrons is scattered from the surface. A sketch of this experiment is given in Fig. 3.1.

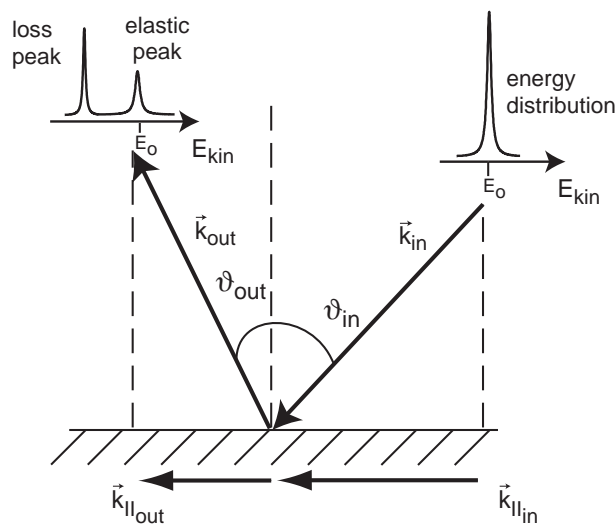


Figure 3.1: An EELS experiment. The momentum transfer parallel to the surface is determined by the electron energy and the scattering geometry.

3.2 Why electrons: The mean free path

One of the main reasons to use electrons in surface science is the mean free path of electrons in matter. This mean free path λ is determined by collisions

$$\lambda(E_{kin}) = v(E_{kin})\tau = \frac{\hbar k}{m}\tau, \quad (3.1)$$

where v is the velocity and τ is the collision time. In the Drude model τ is the mean time between two scattering events. In a quasiparticle-picture τ is given by the imaginary part of the self-energy, i.e. by the lifetime of the quasi-particle. We are interested in energies of the electrons between a few eV and many hundred eV. The mean free path of the electrons in this regime is plotted in Fig. 3.2. The dashed curve shows a calculation of the

mean free path independent of the material and the points are measured data from many elemental solids. The data points scatter more or less around the calculation. The curve is therefore often called a *universal curve*. The reason for this universality is that the inelastic scattering of electrons in this energy range is mostly involving excitations of conduction electrons, which have more or less the same density in all elements. Note that at lower energies other scattering mechanisms will be important, like the scattering with phonons.

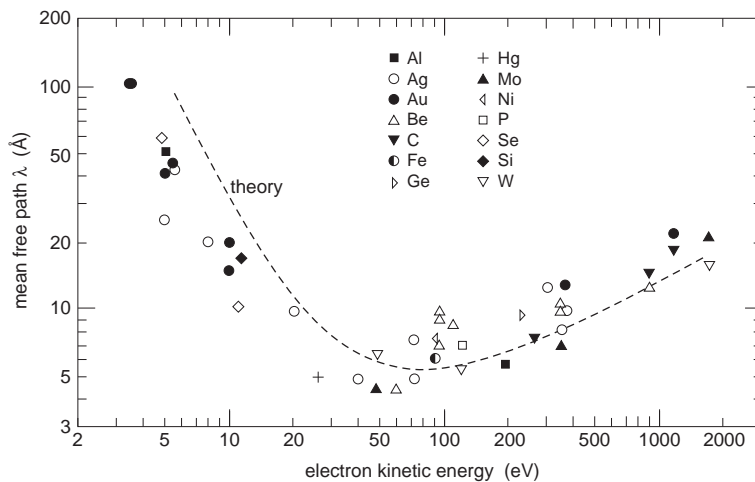


Figure 3.2: The mean free part of the electrons in solid. The dots are measurements the dashed curve is a calculation. After Ref. [13].

The mean free path curve has a broad (note the log-log scale) minimum around a kinetic energy of about 70 eV. There it is less than 10 Å. This means that if we observe an electron with this kinetic energy which has left the solid without suffering an inelastic scattering event it must originate from the first few layers. How do we know that the electron has not been scattered inelastically? Fortunately, the energy loss associated with a scattering from the valence electrons is rather large (as we shall see below). Therefore it is relatively easy to distinguish between inelastically scattered and non-scattered electrons.

3.3 Electron sources and analysers

One big advantage of using electrons is that they are relatively easy to produce. The most common way is electron emission from a hot filament. A

filament is heated by passing a current through it. To “help” the thermally excited electrons out of the metal one additionally puts an anode in front of the filament. The electron beam is focused by placing a so-called Wehnelt cylinder between the anode and the filament. The Wehnelt cylinder is at a negative potential with respect to the filament. The basic principle is shown in Fig 3.3. The simple filament has two disadvantages when one eventually wants to produce a monochromatic beam of electrons. The first is that the voltage drop over the length of the filament (0.5 V) is also reflected in the kinetic energy of the electrons. The second is the thermal broadening due to the high temperature needed to emit the electrons. A better design for emitting monochromatic electrons is an indirectly heated crystal which has a low work function.

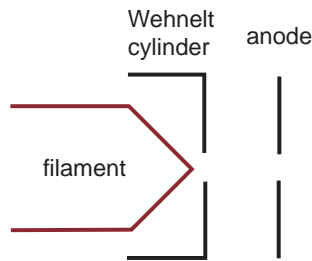


Figure 3.3: An electron gun.

Electrons can be detected using an electron multiplier, usually a so-called channeltron . Such a device is essentially a glass tub with a resistive coating on the inside. A high voltage is applied between the front and the end. An electron which enters the channeltron will be accelerated to the wall where it kicks out more electrons. In this way an electron avalanche is created which eventually leads to a measurable current pulse.

Electron monochromators are needed both for creating a mono-energetic probe-beam and for analysing the energy distribution of scattered or emitted electrons. Electrostatic monochromators are the most common choice. Actual designs represent a trade-off between the need for high count rates and high angular / energy resolution. The so-called cylindrical mirror analyser (CMA) is mostly used for checking the chemical composition of the surface. It consists of two co-axial cylinders in front of the sample. The inner cylinder is held at a positive potential and the outer cylinder at a negative potential. Only the electrons with the right energy can pass through this set-up and are detected at the end. The count rates are high but the resolution (both in energy and angle) is poor. A hemispherical analyser is often used for applications where higher resolution is needed. It consists of two con-centric

hemispheres held a different potentials. The electrons enter and leave through slits. Again, only the electrons with the right kinetic energy, the so-called pass energy E_p can pass the analyser. An electrostatic lens-system can be placed in front of the hemispheres in order to focus the electrons into the analyser and to change the angular acceptance. Such an analyser is shown in Fig. 3.4.

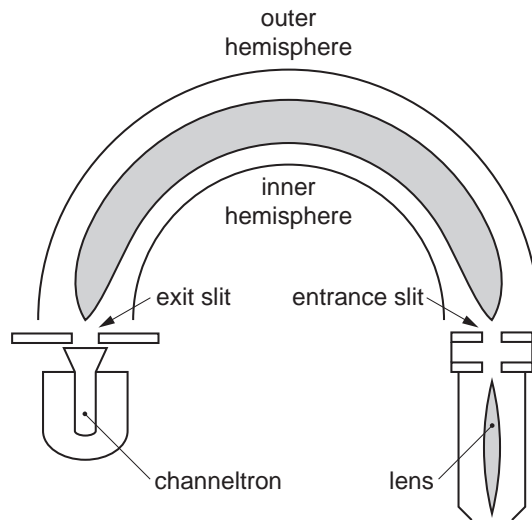


Figure 3.4: A hemispherical electron analyser with a lens system.

In the EELS experiment mentioned above two electron monochromators are needed: one to produce a monochromatic beam and one to analyse the scattered electrons. In a typical apparatus one of these monochromators is movable in order to change the scattering geometry and the momentum transfer (see Fig. 9.3).

3.4 Electrons in solids: elastic and inelastic scattering

Let us now consider the interaction of electrons with solids in some more detail. First consider the scattering of an electron beam from the surface of the solid.

In an elastic scattering event the energy is (by definition) conserved, i.e.

$$E_s = E_0, \quad (3.2)$$

where E_0 is the energy of the incoming electrons and E_s that of the scattered electrons. The momentum parallel to the surface is also conserved apart from a surface reciprocal lattice vector \vec{g}

$$\vec{k}_{\parallel s} = \vec{k}_{\parallel 0} + \vec{g} \quad (3.3)$$

The crystal itself provides perpendicular momentum such that (3.2) and (3.3) can be fulfilled simultaneously. Observing the elastically scattered electrons provides information about the surface reciprocal lattice and the surface geometry. The technique concerned with this is called LEED and will be discussed later.

Here we are more interested in the inelastic scattering since it determines the mean free path of the electrons and hence the surface sensitivity.

3.4.1 The dielectric function

The dielectric function is a very useful concept because it describes the macroscopic absorption of both light and charged particles in solids and, at the same time, has a microscopic interpretation. Let us remind ourselves about some fundamental optical equations. Let the light \vec{E} vector be described by a plane wave which propagates in the x direction.

$$\vec{E} = \vec{E}_0 e^{i(kx - \omega t)}, \quad (3.4)$$

with

$$k = \frac{2\pi N}{\lambda} \quad \text{and} \quad N = n + i\kappa \quad (3.5)$$

Between the complex index of refraction N and the dielectric function ϵ we have the Maxwell relation

$$N = \sqrt{\epsilon} = \sqrt{\epsilon_r + i\epsilon_i} \quad (3.6)$$

The description of the optical properties in terms of N and ϵ is completely equivalent. The two parts of N and ϵ are not independent but can be transformed into each other using the Kramers-Kronig relations

$$\epsilon_r(\omega) = \epsilon_r(\infty) + \frac{\pi}{2} \int_0^\infty \frac{\omega' \epsilon_i(\omega')}{\omega'^2 - \omega^2} d\omega' \quad (3.7)$$

and

$$\epsilon_i(\omega) = \frac{2\omega}{\pi} \int_0^\infty \frac{\epsilon_r(\omega') - \epsilon_r(\infty)}{\omega'^2 - \omega^2} d\omega' \quad (3.8)$$

Note that technically spoken one quantity has to be known over the whole frequency spectrum if we wish to obtain the other. In similar ways both

parts of N or ϵ can be obtained from just measuring the normal-incidence reflectivity over a large spectral range.

The absorption of light in matter is given by Lambert's law

$$I = I_0 e^{-\alpha x} \quad \text{and} \quad \alpha = \frac{4\pi\kappa}{\lambda} \quad (3.9)$$

The probability p for the electrons to suffer an inelastic scattering event is given by

$$p(\omega) \propto \Im\left(\frac{-1}{\epsilon(\omega)}\right). \quad (3.10)$$

This probability is exactly what we are concerned with here. When looking at the mean-free path, there seems to be a scattering probability which is very high for electrons with kinetic energies around 70 eV.

In the following subsections we go quickly through the elementary excitations which are important contributions to the dielectric function, ordered by energy. These excitations provide a detailed microscopic picture for the dielectric function.

3.4.2 Phonons

On its way through the solid and at the surface the electrons can be scattered inelastically by absorbing or creating phonons.

The phonon energies are small (usually less than 100 meV) but the \vec{q} vector can be large. The phonon losses one observes in an EELS spectrum can be used to map the dispersion of the surface phonons or to learn something about the adsorbates by measuring their vibrational frequencies. We will come back to this in a later lecture. In our context here, phonon scattering is not very important because it only has to be considered at low energies.

3.4.3 Excitons

Consider the case that an electron is excited from a bound state to a previously unoccupied state. In a metal, the screening is so strong that the electron and the hole will have very little interaction. In a semiconductor, however, electron and hole can remain loosely bound to form a so-called exciton. This exciton has a spectrum like a hydrogen atom but the Coulomb potential is screened by the dielectric function

$$V_{Coul}(r, R) = -\frac{e^2}{\epsilon|r - R|} \quad (3.11)$$

The energy levels of this “hydrogen atom” lie just below the conduction band in an insulator or semiconductor. Ionizing the exciton means exciting the electron into the conduction band. The exciton is not bound to a particular site: the hole and the electron have some finite probability to hop to an adjacent site. This probability broadens the excitonic energy levels into bands.

At the surface of a solid, the reduced coordination changes both the Coulomb potential for a single exciton and the hopping matrix elements between the excitons. This results in a so-called surface exciton which is shifted and has a different width.

3.4.4 Interband transitions

Another loss mechanism is the creation of electron-hole pairs. In a metal electron-hole pairs can be created with infinitely small energies by lifting an electron from an energy level just below the Fermi energy to a level just above. Electron-hole creation does thus contribute to the dielectric function at all energies. For a semiconductor the situation is different. There is a smallest energy for electron-hole pair creation, the energy of the fundamental gap. In semiconductors, a structure in the dielectric function can be found which corresponds to excitations over the gap. At slightly lower energy, the excitons are found. For both, metals and semiconductors so-called *critical points* in the band structure give rise to strong features in the dielectric function. A critical point is, for example, a situation where the occupied bands and unoccupied bands are parallel in a larger region of k -space. Then the optical transitions from the region all have the same energy and contribute strongly to ϵ .

3.4.5 Bulk and surface plasmons

In the Drude model of metals, the dielectric function is

$$\epsilon(\omega) = 1 - \frac{\omega_P^2}{\omega^2}, \quad (3.12)$$

where ω_P is the so-called plasma frequency

$$\omega_P^2 = \frac{ne^2}{m\epsilon_0}. \quad (3.13)$$

ω_P has a simple interpretation. It corresponds to a longitudinal collective vibration of the electron gas against the positively charged ions (see Fig. 3.5). These excitations are called plasmons .

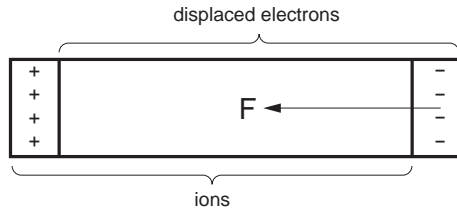


Figure 3.5: A simple picture for a plasma oscillation

The plasma frequency is very important for the optical properties of a metal. We write equ. 3.4 as

$$\vec{E} = \vec{E}_0 e^{i\frac{\omega}{c}\sqrt{\epsilon}x - i\omega t}. \quad (3.14)$$

We can distinguish between two cases: if $\omega < \omega_P$ then ϵ is real and negative and (3.14) gives only exponentially damped solutions. This means that an electric field can not penetrate a metal, the metal is reflecting all the light. Above the plasma frequency (3.14) does permit propagating solutions of the electric field.

For simple metals, there is a good agreement with the calculated plasma frequency ω_P , or plasmon energy $\hbar\omega_P$, and the experimental values.

There is also a plasmon mode which is localized at a metal surface and decays exponentially towards both metal and vacuum. It can be described as a longitudinal wave

$$\Phi(\vec{r}) = \Phi_0 e^{iq_{\parallel}r_{\parallel}} e^{-q_{\parallel}|z|}. \quad (3.15)$$

Fig. 3.6 shows the field and charge distribution for such a mode.

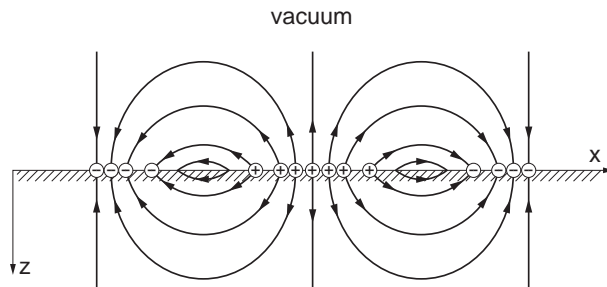


Figure 3.6: Charge and field distribution for a surface plasmon

The planar component of the \vec{E} field associated with this is continuous but

the perpendicular component is not. Just above and below the surface it is

$$E(z + 0) = \Phi_0 q_{\parallel} e^{iq_{\parallel} r_{\parallel}} \quad \text{and} \quad E(z - 0) = -\Phi_0 q_{\parallel} e^{iq_{\parallel} r_{\parallel}} \quad (3.16)$$

Now the $\vec{D} = \epsilon \vec{E}$ field must be continuous. This gives us the condition for the existence of the surface plasmon

$$\epsilon(\omega_{sp}) = -1 \quad (3.17)$$

and hence

$$\omega_{sp} = \omega_P / \sqrt{2} \quad (3.18)$$

The energy loss of electrons due to plasmons and surface plasmons is illustrated in Fig. 3.7. It shows the energy distributions from an electron beam with approx. 2 keV kinetic energy which has been scattered from a surface of α -Ga. Distinct losses are visible which can be ascribed to bulk and surface plasmons. Note that the energy difference between these losses is in good agreement with equ. 3.18. The difference between the spectra is due to the experimental geometry. This will be picked up in the exercises.

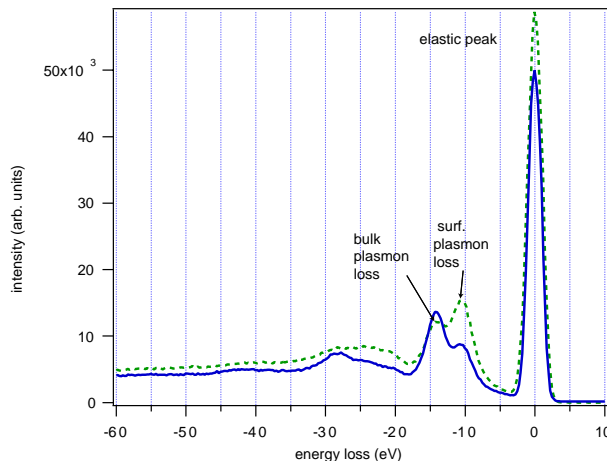


Figure 3.7: EELS spectra from the (010) surface of α -Ga. The surface and bulk plasmon losses can be identified. The difference between the spectra is due to the experimental geometry (to be discussed in the exercises).

The excitation of plasmons and surface plasmons is the major reason for the inelastic scattering of the electrons in the energy regime we are interested in. When looking again at the universal curve we can see that the mean free path is long for lower energies because it is not possible to excite the plasmons. Above the edge for plasmon creation the mean free path drops drastically. At high energies it goes up again because the cross section for the plasmon creation diminishes.

3.4.6 Core levels

At much higher energies, several hundred eV or so, small structures in the dielectric function can be found which are due to the excitation of core electrons.

3.5 Concluding remarks

We have seen that the minimum in the electron mean free path in Fig. 3.2 is mainly determined by the excitations of plasmons. Below the edge for plasmon excitation, the most important loss mechanism is interband transitions. This raises the question about how universal the curve actually is. If we take, for example, a wide band semiconductor, then interband transitions below the gap energy will not be possible and this will increase the mean free path considerably.

The fact that plasmon creation is the most important mechanism for inelastic scattering makes it clear why it is simple, in most cases, to distinguish elastically scattered (emitted) electrons from electrons which have been scattered by plasmons. The reason is that the plasma energies are rather large so that the loss peaks are far away from the elastic peak (see Fig. 3.7).

The most common way to measure the mean free path of electrons in a material is to evaporate a thin film of the material on a substrate. Then the intensity of characteristic Auger transitions in the substrate is measured as a function of film thickness.

3.6 Further reading

The basic principles of electron spectroscopy are discussed in most surface science books [3, 2, 1, 4]. A good section about analysers and electron optics can be found in [4]. The elementary excitations which contribute to the dielectric function are discussed nicely in [3]. The basic physics of the Drude model and the plasmons is discussed in [11]. Surface plasmons are described in [3].

Chapter 4

Surface cleaning and chemical analysis

4.1 Surface cleaning

In the first lecture we have learned about UHV techniques and how to keep surfaces clean for a long time. The next question is obviously how to obtain a clean surface in the first place. There are various ways of doing this, the most common being

1. cleavage of the bulk crystal
2. heating
3. ion bombardment (sputtering) with noble gas ions (Ne^+ or Ar^+)
4. *in situ* chemical treatment
5. Growing a thin film of the desired material on a surface of another material.

Cleaving a bulk crystal is a very elegant way of obtaining a clean surface but it can only be applied to materials which have a natural cleavage plane. Important examples are some semiconductors and layered compounds like graphite or the new high T_C superconductors as well as molecular crystals which are merely bound by van der Waals forces like fcc C_{60} . A disadvantage of cleaving is the fact that a new preparation requires a new cleavage and most samples can only be cleaved once. Another potential problem is that the surface structure obtained by cleaving might be a meta-stable structure. The surface atoms may be left at the bulk position while the most stable structure would actually be a reconstruction. Yet another problem is that

some samples are so unstable, that some of their constituents are evaporating out of the freshly cleaved surface and are thus depleted in the vicinity of the surface. An example is the oxygen depletion in certain high T_C superconductors which occurs unless the cleavage is performed at very low temperatures.

Some materials can simply be cleaned by heating, in order to flash off an oxide layer and all contaminations. The most important examples are Si and the refractory metals Mo and W. For most materials, however, the bulk melting point lies under the temperature which would be required to clean the sample. Even below the melting temperature, heating might damage the crystal too much by changing the stoichiometry.

Ion bombardment (sputtering) of the sample is a very broadly used method, especially for metals. It is possible to clean the surface but the cost is that the surface is heavily damaged. This damage can often be repaired by heating. This, in turn, might cause impurities from the bulk to migrate to the surface such that more ion bombardment is needed and so on. Usually many cycles are needed to obtain a clean surface. When used for compounds, ion bombardment has the problem, that some elements in the compound are more easily removed than others. This leads to a sample with the wrong stoichiometry.

The sample can be chemically treated in order to “react the impurities away”. Carbon contaminations can often be removed by heating the sample in a low oxygen pressure (to create desorbing CO) and the remaining oxygen can be removed by a hydrogen treatment (to create desorbing water).

4.2 Surface chemical analysis

Chemical analysis is essential for almost every experiment in surface science. Many questions are concerned with chemical reactions on surfaces where one has to learn about the reactants and the products and last but not least one has to determine if the surface is indeed clean after cleaning it.

We want to concentrate on non-destructive techniques for analysing the chemical composition of a surface. One can probe the geometric, electronic or vibrational properties in order to check if they correspond to those of the clean surface. The electronic structure is of particular importance because the binding energies of the core electrons, i.e. the electron in the atom’s inner shells, are very characteristic for the different elements. The techniques of x-ray photoelectron spectroscopy (XPS) and Auger electron spectroscopy (AES) rely on this. An alternative is to probe the surface vibrations. Adsorbed atoms or molecules have characteristic vibrational modes which often have higher energies than the bulk vibrational frequencies.

In the following we will describe XPS in some detail and Auger rather briefly. The reason is the higher potential in the former technique. XPS can not only give an answer about which elements are present on the surface, it can also give some information about the chemical state the elements are in.

4.3 X-ray photoelectron spectroscopy (XPS)

XPS relies on the photoelectric effect. In the most simple picture, the photons which hit the solid kick out electrons which are detected outside. The photon energy must be high enough for the electrons to overcome the work function of the solid. If one analyses the energy distribution outside the solid, it reflects the density of states inside (see Fig. 4.1). The energy is conserved:

$$E_{kin} = h\nu - E_{bin} - \Phi, \quad (4.1)$$

where E_{kin} is the kinetic energy, $h\nu$ is the photon energy, E_{bin} is the binding energy and Φ is the work function. For XPS the photon energy has to be high enough to ionize the core levels from the atoms of interest. Fig. 4.1 suggests that the photoemission intensity $I(E_{kin})$ is simply given by $I(E_{kin}) = DOS(h\nu - E_{bin} - \Phi)$ where $DOS(E)$ is the density of states of the sample as a function of binding energy. We shall see later that this simple picture is rather poor, in particular for spectroscopy of the valence states.

We have to keep in mind, however, that identifying the photoemission intensity with the occupied density of states is much too simple, mainly because of the fact that the photoemission intensity depends strongly on photon energy and emission direction.

4.3.1 X-ray sources

To make use of the difference in core-level binding energies for chemical analysis, one needs a monochromatic x-ray source. Most x-ray sources are based on the following principle: a hole is created in the inner-shell core levels of the atoms in an anode by bombardment with high-energy electrons. There are two competing ways to fill up this hole: x-ray emission and Auger decay. Both are shown in Fig. 4.2.

The Auger process is important for relatively low core-binding energies and for light elements. Below 10 keV binding energy and $Z = 12$ (Mg), the x-ray decay is extremely unlikely.

For the x-ray sources employed in surface chemical analysis, one normally uses Al or Mg as an anode material. The most intense lines are called K_{α_1} and K_{α_2} , according to the old x-ray nomenclature (see Fig. 4.3). Often the

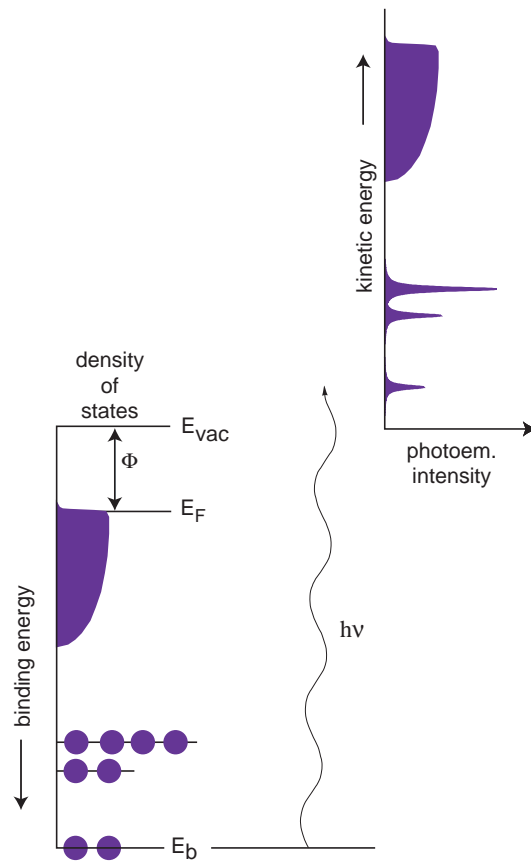


Figure 4.1: Sketch of the energies involved in photoelectron spectroscopy.

doublet is viewed as one line and called $K_{\alpha_{12}}$. It has an energy of 1253.6 eV and 1486.6 eV, for Al and Mg, respectively. Note that in the light of what we have just said about the probability of an x-ray decay, these sources are very un-efficient. Why does one use these materials anyway?

The $K_{\alpha_{12}}$ is the most intense line in the x-ray spectrum but not the only one. The most important other contributions are due to double-ionization (the $K_{\alpha_{34}}$ line), transitions from the valence band (the K_{β} line) and a bremsstrahlungs background caused by the de-acceleration of the fast electrons in the material. These lines lead to “satellite” peaks in the spectra. The K_{α_1} and K_{α_2} lines do also have a certain width themselves which, together with their separation, determines the ultimate resolution achievable with an x-ray source. It is determined by lifetime of the core hole. The total width for the Al and Mg $K_{\alpha_{12}}$ line is of the order of 1 eV.

For a detailed chemical analysis, it is very desirable to have a higher en-

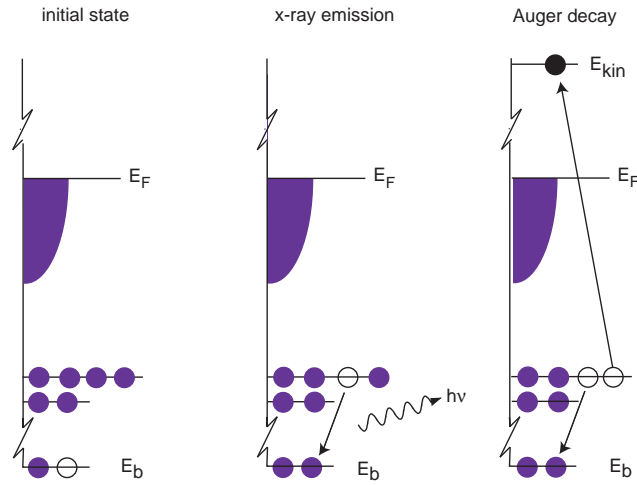


Figure 4.2: Decay of a core-hole by x-ray emission or the Auger process.

ergy resolution. In order to achieve this, the x-ray source can be equipped with a monochromator. This will increase the energy resolution and at the same time remove the “satellite” lines which are due to photoemission induced by, for example, the $K_{\alpha_{34}}$ line.

Alternatively, one can use synchrotron radiation as an x-ray source. This radiation is caused by accelerating ultra-relativistic charged particles (mostly electrons), typically by forcing them to go around the corners of a storage ring (see Fig. 4.4).

This leads to a continuous spectrum from the infrared over the visible and uv to the x-ray regime (see Fig. 4.5)

Above the so-called critical energy, the synchrotron radiation intensity drops quickly to zero. The critical energy is given by the kinetic energy of the electrons in the ring

$$E_C \propto \frac{E_{kin}^3}{R}, \quad (4.2)$$

where R is the bending radius in the ring. If one wants to do XPS at a synchrotron radiation source, one does of course also need a monochromator.

Synchrotron radiation has several advantages over conventional sources: the resolution can be very high, the radiation is polarized and, most importantly here, the photon energy can be changed. The last point allows us to shift the peaks in an x-ray spectrum to exactly the kinetic energy we want. In surface science, this is often the energy where the mean free path of the electrons is shortest. The obvious disadvantage of synchrotron radiation is that you have to build a storage ring to get it.

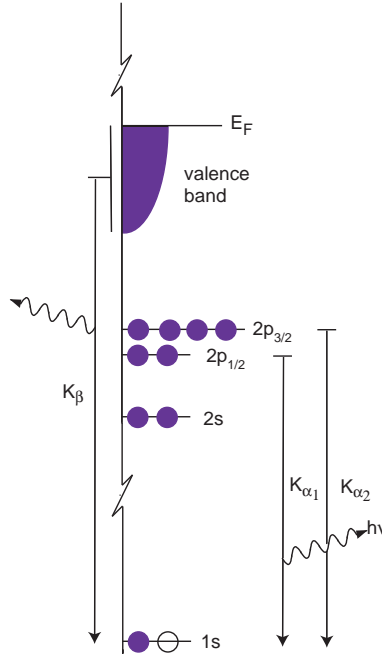


Figure 4.3: Nomenclature in the x-ray decay in Al and Mg.

4.3.2 XPS cross sections

The XPS cross section is given by a matrix element $\langle f | \vec{H}' | i \rangle$. The field-atom interaction hamilton can be written as

$$\vec{H}' = -\frac{e}{2mc}(\vec{p}\vec{A} + \vec{A}\vec{p}) - e\Phi + \frac{e^2}{2mc^2}|A|^2 \quad (4.3)$$

This may be simplified using various approximations (for a detailed discussion of the photoemission process, see section 7.3.2). The result is

$$\langle f | \vec{H}' | i \rangle = \frac{i}{\hbar} \langle f | \vec{p} | i \rangle. \quad (4.4)$$

Decomposing this into a radial part and an angular part gives the dipole-selection rules

$$l' = l \pm 1 \quad \text{and} \quad m' = m, m \pm 1. \quad (4.5)$$

The actual cross section is contained in the radial integral. As a rule of thumb, the cross section for a given initial state, e.g. the 1s electron, increases very rapidly with the atomic number of the element. This means that is easier to see a contamination of oxygen than a contamination of carbon when looking at a conventional XPS spectrum from a surface.

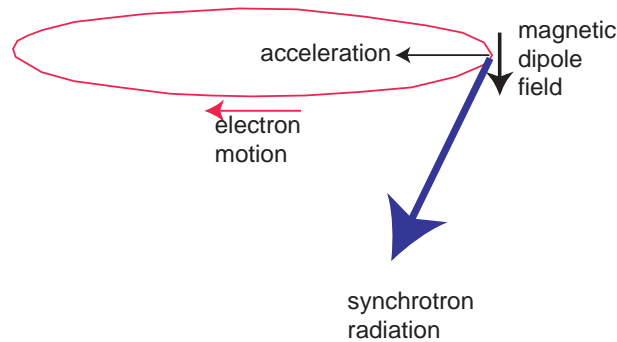


Figure 4.4: Acceleration of electrons in a storage ring and emission of synchrotron radiation.

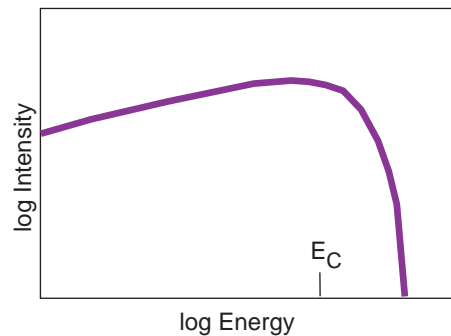


Figure 4.5: Spectral distribution of synchrotron radiation.

Qualitatively, a lot can be learned about the cross sections by just looking at the radial part of the atomic, i.e. bound, wave function and of the free electron wave leaving the atom. Fig. 4.6 shows such a comparison. Consider first the upper part which shows the radial wave function of Ne $2p$ together with the radial part of the photoemitted electron just at the threshold, i.e. at zero kinetic energy. Qualitatively, the matrix element is given by the integral over the product of the two wave functions. This integral is positive. When we now increase the energy of the outgoing electron then the wavelength of the photoelectron will become smaller and the value of the integral will increase. At very high energies, on the other hand, the wavelength of the outgoing electron will be so short, that the integral contains very many positive and negative contributions of equal size and vanishes. This means that for increasing the photoelectron energy, we expect the photoemission cross section to increase right after the threshold, to rise to a maximum value and

to decrease slowly after reaching this value.

Now consider the case of Ar $3p$. The behaviour here is qualitatively different because the radial wave function of the atom has a node. Right at threshold the integral is large and negative. Increasing the energy of the outgoing electron will lead to a situation where the first node of the outgoing wave divides the large negative area of the $3p$ area in almost equal parts. At this point, the integral will be close to zero. Upon a further increase of the energy, the integral will also increase again. Finally, for very high energies, it will vanish for the same reasons as above. The minimum occurring in the cross sections for initial states with a radial node is called a *Cooper minimum*.

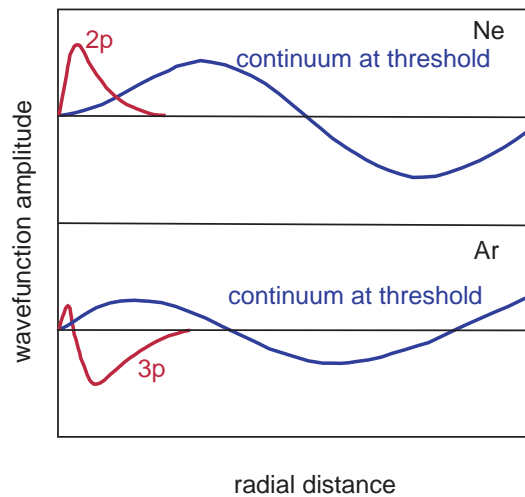


Figure 4.6: Radial part of the Ne $2p$ and Ar $3p$ wave functions together with the continuum wave function for the $l+1$ channel at zero kinetic energy. After Ref. [14].

4.3.3 Qualitative analysis: typical spectra

Fig. 4.7 shows an XPS spectrum from an Al surface. The most pronounced peaks in the spectrum are due to the excitation of the Al core levels and the corresponding plasmon losses. Apart from these, several other structures are visible. Some can be identified as lines from contaminations which are adsorbed on the surface. One is due to an Auger transition which occurs to fill up the core hole under the emittance of an electron. When using synchrotron radiation, it is simple to distinguish between the Auger and the XPS peaks:

One takes the same spectrum at a slightly different photon energy. The XPS peaks will also shift in kinetic energy by the same amount but the Auger peaks will not. They have a fixed kinetic energy. The possibility of moving the photon energy is also very useful if some adsorbate XPS peaks fall too close to some substrate Auger peaks and are therefore invisible.

There is also a background under the whole spectrum which is caused by inelastically scattered electrons. This background is quite structureless, only increasing at low kinetic energies. We see that we can really distinguish between the directly emitted electrons and those which have undergone an inelastic scattering process.

For a practical surface chemical analysis one can compare the measured spectra to tabulated data, like in the “Handbook of x-ray photoelectron spectroscopy” [17].

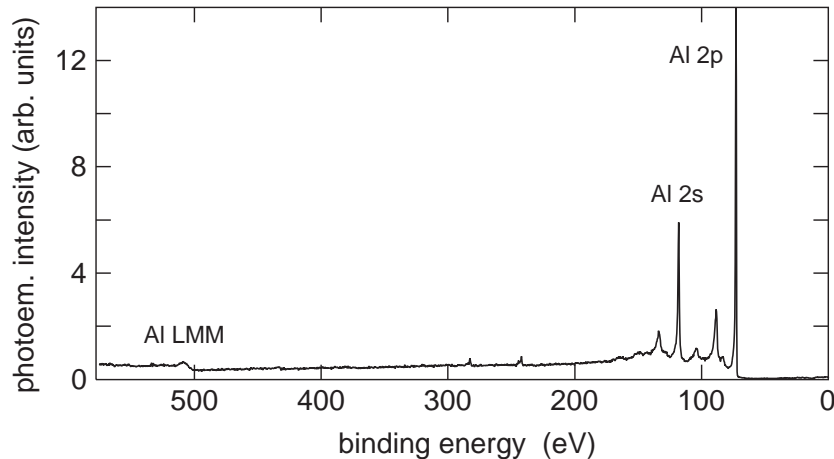


Figure 4.7: XPS spectrum taken from an Al(001) surface with synchrotron radiation at $h\nu = 600\text{eV}$.

4.3.4 XPS binding energies

The precise value of the XPS binding energy gives very valuable information about the system. However, an exact understanding of the observed binding energy is rather complicated. We distinguish between initial state effects and final state effect. The former affect the binding energy of the initial state before the photoemission event, for example by the chemical environment of the atom of interest. The latter are due to the photoemission event itself and the nature of the final state.

Let us start with the initial state effects. If one finds, for example, a C 1s peak in the XPS spectrum from a surface, then one may be able to decide if the carbon is present in a CO₂ or in a CF₄ molecule. The reason is, that the electronic environment of the carbon atom determines the electrostatic potential at the position of the carbon core. In the case of CF₄ the F atoms draw the C valence electrons strongly away from the carbon. For the 1s electron, this leads to an effective increase of the nuclear charge and it therefore increases the binding energy observed in XPS. Fig. 4.8 shows the measured and calculated (see below) binding energies for the C 1s line in different chemical environments. The *chemical shift* over the whole range is rather large, so large that it can be observed even with a conventional x-ray source.

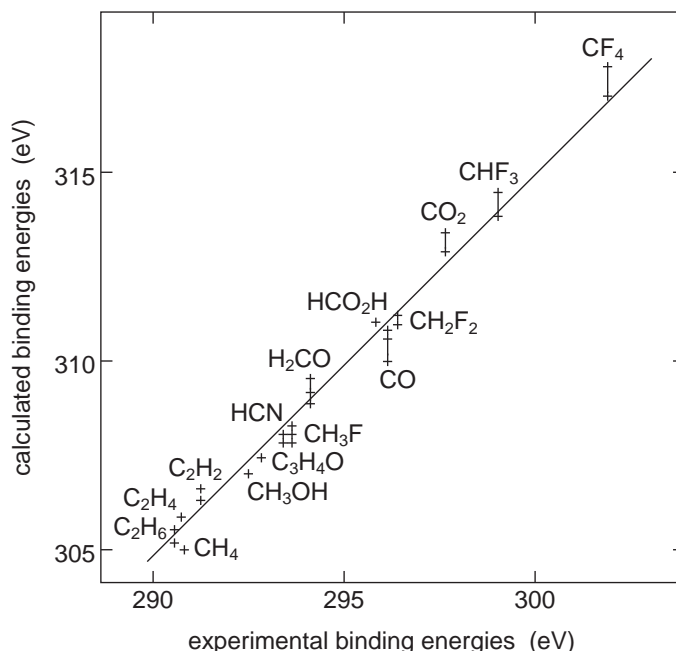


Figure 4.8: Comparison between experimental and calculated (from Koopman's theorem) C1s binding energies. Note that the agreement is very good but only if one of the axes is shifted by 15 eV. The good agreement is underlined by the line of slope 1 After Ref. [15].

The use of synchrotron radiation and the high resolution associated with this permits now to observe much smaller shifts. Fig. 4.9 shows the Ru 3d core level spectrum from a *clean* Ru surface. Apart from the bulk peak two others are visible which can be assigned to emission from the first two layers

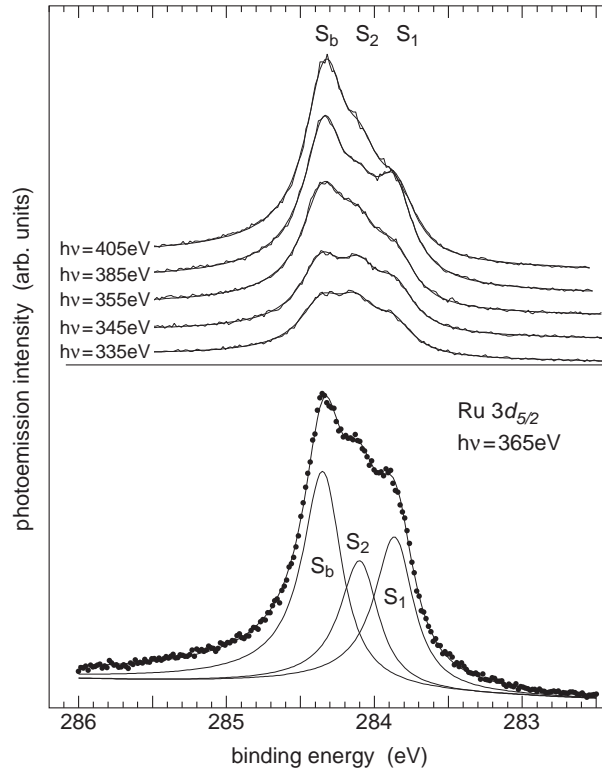


Figure 4.9: A Ru $3d_{5/2}$ core level spectrum from a clean Ru surface. Apart from the bulk peak two surface-related peaks are visible, one from the first and one from the second layer. After Ref. [16].

of this surface. Such *surface core level shifts* (SCLS) have often been observed for the transition metals and have been explained using the simple picture given in Fig. 4.10. When the surface is created, the d -band is narrowed due to the smaller number of nearest neighbours. Consider the case of less than half filling. A band narrowing would also move the whole band over the Fermi level. This would mean that the surface is charged: it is at a chemical potential different from the bulk. In order to avoid this energy-expensive situation, an electrostatic potential is needed which shifts the whole band down to lower energies. This electrostatic potential does also shift the core level. The analogue argument is made for the case of more than half filling.

So far, we have only considered initial state effects on shifting the binding energy. We have not said anything about the importance of final state effects or how to calculate the binding energy in the first place. The most simple assumption for such a calculation is that the measured binding energy is the

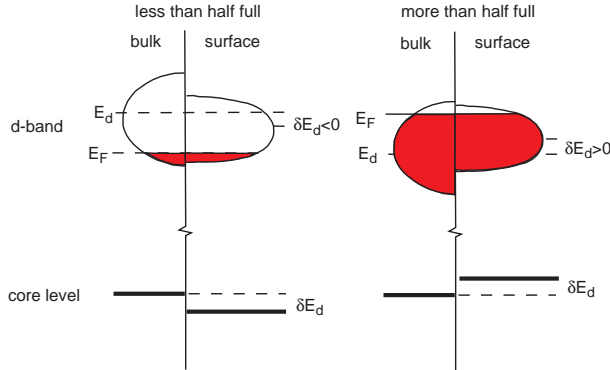


Figure 4.10: Surface core level shift caused by d -band narrowing and an electrostatic shift for transition metals with less and more than half filling of the d shell.

orbital energy of the photoionized electron. This is known as Koopman's theorem. It has been used to calculate the binding energies in Fig. 4.8 and obviously leads to a large but constant error of about 15 eV.

The most severe error in Koopman's theorem is the following: if an electron is adiabatically removed from the core, the other electrons in the system have to reach a new ground state. This new ground state has a lower energy due to the increased effective nuclear number of the photoemitting atom. The *relaxation energy* associated with reaching the new ground state is partially transferred on the photoelectron (Fig. 4.11). This increases the kinetic energy and decreases the apparent binding energy. We can write:

$$E_{kin} = h\nu - E_{bin} + E_r = h\nu - (E_{bin} - E_r) \quad (4.6)$$

We assume a zero work function here for simplicity. The expression in brackets would be the binding energy determined by the experiment. The picture where the electron is taken out of the system adiabatically, i.e. very slowly, is actually not a good one. On the contrary, we should rather think of the electron as being removed very quickly. In such a situation, the system is not necessarily left in the ground state. It could be in some excited state and the energy of this excitation would be missing from the photoelectrons. This leads to satellite peaks in the photoemission spectra. In the case of metals the most pronounced satellite peaks correspond to plasmon excitation. The excitation of electron-hole pairs, on the other hand, does not lead to separate peaks but it renders the lineshape of the core level peak itself asymmetric.

In summary, we can note that the precise binding energy of a core electron is very sensitive to the environment of the emitting atom and much can be

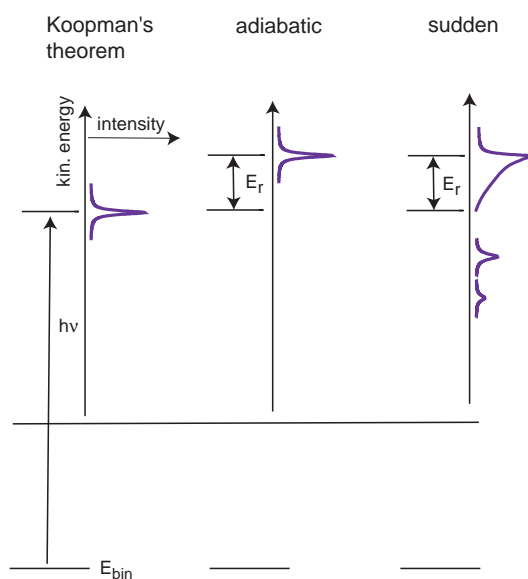


Figure 4.11: Final state effects in the photoemission process.

learned from the XPS spectra. On the other hand, one has to be very careful when it comes to interpreting spectra with several shifted components because the shift itself is a very complicated interplay of initial and final state effects. An “intuitive” assignment of the various peaks could be wrong.

4.4 Auger electron spectroscopy (AES)

Auger electron spectroscopy can be used for surface chemical analysis in a way very similar to XPS. Since core levels are involved, the energy of the Auger electrons is also very characteristic for the various elements. AES is, however, rather limited when it comes to very high resolution studies. Therefore, we discuss it only briefly here. On the other hand, a qualitative chemical analysis of the surface is still very often performed using AES with a simple spectrometer based on a cylindrical mirror analyser. The importance of AES for the practitioner justifies a short discussion.

The Auger effect (depicted in Fig. 4.2) was discovered by Pierre Auger in 1923. In photoemission experiments, he observed electrons with kinetic energies independent of the incident x-rays.

The process starts from an atom with a core hole in the level A. This core hole is filled by an electron from the level B. The remaining energy is used to kick out an electron from the level C. The kinetic energy of an Auger

electron is then

$$E_{kin} = E_A - E_B - E_C - \Phi \quad (4.7)$$

This formula is not a very good one because it is only based on the atomic levels. Actually we are concerned with a transition from an atom with one core hole to an atom with two core holes. One often takes this into account (with little justification but some success) by inserting the average between the Z and $Z + 1$ energy levels for E_B and E_C into equations (4.7).

4.4.1 Auger nomenclature

The Auger nomenclature follows the old x-ray notations. The Auger transitions are labelled ABC for the initial state hole (A) and the two final state holes (B) and (C). For ABC one sets the letter denoting the shell. A KLL Auger transition would be a transition starting from a hole in the $1s$ level which would be filled up from the $2p$ level. A $2p$ electron would also be emitted. The more complicated nature of the upper levels causes a multiplet splitting in the Auger spectra.

4.4.2 Experimental

An important point in AES is, that it does not make any difference, how the initial core hole is created. In most practical cases this is achieved by bombarding the sample with electrons of 2-3 keV kinetic energy. The Auger electrons are detected with the electron analysers we have already discussed. For a quantitative analysis, the energy of the exciting electrons does, however, come into play because of the energy- and element-dependent ionization probability.

4.4.3 Qualitative analysis: typical spectra

Fig. 4.12 shows a typical Auger spectrum from a Cu surface. It shows pronounced peaks due to the Cu Auger peaks and some small peaks which have been assigned to contaminations of the surface. Note that the spectrum is taken in a derivative mode using a lock-in amplifier in order to reduce the contribution of the inelastically scattered electrons.

4.4.4 Quantitative analysis

An example for the quantitative analysis of Auger spectra is given in the Exercises.

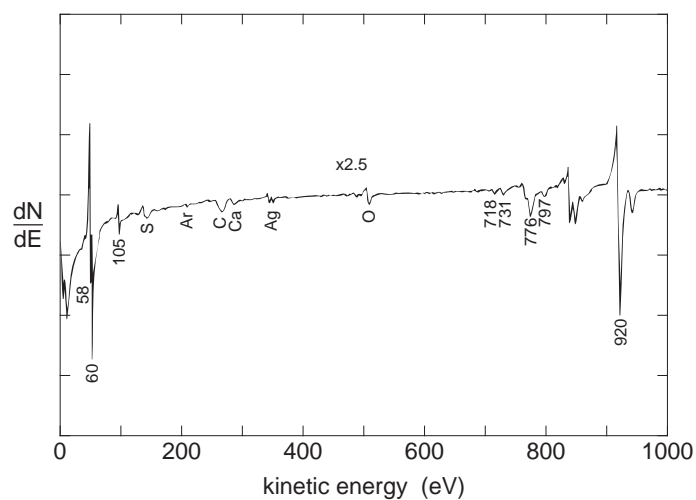


Figure 4.12: Typical Auger spectrum from a Cu surface.

4.5 Further reading

If you are interested in preparational details for a specific system, it is best to consult some recent original publications (if these do not exist you have to try for yourself!). XPS and AES are discussed in most surface science books and in great detail in [2].

Chapter 5

Adsorption, Desorption and Chemical Reactions

5.1 Introduction

The adsorption and desorption of atoms and molecules on surfaces and the chemical reactions between them while on the surface are important areas in surface science because they are close to heterogeneous catalysis, corrosion and the growth of thin films. The scenario for heterogeneous catalysis is, for example, the adsorption of the reactants on the surface, the dissociation of some of the reactants and the desorption of the products. A simple and yet important example is the NH_3 synthesis in Fig. 5.1.

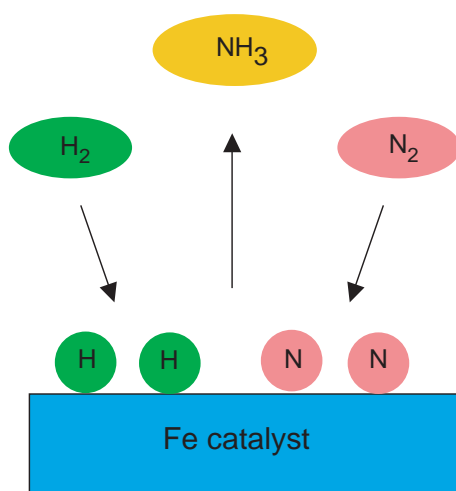


Figure 5.1: NH_3 synthesis on an iron surface.

The figure also illustrates two fundamental concepts in adsorption. One is the question if a molecule is adsorbed as a single unit or dissociated upon adsorption. This is called associative and dissociative adsorption. The other is that such adsorption processes might be reversible or irreversible.

In the following, we discuss the mechanisms which bond adsorbates to surfaces and the forces between them. Then we look at the kinetics of adsorption under very simple circumstances. At last we take a brief look at chemical reactions on surfaces. We do not discuss any effects of the adsorption geometry on the bonding at this point.

5.2 Physisorption

Bonding of adsorbates to a surface is very similar to the usual chemical bonding between atoms. The major differences are that one of the bonding partners now contains very many electrons and is much larger than the other.

The weakest interaction which can lead to bonding between a surface and an adsorbate is the van der Waals interaction, which is the force caused by the interaction of a fluctuating dipole in the adsorbate with a polarizable solid. This van der Waals bonding already illustrates the difference in bonding between two molecules and one molecule with a solid. A van der Waals bonding between two molecules can be described as the interaction between two point dipoles. The dipole moment p_1 at the first molecule leads to opposite induced dipole moment at the second molecule $p_2 \propto \alpha p_1 / r^3$ which has a polarizability of α and is placed a distance r of the first molecule. The attraction results from the interaction between the dipoles p_1 and p_2 . Such a potential has a r^{-3} dependence. This together with the r^{-3} dependence of p_2 creates a total r^{-6} dependence of the potential.

In the case of bonding to a (metal) surface the situation is different. The van der Waals forces are acting between the charges outside the surface and their images inside. This leads to a r^{-3} dependence of the interaction. At short distances to the surface, the electron cloud of the adsorbate overlaps with that of the substrate. The electrons have to raise their kinetic energy to orthogonalize. This leads to a steep increase of the interaction potential at short distances. A typical total potential is shown in Fig. 5.2. Its minimum is very shallow (a few meV) and rather far away from the surface (more than 3 Å). This type of bonding is called physisorption.

We can immediately draw some conclusions about this type of bonding. First of all, all atoms or molecules will be able to physisorb on a surface. For reactive species, however, the physisorption may only be a precursor state before establishing a real chemical bond. Noble gases, on the other hand,

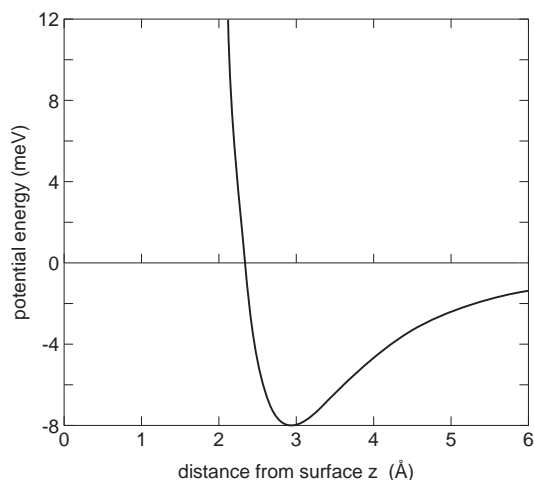


Figure 5.2: A physisorption potential for He on Au. After Ref. [19].

will only physisorb on a surface. Looking at the depth of the well we can conclude that the temperature has to be very low if we want to observe a stable physisorbed state (at room temperature $kT \approx 25\text{meV}$) and one would not be able to observe physisorption. Furthermore, the large distance of the adsorbate to the surface renders the adsorbates highly mobile.

5.3 Chemisorption

Far more interesting than physisorption, at least from a practical point of view, is the case where we have a real chemical bond between the surface and an atom or a molecule. The scenario is similar to chemical bonding between atoms and the whole complex of surface and adsorbate may be viewed as one giant molecule. For chemisorption on simple metals, the molecular orbitals of the adsorbate interact with the whole Fermi sea whereas in the cases of semiconductors and insulators the interaction is typically limited to the surface atoms in the immediate vicinity of the adsorbate. Transition metals are a case which lies somewhat in between: on one side one has the interaction with the delocalized sp electrons, on the other hand the rather localized d electrons.

The energy scale for chemisorption is much higher than for physisorption. Here we deal with bonding energies of several electron volts. In fact, the energy for the individual bonds can be so high that it is favourable to crack the intramolecular bond of the adsorbate molecule and to adsorb the two

resulting fragments. This is called dissociative adsorption in contrast to the so-called associative adsorption. O_2 is a molecule which frequently dissociates upon adsorption. Dissociative adsorption is a key-step in heterogeneous catalysis and therefore the understanding of the chemisorption process is of great interest.

We will now discuss the chemisorption process in terms of a very simple model dealing with the adsorption on metal surfaces. Those interested in more sophisticated models are referred to the course in theoretical surface science. In the so-called Newns-Anderson model, one establishes a connection between the adsorbate and the Fermi sea in the substrate by introducing a matrix element $\langle a|H|\vec{k}\rangle$ between the states of the adsorbate $|a\rangle$ and those of the metal $|\vec{k}\rangle$. One then looks at the density of states (DOS) at the adsorbate. When the adsorbate is brought close to the surface the initial delta function-like DOS is broadened into a Lorentzian line and shifted from its value in the free molecule (see Fig. 5.3). The shift is a direct consequence of the coupling matrix elements which change the eigenvalues of the substrate/adsorbate system. The broadening is due to the reduced lifetime in the molecular states because now the electrons can hop into the substrate as well.

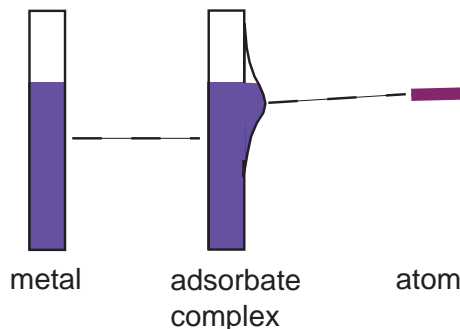


Figure 5.3: Schematic energy level diagram for an adsorbate / substrate system in case of a simple metal.

A more complicated situation arises when we consider the adsorption on a transition metal surface. Then we have a flat d -band with a high DOS in addition to the sp band above. Let's focus on the d -band first. We assume that these states are so localized that we can adopt the familiar concept of chemical bonding. The metal d states interact with the adsorbate to form a bonding and an antibonding molecular orbital like shown in Fig. 5.4. Interaction with the sp band then leads to an additional shift and broadening of these levels.

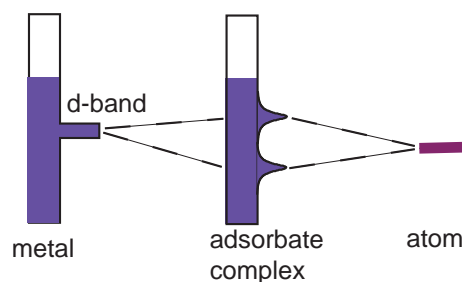


Figure 5.4: Schematic energy level diagram for an adsorbate / substrate system in case of a transition metal.

These figures make it plausible that chemisorption exists and we can explain what happens on transition metal surface in a rather coarse qualitative way. Unfortunately, there is no quantitative predictive power whatsoever in the model. More recently, rather sophisticated theoretical tools have been build, based on Density Functional Theory and the local density approximation . These tools do still not have real predictive power but in combination with experimental data one can learn a lot about the physics and chemistry of adsorption. In the following we will look at the results of such calculations.

A classical example is the adsorption of Li, Si and Cl on a jellium surface with the charge density of Aluminium (Lang and Williams [20]). Fig. 5.5 shows the change in state density due to adsorption of the three atoms on the surface. It was obtained using Density Functional Theory within the Local Density Approximation. The Li $2s$ level has been emptied and lies above the Fermi level. The Cl $3p$ level has been filled upon adsorption. For these two cases we have an almost ionic bond, as we could have expected. Si represents a state in between: we observe two peaks. The one with the higher binding energy corresponds to Si $3s$ which is of course fully occupied. The other peak, corresponding to Si $3p$ just straddles the Fermi level. Here we have a case of covalent bonding.

This view of the bonding is confirmed when looking at the charge density plots for these three adsorbate systems in Fig. 5.6. The difference plot on the lower panel is particularly instructive: it shows that the charge is drawn away from the Li and pushed into the direction of the Cl. In the case of Si charge is found on both sides of the adsorbate, slightly more in the direction of the surface. This situation corresponds to the bonding $3p$ orbitals.

A more complicated and important example is the adsorption of CO on transition metal surfaces. The jellium model is inadequate to describe such bonding because of the directional character of the d . Fig. 5.7 shows

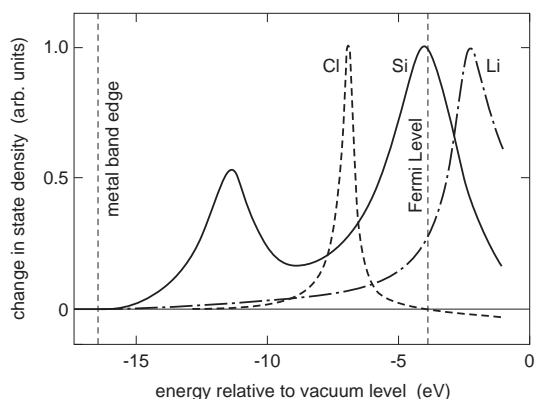


Figure 5.5: Change in state density due to adsorption of Li, Si and Cl on jellium. After Ref. [20].

the energy diagram for the molecular orbitals of CO. The highest occupied molecular orbital is the 5σ orbital which is located on the carbon end of the molecule. The lowest unoccupied molecular orbital is the antibonding 2π orbital. The bonding to the surface is achieved by donating 5σ electrons to the metal. This explains why CO is always adsorbed carbon end down on the surface. At the same time, there is a “back-donation” of electrons into the 2π orbital of the CO molecule.

Fig. 5.8 shows the results for a calculation of CO adsorbed on a Ni surface. The calculation goes beyond jellium and incorporates the “real” Ni surface geometry. This gives significantly more insight into the bonding process. Part (c) of Fig. 5.8 clearly shows that the bonding to the Ni is achieved by the donating 5σ electrons to the substrate, i.e. by an interaction between the 5σ electrons and the d electrons of the substrate. It can also be seen that the 2π orbital gets more occupied, establishing a bonding between CO and the substrate and at the same time weakening the internal CO bond.

A picture like Fig. 5.8 makes it at least plausible, how chemisorption on a transition metal surface can lead to the dissociation of molecules as required for catalysis. Upon adsorption, the intra-molecular bond can be weakened to such a degree that the molecule simply falls apart (although CO is not a good candidate for this to happen). This process can be made more efficient by modifying the electronic structure of the catalyst, e.g. by co-adsorbing alkali atoms.

A good qualitative picture of the dissociation process was given by Lennard-Jones (1932). Consider the potential energy of a molecule as a function of

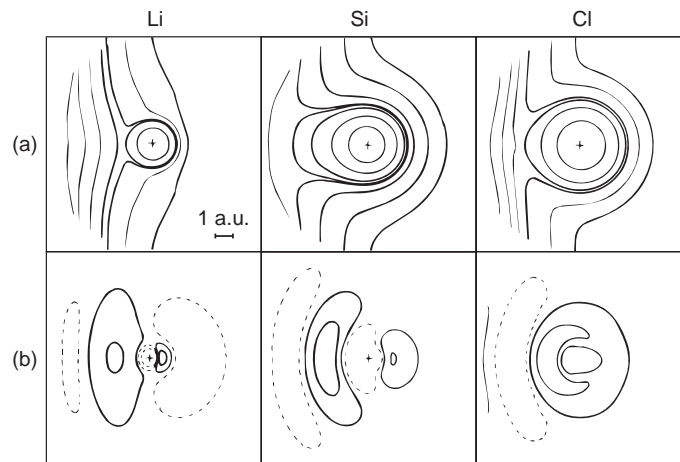


Figure 5.6: Electron density contours for Li, Si and Cl on jellium. The upper panel displays the total charge density. The lower panel the total charge density minus the superposition of the individual charge densities. Solid lines correspond to a charge accumulation, dashed lines to a charge depletion. After Ref. [20].

distance from the surface and compare it to sum of the potentials of its constituents (Fig. 5.9). Far away from the surface, the energy for the molecule will be lower and the separation of the two curves is the dissociation energy of the free molecule. As one moves closer to the surface, the curves will at least show a physisorption minimum and maybe even a chemisorption minimum. Fig. 5.9 illustrates different possible scenarios. Some are: (a) the potential energy for the molecule stays always lower than that of the constituents and a physisorption plus chemisorption minimum develops. In this case we will have molecular chemisorption. (b) the two potential energy curves cross and yield an absolute minimum for the dissociative chemisorbed state which, however, can only be reached if a large activation energy maximum is overcome from a molecular physisorbed state. In this case we will find molecular physisorption. (c) the dissociated state has the lowest energy and can be reached directly without a high activation barrier. In this case we will have a dissociative chemisorption. This model lacks of course any predictive power. Actually, it is first now, 70 years after Lennard-Jones, that one can calculate such potential energy surface rather accurately and “simulate” the dissociation of simple molecules (i.e. H_2). Such curves are of course multi-dimensional because one has to track the motion of every atom in the molecule and, in principle, also of the substrate atoms close to the molecule.

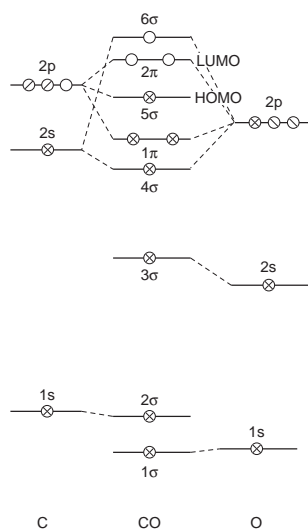


Figure 5.7: Energy-level diagram for the molecular orbitals in CO.

5.4 Interaction between adsorbates

At this point we want to discuss the interaction between adsorbed atoms or molecules but without going into any detail. Such interactions are ultimately what can be used to, for example, promote the catalytic properties of a surface but they manifest themselves already on a much more basic level. One finds, that many adsorbates on surfaces form ordered layers, the symmetry and spacing of which are dictated by the adsorbate-adsorbate interaction. We can think of several mechanisms for this interaction

- The van der Waals interaction between adsorbates is always present but only important for physisorbed layers, unpolarized and inert layers. Because of its small magnitude it immediately turns unimportant if any of the other interactions are present.
- Forces between the permanent dipolar moments of the adsorbates.
- Direct orbital overlap.
- Interactions mediated by the properties of the substrate (electronic / elastic)

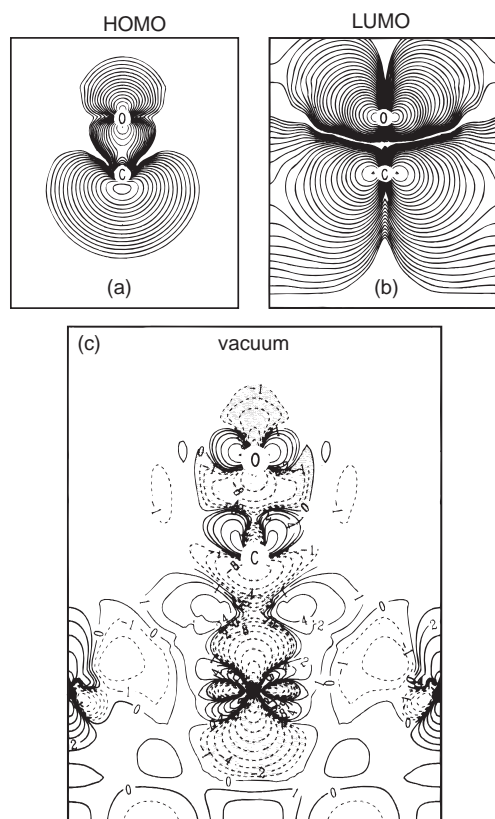


Figure 5.8: Charge density contour plots for a layer of CO adsorbed on a Ni surface. (a) and (b) show the 5σ and 2π orbitals of the free molecule, respectively. (c) shows the difference in charge density between the actual adsorption system and the unsupported monolayer. Solid lines correspond to a charge density increase and dashed lines to a depletion. After Ref. [21].

The second and third force will keep the adsorbates apart from each other in densely packed layers. The last force could be either attractive or repulsive

5.5 Kinetics

So far we have been focusing on the detailed physical mechanism of adsorption. Now we will adopt a different point of view. When dealing with adsorption kinetics one wants to study the influence of certain macroscopic external variables on processes like adsorption, desorption or, in general, reactions. A typical question is: how reactive is a certain surface towards the dissociative adsorption of N_2 ? When interpreting kinetic data, one has to

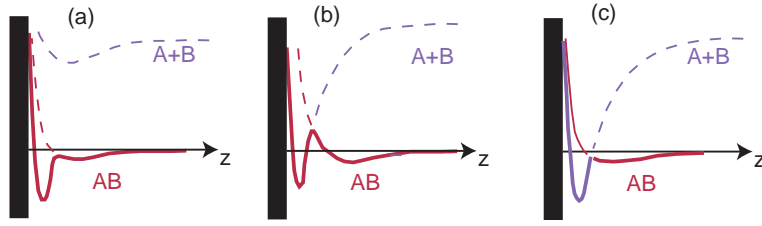


Figure 5.9: Schematic diagram of the potential energy of a molecule and its constituents as a function of distance from the surface. Different scenarios are possible (a) molecular chemisorption (b) molecular physisorption and (c) dissociative chemisorption. After Ref. [22].

make certain model assumption about the microscopic processes underlying the reactions. One can check the plausibility of such models by fitting their parameters to the experimental results. In case of a good fit, one can hope that the model parameters have some meaning.

5.5.1 Adsorption

The most simple model for adsorption one encounters is that of Langmuir (see Fig. 5.10). The molecules from the gas-phase are adsorbed on the surface when they hit an empty site. We define the relative surface coverage Θ as the ratio between occupied sites and available sites. We assume that we have N_0 available sites per unit area on the clean surface. All sites on the surface are equivalent and the adsorption energy is independent from the coverage of the surface, i.e. all the adsorbate-adsorbate interaction which we have discussed above are turned off.

We can calculate the adsorption rate for a surface assuming that the molecules only adsorb and do not desorb again. The rate of incoming molecules is given by the kinetic gas theory. For a unit area it is

$$\frac{dN}{dt} = \frac{P}{\sqrt{2\pi M k T}}. \quad (5.1)$$

where M is the mass of the incoming molecules. The adsorption rate is now given by the product of the incoming flux with a suitably defined sticking coefficient.

$$\frac{d\Theta}{dt} = \frac{1}{N_0} S \frac{dN}{dt} = S \frac{P}{\sqrt{2\pi M k T}}. \quad (5.2)$$

Let's assume for the sticking coefficient that

$$S = c(1 - \Theta)^n e^{-E_a/kT} = S_0(1 - \Theta)^n, \quad (5.3)$$

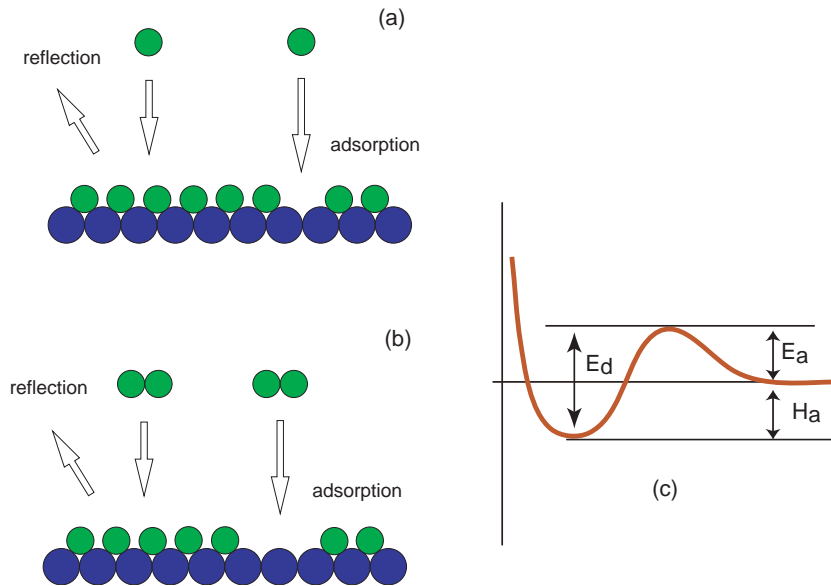


Figure 5.10: The Langmuir model for adsorption: (a) associative adsorption (first order process); (b) dissociative adsorption (second order process). (c) simple energy diagram with activation energies for adsorption and desorption (E_a and E_d) and the heat of adsorption H_a .

where S_0 is the sticking coefficient for the clean surface. This leads to

$$\frac{d\Theta}{dt} = \frac{p}{\sqrt{2\pi M k T}} c (1 - \Theta)^n e^{-E_a/kT}. \quad (5.4)$$

The factor c takes care of the fact that only a fraction of the incoming molecules actually adsorb, even if they find a site. They can also simply bounce back if they can not get rid of their kinetic energy or if they come in “turned the wrong way”. The factor $(1 - \Theta)^n$ takes the available sites into account where Θ is the relative coverage and n is the order of the process. The last factor takes care of a possible activation energy necessary to adsorb a molecule. Rewriting the expression using S_0 highlights the sticking coefficient for the clean surface.

Using this model one can already try to analyse a lot of simple experiments. Assume that we dose gas on a surface and measure the coverage as a function of dosage. From the slope of the curve we can work out the sticking coefficient as a function of coverage and compare it to our simple model. Fig. 5.11 shows that the results are often not too good.

The reason for this disagreement is that the adsorption potential is actually more complicated. Instead of one deep minimum for chemisorption

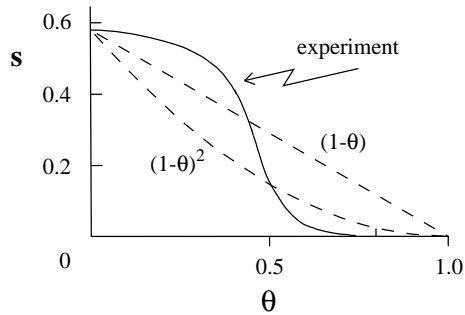


Figure 5.11: Sticking probability of N_2 on tungsten as a function of coverage. After Ref. [23].

there is also a shallow minimum for physisorption. This minimum can act as a precursor state such that the incoming molecule can “stay” at the surface and find an empty site even if it impinges on a filled site. A more elaborate model which takes this into account improves the agreement between experiment and theory.

5.5.2 Desorption

For the desorption of adsorbates we consider the Langmuir model again (Fig. 5.12). Desorption takes place if a molecule has enough energy to overcome an activation energy E_d for desorption. Alternatively, two atoms or molecules from neighbouring sites might desorb together, forming a new molecule.

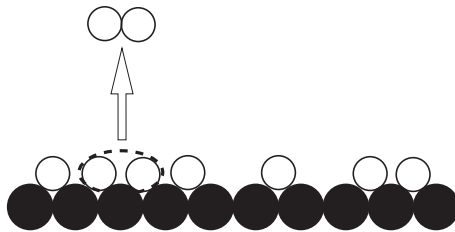


Figure 5.12: Desorption in the Langmuir model.

We write

$$-\frac{d\Theta}{dt} = \nu_n \Theta^n e^{-E_d/kT}. \quad (5.5)$$

Again, this equation contains a factor such that not all the molecules with sufficient energy desorb, a factor describing the probability of finding two

neighbouring sites which are occupied (for $n = 2$) and a factor for the activation energy.

Thermal desorption is directly used in a very common experimental technique called Thermal Desorption Spectroscopy (TDS). In TDS, one prepares an adsorbate layer with a certain coverage on a surface. Then one places this surface in front of a mass spectrometer and measures the partial pressure from a certain mass one is interested in while (linearly) increasing the temperature of the sample. Let's assume

$$T = T_0 + \beta t. \quad (5.6)$$

and

$$-\frac{d\Theta}{dt} \propto p_{\text{partial}} \quad (5.7)$$

The first condition can be realized by an electronically controlled ramping of the temperature. The second condition is only valid at very high pumping speed in the UHV vessel. The measured increase in partial pressure as a function of time can now be fitted with the model equation 5.5 to obtain the relevant parameters, in particular the desorption energy E_d . Much information can already be gained just by looking at desorption curves like in Fig. 5.13. The figure shows two sets of curves for first and second order desorption. Every set contains curves for different initial coverages. One finds that the maximum of the desorption curves is independent from the initial coverage for a first order process but not for a second order process.

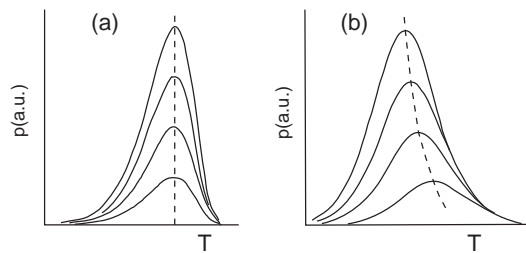


Figure 5.13: Thermal desorption curves for a linear heating rate: (a) a first order process ($n = 1$) and (b) a second order process $n = 2$.

Thermal desorption spectra can contain a lot of information and can be quite complicated. Fig 5.14 shows a thermal desorption spectrum of H_2 from a tungsten surface. An obvious implication of such a curve is that there are at least four different binding configurations of hydrogen on the surface.

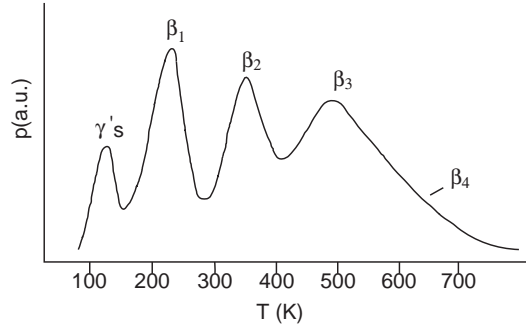


Figure 5.14: Thermal desorption spectrum for H_2 from a tungsten surface. After Ref. [24].

5.5.3 Adsorption-desorption equilibrium

Again we use Langmuir's model to study the equilibrium between adsorption and desorption. We set (5.4) equal to (5.5) and obtain

$$\frac{P}{\sqrt{2\pi mkT}} c(1 - \Theta)^n e^{-E_a/kT} = \nu_n \Theta^n e^{-E_d/kT}. \quad (5.8)$$

or

$$P = \nu_n \left(\frac{\Theta}{1 - \Theta} \right)^n \frac{\sqrt{2\pi mkT}}{c} e^{-H_a/kT}. \quad (5.9)$$

where H_a is the heat of adsorption, i.e. $H_a = E_d - E_a$ (see Fig. 5.10).

It is actually possible to obtain values for H_a using the Clausius-Clapeyron equation on isostere data, i.e. data where one measures the pressure to keep a certain surface coverage as a function of temperature.

$$H_a = -R \left(\frac{\partial \ln(P)}{\partial (1/T)} \right) \Big|_{\Theta} \quad (5.10)$$

where R is the gas constant. The data for the Clausius-Clapeyron analysis can either be taken from a real isostere measurement or the isostere points can be figured out from measured isotherms. One thing one has to keep in mind, though, is that the major trouble with the equilibrium approaches is that they can not be used to study irreversible processes!

5.6 Single-crystal adsorption calorimetry

To conclude our discussion about adsorption we want to discuss a very recent and sophisticated experiment which directly measures the heat of adsorption

[25]. The principle of the experiment is shown in Fig. 5.15. A pulsed molecular beam is directed at a very thin single crystal (about 2000 Å thick). A proportion of these molecules adsorb at the surface and cause the liberation of adsorption heat within the surface region. The small heat capacity of the crystal leads to a measurable rise in temperature (the adsorption of 1 percent of a monolayer typically leads to a temperature rise of 0.1 K). The heat is conducted very efficiently to the back of the crystal and very in-efficiently to the sides. This means that the cooling of the crystal occurs mostly by the emission of thermal radiation. For this reason the back-side of the crystal is made black with a carbon film such that it will emit most of the radiation which is then measured with an infrared detector. The detector measures a short infrared pulse and the crystal is cooled down again before the next pulse of molecules arrives.

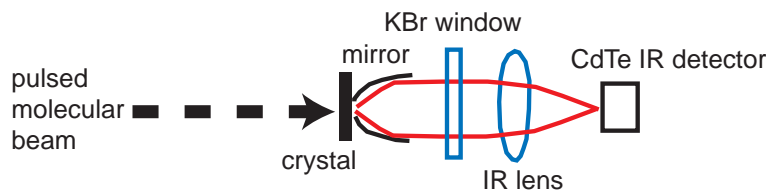


Figure 5.15: A single-crystal adsorption calorimeter.

In this way the heat of adsorption can be measured reliably and directly even for systems where the adsorption is an irreversible process.

5.7 Chemical reactions and catalysis

To my great shame, I have to admit that the intention of this brief section about chemical reactions is more to avoid a bad conscience for not mentioning them at all rather than for the reader to learn a lot! Anyway, you might get the flavour.

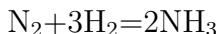
One of the major technical motivations for doing research on surfaces has always been the understanding of heterogeneous catalysis. So let's discuss a little what this actually is. In heterogeneous catalysis the presence of a solid (the catalyst) speeds up chemical reactions which are slow or impossible in the gas phase. Why?

One obvious advantage of the catalyst's surface is that adsorbed molecules are much more likely to meet each other than in the gas phase. It is the pure presence of a surface which enhances the reaction speed. Therefore an

industrial catalyst is always build such as to have a high surface area. There is also another reason for this: if the really active catalyst is a precious metal then it is much wiser to distribute small metal particles on a cheap oxide or ceramic support than to have a small surface enclosing a big, expensive and useless chunk of bulk metal.

A more exotic variation of this theme is the following: in the interstellar medium (the pure presence) of dust particles is needed if one wants to form hydrogen molecules. The particles are needed to get the momentum / energy balance right when the molecule is formed.

Another purpose of the catalyst is to be chemically involved in the reaction. Take for example the ammonia synthesis (Haber-Bosch-process) .



The catalyst must have chemical properties such that both H_2 and N_2 chemisorb on the surface and get dissociated. Then they must react to form ammonia and this has to desorb again (Fig. 5.1). This is a complicated process involving not only the actual reaction but all the chemisorption (adsorption and desorption) processes mentioned above. It is easy to see that the whole thing will not work or will be very slow if there are problems with one single step in the reaction pathway.

Surface Science experiments can help to understand all steps in such a pathway and one can try to find concepts to improve the catalyst. On the other hand, the experiments are typically performed under ideal conditions, in UHV on a single-crystal surface, and one has to pay attention when applying the results to real catalysts which are often just small metal particles dispersed on some support, working under high pressure and high temperatures.

In the following we briefly discuss some central concepts in heterogeneous catalysis.

The first question one has to ask is how the reaction pathway actually looks like. A classical example is the oxidation of carbon monoxide. Two pathways have been suggested:

1. Langmuir-Hinshelwood:



2. Eley-Rideal:



Issues like this can be solved by molecular beam studies. One adsorbs oxygen and directs a CO beam on the surface. Then one measures the CO_2

desorption from the surface. The time difference between the CO hitting the surface and the CO₂ being desorbed directly points to the reaction pathway.

Other central concepts in the design of a catalyst are the activity and the selectivity. The activity describes the degree of acceleration for the desired chemical reaction. The selectivity describes how much the converter catalyses the desired reaction as opposed to other possible reactions which are unwanted. One can change all sort of parameters in a giant parameter space to influence both reactivity and selectivity.

Two other important concepts are promotion and poisoning of a catalyst. Let us give an example for promotion. We consider the CO dissociation. Such a reaction is often promoted by some small amount of alkali atoms into the catalyst. We can make plausible why this is so by looking at Fig. 5.8. The CO bond is already weakened upon adsorption on the surface. Co-adsorption with alkali atoms will modify the electronic structure of the substrate such that the bond will be weakened even more. Poisoning is simply the opposite effect. The catalyst “dies” sooner or later by adsorbing “poison” on its surface. The poison can have different effects. The trivial one is that it simply sticks to the surface without ever being desorbed again. In this way, it will sooner or later block the surface for the real, wanted reaction. But it could also have the opposite effect as shown above for the alkali atoms: it could in some way influence the electronic structure of the substrate such that a particular reaction becomes impossible. In the latter case only a very small amount of “poison” could do a big damage to the catalyst.

The last concept we want to mention here is that of active sites. The idea is the following: Suppose the reaction only takes place at some sort of defects on a metal surface. The defect could be such that the atoms at the defect have a smaller co-ordination than the other surface atoms and therefore a different chemical reactivity. Such a defect could be a step on a surface. In some way, the active site idea is the kiss to death for a surface science experiment where one deals (or tries to deal with) almost perfect surfaces. On the other hand, choosing different crystal faces of a material will give surface atoms with different co-ordination numbers and one might learn something about the influence of co-ordination. There are several ways out of the problem: one can prepare surfaces with a controlled number of steps such as to increase the active sites. One can use a local technique such as Scanning Tunnelling Microscopy 6.7 to look only at one active site and study it. Or one can try to “build” something which looks much more like an industrial catalyst but which is still a very-well characterized system. An example would be the controlled adsorption of size-sorted metal clusters on a well-prepared oxide surface and catalytic studies on such systems. This is, admittedly, very difficult but not impossible.

5.8 Further reading

A good discussion about adsorption and desorption phenomena can be found in [3]. For more information on actual surface chemistry see for example [26]. A good description of the theory can be found in [27].

Chapter 6

Surface Structure

The questions of surface structure can be roughly divided into the “large scale” and the “small scale” structure. The two are divided by an arbitrary and unclear borderline. Some interesting and more macroscopic phenomena still lack a detailed understanding on the microscopic level, for example catalysis or friction. Here we discuss the “large scale” structure only very briefly in connection with surface free energies and crystal shape. We also mention some very interesting phenomena such as the roughening transition and surface melting. This discussion is done in the framework of thermodynamics. All the rest of the chapter is concerned with the microscopic structure. We are interested in questions like: What is the structure of clean and adsorbate-covered surfaces? Why is the structure like this? How does one measure the structure?

6.1 Surface Thermodynamics and general crystal shape

We start this section off with the expression for the internal energy of a homogeneous thermodynamic system, having in mind the bulk crystal. This is given by the Euler equation

$$U = TS - PV + \mu N. \quad (6.1)$$

Now suppose that this crystal is cleaved and a surface area is created. Suppose further that this process is carried out reversibly at a constant temperature, system volume and chemical potential. The creation of the surface adds a term to the energy which must be proportional to the amount of surface area created and positive because otherwise bulk crystals would cleave

spontaneously. The energy is then

$$U = TS - PV + \mu N + \gamma A, \quad (6.2)$$

where the constant γ has the dimension of energy per surface area and is called the surface tension. It would be very desirable to measure the surface tension (or energy) of a solid/vacuum interface because it is the most fundamental quantity emerging from a modern total-energy calculation of the surface properties. The theory would greatly benefit from a comparison to reliable experimental numbers. Unfortunately, it is very difficult to measure the surface tension. Some hint about the magnitude of the quantity can be taken from measurements of the liquid gas interface but this is not sufficient to test the interesting details in the theory.

When we think about the microscopic origin of γ it is obvious that it will be different for the various possible surface planes of a crystal. As we shall see below, the number of bonds which have to be broken to generate a certain surface plane depends on the orientation of the plane. A surface with many steps might be particularly unfavourable because several of bonds have to be broken to create a low-coordination step atom. Therefore we write γ with a directional dependence $\gamma(\vec{n})$.

These considerations have important consequences on the macroscopic shape of crystals. While liquids are always found in the shape of smallest surface area (a sphere) this is not the case for solids. The solid crystal wants to have a shape where a large fraction of the surface area is given by crystal planes with a low γ . More formally, if we look for the minimum in the free energy (but at zero temperature) we have to require that

$$\int_A \gamma(\vec{n}) = \text{minimum}. \quad (6.3)$$

This requirement leads to quite complex equilibrium shapes of crystals. If $\gamma(\vec{n})$ is known, the problem can be solved graphically by the so-called Wulff construction shown in Fig. 6.1. The procedure for finding the equilibrium crystal shape at 0K is as follows: Draw $\gamma(\vec{n})$. Draw a plane perpendicular to the radius vector which intersects $\gamma(\vec{n})$ at each point. The inner envelope of all these planes is the equilibrium crystal shape.

It is interesting to consider this crystal shape if we want to prepare a surface by cleaving a crystal. The cleaving process will only work (if at all) for surfaces which also appear on the equilibrium crystal. If we attempt a cleavage in another direction, the result will be a surface with facets of low-energy planes.

At finite temperature the situation changes. Now excitations which do not cost much energy but increase the entropy of the system become important. Such excitations are steps and other defects. As the temperature is

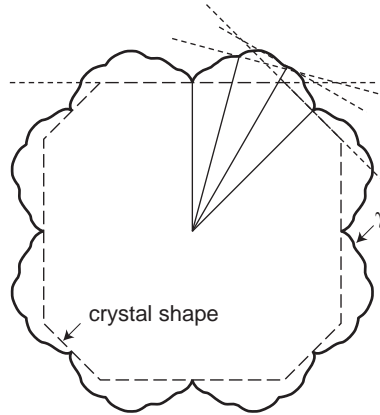


Figure 6.1: The Wulff construction for the determination of equilibrium crystal shape.

raised, the free energy for the steps decreases. The sharp edges of the Wulff-crystal disappear and the facets decrease. Eventually, the facets will vanish completely and the crystal will have a round shape. This behaviour can be described by a phase transition, the so-called roughening transition. It can also be observed on certain crystal surfaces, well below the actual melting temperature of the crystal.

Another process worth mentioning is the phenomenon of surface melting. This is the formation of a thin, liquid-like phase on the surface below the melting temperature of the bulk. The most important example of this phenomenon is the surface melting of ice which permits for example skating. The existence of surface melting can be made plausible by considering the Lindemann formula for bulk melting. It states that

$$T_m \propto \Theta_D^2 \quad (6.4)$$

where T_m is the melting temperature and Θ_D is the Debye temperature. The latter is often found to be much smaller at the surface. A rule of thumb is that the surface Debye temperature is about a factor of $\sqrt{2}$ smaller than its bulk counterpart. This simply means that the surface atoms vibrate more strongly than the bulk atoms at a given temperature and this eventually leads to melting. But one has to keep in mind that this point of view is much too simple. Note that also the completely counter-intuitive phenomenon of surface overheating is found in which the bulk melts at a lower temperature than the surface.

6.2 Surface geometry: truncated bulk, relaxation, reconstruction, defects and superstructures

6.2.1 General phenomena

The simplest picture of a microscopic surface structure is that of the truncated bulk (the so-called ideal surface). Suppose the crystal is cleaved along a plane specified by its Miller indices (hkl) . In the truncated bulk model, all the atoms on the cleaved crystal's surface stay exactly where they have been in the bulk crystal. This means that one can immediately draw the surface geometry of the crystal. Fig. 6.2 shows the surface geometry for the fcc(111) surface.

When looking at a surface, we think of the bulk as being made of planes parallel to the surface plane. We define a unit cell in the first plane and, if required, a basis. We define furthermore a vector \vec{r} connecting the atoms in successive planes. A “plane” does of course not necessarily mean that all the atoms have the same z value (z being the distance perpendicular to the surface). We can extend the unit cell over several layers if we want to. In Fig. 6.2, however, we have chosen a primitive unit cell and all the atoms in one layer are at the same height. We call the z component of \vec{r} the distance between the planes. In the side view of the surface in Fig. 6.2 we can see the familiar ABCABC... stacking sequence of the fcc lattice.

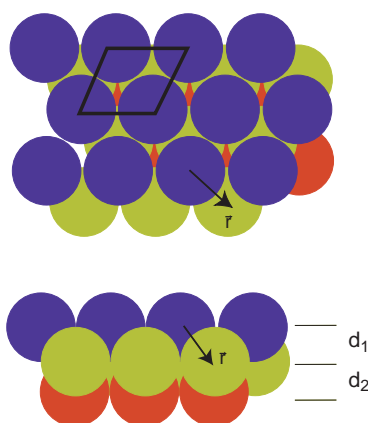


Figure 6.2: The (111) surface of an fcc crystal.

In Fig. 6.3 the truncated bulk surfaces of a few important cases are shown.

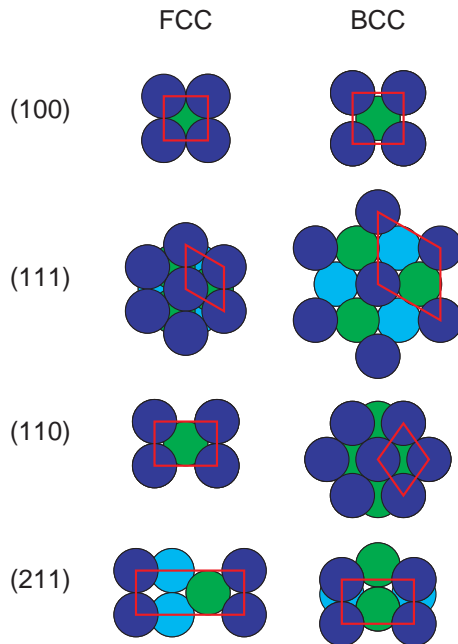


Figure 6.3: A few important truncated bulk surface structures.

The most severe problem with the truncated bulk model is that it completely neglects the dramatic change in the coordination and potential due to the abrupt termination of the crystal in the direction normal to the surface. This change will for almost all surfaces lead to a phenomenon called *relaxation* (see Fig. 6.4). A relaxation is a change in the distances between the first few layers with respect to the bulk values. For most surfaces the distance d_1 is smaller than the corresponding bulk value. This can be made plausible by the model of Finnis and Heine shown in Fig. 6.5 [28]. In the bulk (of a metal) the ion cores are screened by the conduction electrons around them. If we divide up the crystal in Wigner-Seitz cells, it is easy to see what happens in the surface case: the original distribution of electrons in the Wigner-Seitz cells would lead to a highly corrugated electron distribution at the surface. This is, however, very unfavourable because of the high kinetic energy of “bent” wave functions. The electrons at the surface will re-distribute themselves leading to a smooth charge density at the surface. This creates an asymmetric screening of the ion cores in the first layer and a net electrostatic force which pushes them “into” the crystal and thus reduces d_1 . The charge smoothing at the surface is called the Smoluchowski effect .

A more severe change of structure is the phenomenon of surface *reconstruction* (see Fig. 6.4). In a reconstruction the periodicity parallel to the

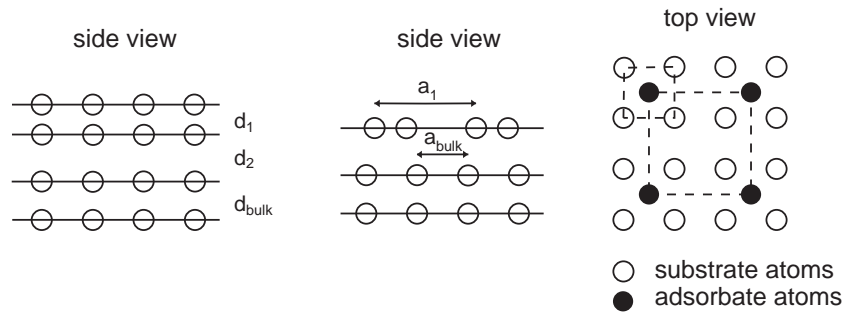


Figure 6.4: Relaxation (left) and reconstruction (middle) and adsorbate superstructures (right) on surfaces.

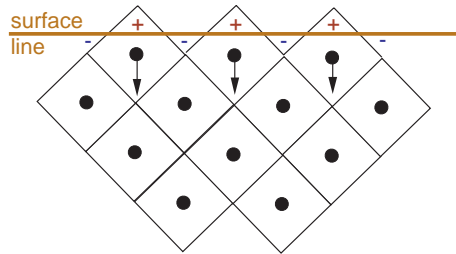


Figure 6.5: The Finnis Heine model for inward relaxations on metal surfaces [28].

surface is changed with respect to that of the bulk. Surface reconstructions are the rule in the case of semiconductors. There the bonds are highly directional. Cleaving the crystal leaves the structure in a unfavourable elastic state and also gives rise to half-occupied “dangling” bonds. Reconstructions give a considerable gain in energy and reduce the number of dangling bonds. The resulting structures can be rather complicated. Most metals surfaces do not reconstruct but some do. In most cases, this happens for metals where localized d or f electrons take part in the bonding for reasons similar as on the semiconductor surfaces. But there are also a few simple metal surfaces which reconstruct.

Another phenomenon, somewhat similar to reconstruction, happens when atoms or molecules are adsorbed on a surface. The adsorbates often form ordered structures (due to their mutual interaction) which have unit cells larger than the substrate unit cell (see Fig. 6.4). In most cases, however, there is still a simple ratio between the substrate and adsorbate unit cell (due to the adsorbate - substrate interaction). Adsorbates will in general change

the structure of the underlying substrate. In particular, they can induce a lift of the reconstruction of the clean surface.

Apart from these simple phenomena there are many things which can make life much more complicated: adsorbate structures have domains and domain boundaries, the surface may have many imperfections such as steps and terraces, the atoms and molecules which are adsorbed on the surface do not show any long-range order and so on.

6.2.2 Lattice and reciprocal lattice

The concepts for lattice and reciprocal lattice on surfaces are very similar to what we know from the bulk. In any case, it is worth repeating them!

The 14 possible Bravais lattices of the bulk are reduced to 5 two-dimensional surface Bravais lattices which are shown in Fig. 6.6.

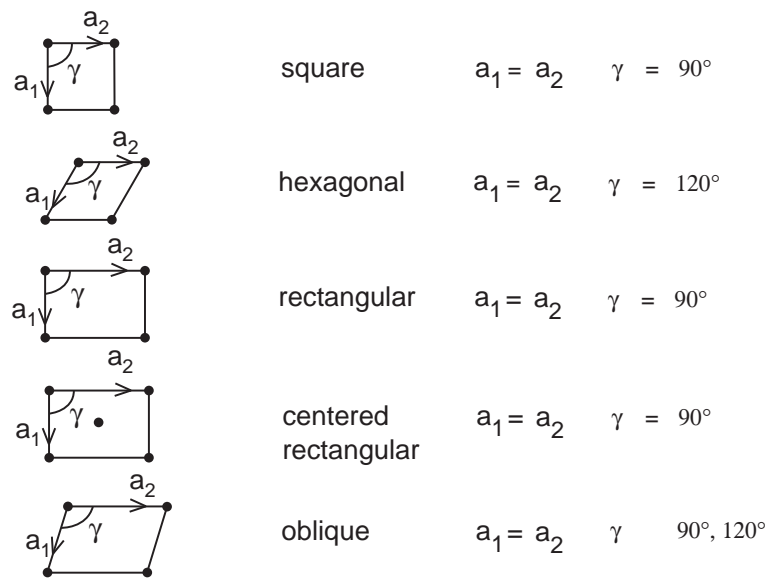


Figure 6.6: The 5 possible two-dimensional Bravais lattices.

The two-dimensional lattice is then the combination of one of the Bravais lattices and a basis. It is important to notice that since a surface is not two-dimensional, the basis atoms need not be in one plane. Once the basis is assigned one can find out the two-dimensional point group of the lattice. The point group will be some sub-group of the highest possible symmetry compatible with the Bravais lattice under consideration. The final symmetry of the system, the space group, is then formed by a combination of the

translation group (i.e. the Bravais lattice) and the point group. Like in the three dimensional case this combination can lead to entirely new symmetry elements which are glide-lines in the two-dimensional case. In total, there are 17 possible two-dimensional space groups.

The phenomena of reconstruction and ordered overlayers make it necessary to have a nomenclature which describes the periodicity and symmetry of the surface with respect to that of the bulk. Suppose the two-dimensional lattice vectors of the bulk are \vec{a}_1 and \vec{a}_2 . By “two-dimensional lattice vectors of the bulk” we mean the lattice vectors for the bulk-truncated crystal or, equivalently, the vectors which represent the lattice of the bulk projected onto the surface. Let the lattice vectors of the surface including possible adsorbate overlayers be \vec{b}_1 and \vec{b}_2 . A simple nomenclature of surface structures is that of Woods . The surface structure is described by

$$N \left(\frac{b_1}{a_1} \times \frac{b_2}{a_2} \right) R\Theta \quad (6.5)$$

where $N =$ ”p” or “c” for primitive or centred cells, respectively, and Θ is the angle by which the surface vectors have to be rotated with respect to those of the bulk (see Fig 6.7). The nomenclature of Woods has the advantage of simplicity. It is, however, not possible to describe all surface structures because the rotation angle might not be the same for both vectors.

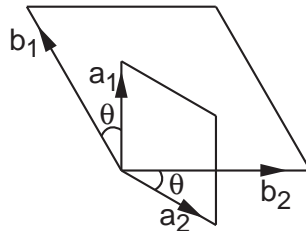


Figure 6.7: The Woods terminology for surface lattices.

Some examples for the application of the Woods nomenclature are given in Fig. 6.8. Note that despite of its lack of generality the Woods nomenclature is still useful because many structures can be described by it.

A more general description of the surface structure is the so-called matrix notation . One writes

$$\vec{b}_1 = m_{11}\vec{a}_1 + m_{12}\vec{a}_2, \quad (6.6)$$

$$\vec{b}_2 = m_{21}\vec{a}_1 + m_{22}\vec{a}_2. \quad (6.7)$$

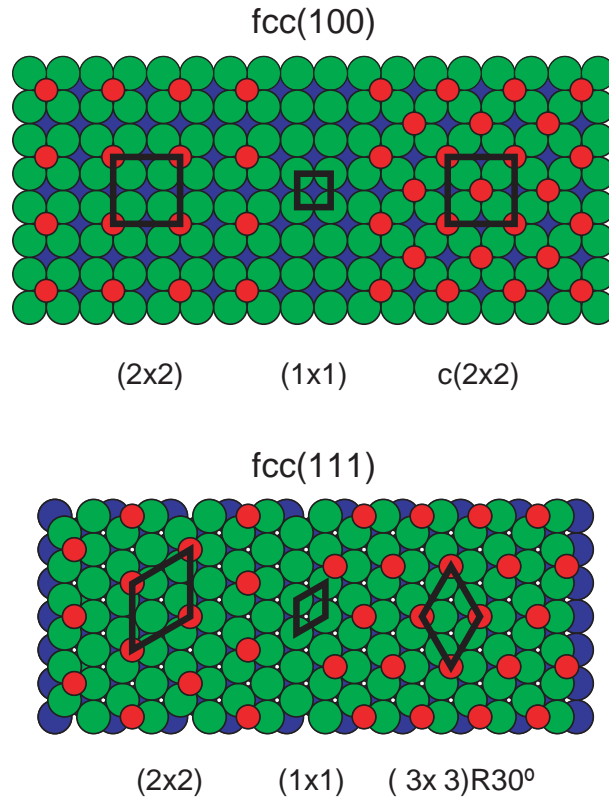


Figure 6.8: Examples for structures described by the Woods terminology.

or, in other words

$$\begin{pmatrix} \vec{b}_1 \\ \vec{b}_2 \end{pmatrix} = \begin{pmatrix} m_{11} & m_{12} \\ m_{21} & m_{22} \end{pmatrix} \begin{pmatrix} \vec{a}_1 \\ \vec{a}_2 \end{pmatrix}. \quad (6.8)$$

The inspection of the matrix directly allows the classification of the over-layer structures into three types which are illustrated in Fig. 6.9:

1. All the matrix elements are integer: the adsorbate and substrate lattices are called simply related and the lattice of the whole surface (adsorbate and substrate) has the same translational symmetry as the adsorbate lattice.
2. Some matrix elements are rational: the adsorbate and substrate lattices are called rationally related . The lattice of the whole surface (adsorbate and substrate) has a translational symmetry which is given by the distance it takes before adsorbate lattice and substrate lattice come into coincidence again.

3. Some matrix elements are irrational. In this case the adsorbate lattice is incommensurate with the substrate and no true lattice for the whole surface (adsorbate plus substrate) exists.

It is obvious that the relative strength of the substrate-adsorbate and adsorbate-adsorbate interactions will favour one type of structure over the others.

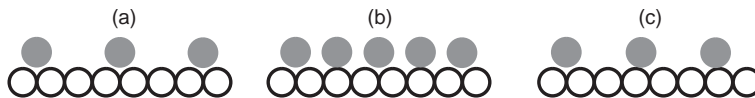


Figure 6.9: Three types of overlayers: (a) simply related to the substrate, (b) rationally related and (c) a incommensurate structure with no common periodicity between substrate and adsorbate lattice.

The reciprocal lattice of the surface is defined in the same way as that of the three-dimensional crystal:

$$\vec{g}_1 = \frac{2\pi(\vec{a}_2 \times \vec{n})}{|\vec{a}_1 \times \vec{a}_2|}, \vec{g}_2 = \frac{2\pi(\vec{n} \times \vec{a}_1)}{|\vec{a}_1 \times \vec{a}_2|}, \quad (6.9)$$

This means that

$$\vec{a}_i \vec{g}_j = 2\pi \delta_{ij}. \quad (6.10)$$

and

$$|\vec{g}_i| = \frac{2\pi}{a_i \sin \angle(\vec{a}_i, \vec{a}_j)}, \quad i, j = 1, 2. \quad (6.11)$$

The two last equations also give a simple recipe to construct the reciprocal lattice.

6.3 Low energy electron diffraction (LEED), LEED patterns and quantitative structure determination

Low-energy electrons are for surface structure what x-rays are for the bulk. We already know the two reasons for this: (1) the mean free path for low energy electrons in solids is short and therefore any technique based on such electrons is rather surface sensitive and (2) the electron de Broglie wavelength $\lambda = h/p$ fits very well with the typical distances in crystals and thus diffraction phenomena are to be expected. The discovery of the fact that the electron has indeed a wave nature was a milestone in the development of

modern physics: The first LEED experiment from Ni single-crystals by Davisson and Germer was published in 1927. However, the quantitative structure determination with electrons instead of x-rays also leads to some difficult problems: the electrons interact with the solid much more strongly than x-rays. This results in a refraction of the electron wave at the crystal-vacuum boundary and, even worse, it leads to a high degree of multiple scattering .

As we shall see below there are two major applications for LEED. The first one is to learn something from the pure inspection of the surface diffraction pattern. One short LEED experiment gives immediate and direct information about the surface order and quality. When the surface is reconstructed or covered with adsorbates, the LEED images can quickly give some information about the surface symmetry and periodicities. The second application of LEED is the quantitative structure determination. This is much more difficult. One has to measure the diffraction intensities as a function of the incidence electron energy and compare them to sophisticated multiple-scattering calculations for a model system. This model system has to be changed until good agreement between calculations and experimental intensities is achieved. Despite of this complicated procedure, LEED is the most important tool for quantitative surface structure determination.

6.3.1 Instrumentation

Fig. 6.10 shows a typical LEED apparatus which can be found in almost every surface science vacuum chamber. The LEED system has two major components: (1) an electron gun producing monochromatic electrons and (2) a detector system which detects only the elastically scattered electrons.

We know already how the electron gun works. The detector consists of four metal grids at different voltages and a fluorescent screen. The first grid (counted from the sample) is on ground potential to ensure a field free region around the sample. The next two grids are set to the so-called retarding voltage. This voltage is slightly lower than the kinetic energy of the electrons produced by the gun. It repels almost all the inelastically scattered electrons. The elastically scattered electrons pass the next grid which is set to ground voltage again and are then accelerated towards the fluorescent screen which is set to a high positive voltage. Behind the screen there is a window in the vacuum system so that the LEED pattern can be observed directly or recorded with a video camera.

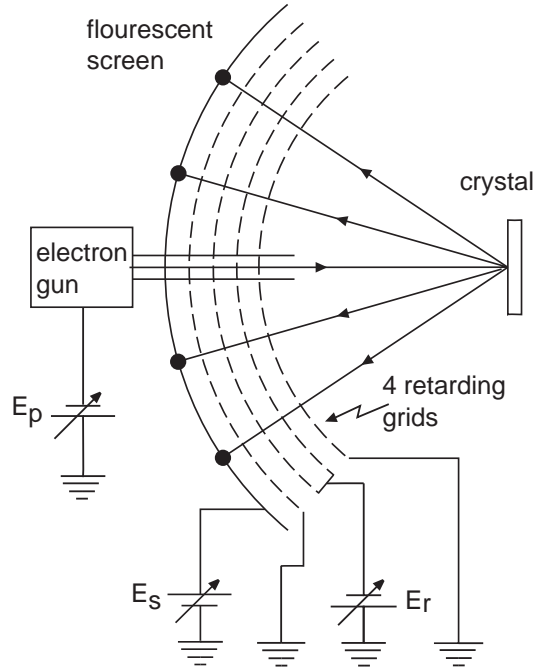


Figure 6.10: A LEED system.

6.3.2 Diffraction pattern and their analysis

Diffraction from a two-dimensional lattice

The discussion of diffraction from a two-dimensional lattice is very similar to that of a three dimensional crystal. We will therefore only give a very short overview. The diffraction conditions for a two dimensional lattice are given by the two Laue conditions

$$(\vec{k}_i - \vec{k}_f)\vec{a}_1 = 2\pi h, \quad (\vec{k}_i - \vec{k}_f)\vec{a}_2 = 2\pi k \quad (6.12)$$

where h and k are arbitrary integers. We know of course that this condition is fulfilled by any vector of the reciprocal lattice. This gives us the diffraction condition associated with the momentum transfer *parallel* to the surface

$$\Delta\vec{k}_{\parallel} = h\vec{g}_1 + k\vec{g}_2 \quad (6.13)$$

The vertical momentum transfer did so far not enter the discussion at all. This makes sense since for a two-dimensional lattice k_{\perp} is not a good quantum number and does not have to be conserved. This is also true for the semi-infinite solid when electrons cross the vacuum-solid interface. However, the

energy conservation imposes a restriction on k_{\perp} because we have to require that

$$|\vec{k}_f| = |\vec{k}_i|. \quad (6.14)$$

These two conditions can be made visible by changing the Ewald construction known from x-ray scattering to the surface case as shown in Fig. 6.11. Instead of a three dimensional reciprocal lattice we have our two dimensional lattice. In the third dimension the real-space periodicity is infinite which means that in reciprocal space the lattice points have to be infinitely close to each other. This leads to reciprocal lattice rods instead of points. We know draw a \vec{k}_i -vector which ends at the origin of the reciprocal lattice and has the right length and direction corresponding to our experimental setup. Then we draw a circle of radius $|\vec{k}_i|$ around the starting point of the vector. The intersection of this circle and the lattice rods gives the possible final \vec{k}_f vectors for which we will observe scattering maxima. It is evident that we will see many more spots in the two-dimensional case than in the three dimensional case because the circle does not have to hit points in k-space, it just has to intersect with the rods.

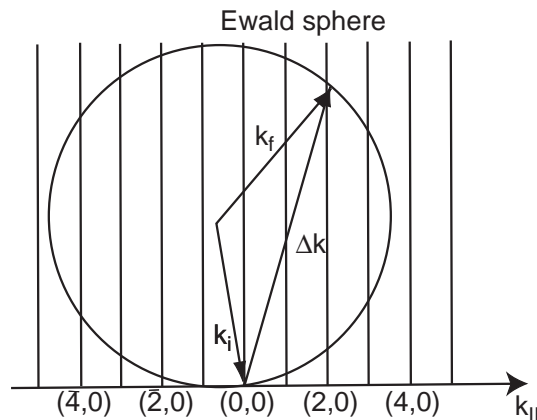


Figure 6.11: The Ewald construction for the surface case.

Diffraction from a surface

We now apply the concepts from the last section to the real LEED experiment. In most cases, the sample in the LEED setup shown in Fig. 6.10 is adjusted such that the electron beam hits the surface at normal incidence, i.e. such that \vec{k}_{\parallel} is 0 for the incident electrons. This greatly simplifies the

analysis of the resulting diffraction patterns because (1) the resulting diffraction maxima can be directly associated with the reciprocal lattice and (2) the diffraction pattern represents the symmetry of the surface. In fact, for such a system the diffraction pattern will be an image of the surface reciprocal lattice. According to equ. 6.13 we will find high intensities at $\vec{k}_{\parallel} = h\vec{g}_1 + k\vec{g}_2$. At the same time we know the magnitude $|\vec{k}|$ of the outgoing electrons and this gives us the emission angle $\sin \Theta_{hk} = |\vec{k}_{\parallel}|/|\vec{k}|$. Now we consider the imaging by the LEED apparatus (Fig. 6.12). The position of the intensity maxima on the window is given by

$$d_{hk} = R \sin \Theta_{hk} = \frac{R}{|\vec{k}|} (h\vec{g}_1 + k\vec{g}_2) = R \sqrt{\frac{\hbar^2}{2m}} \frac{1}{E^{1/2}} (h\vec{g}_1 + k\vec{g}_2). \quad (6.15)$$

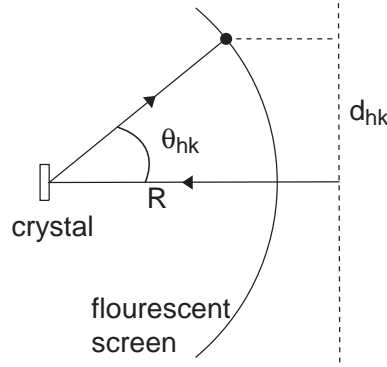


Figure 6.12: Linear imaging of the reciprocal lattice by LEED.

From equ. 6.15 it is also obvious what happens when one changes the primary energy E of the electrons. When increasing the energy we will still see the same spots but they will move closer to the centre of the window. New spots will move in on the sides of the screen which have not been visible before. It is obvious that for every reciprocal lattice point (except the origin) there is a smallest energy of the primary electrons which is required to see its image on the screen. The effect is illustrated in Fig. 6.13 which shows two LEED images taken at different energies E for the W(100) surface. The surface unit cell of W(100) is a square and hence the reciprocal lattice is also a square.

On the right-hand side of Fig. 6.13 we also give the indexing of the first LEED spots. This nomenclature refers to the reciprocal net of the bulk-terminated surface. This means for example that if a reconstruction or an overlayer with double periodicity is present, then we will have $(1/2,0)$ spots

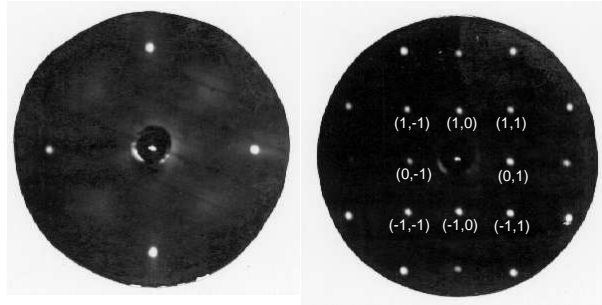


Figure 6.13: LEED patterns of W(100) taken at a electron kinetic energy of 45 eV (left) and 145 eV (right), respectively.

and so on. The $(0,0)$ spot is invisible in a normal normal-incidence LEED image because of the electron gun which is in the way.

When considering the diffraction from the surface instead of a perfect two-dimensional lattice we have to take into account the three-dimensional nature of the solid. Our picture of the Ewald-sphere with rods giving the same intensity in every LEED spot and at every kinetic energy is not quite correct because the electrons penetrate into the solid and “feel” the third Laue condition as well. This leads to very strong intensity variations in the LEED spots as a function of energy. Fig. 6.14 shows the intensity of the $(0,0)$ spot from Ni(100) as a function of electron kinetic energy. Measurements like this are called an I-V curves (intensity vs. accelerating voltage of the electrons). A substantial intensity variation is visible and some of the highest maxima lie close to the energies which are calculated by application of the third Laue condition (indicated as arrows on the figure). The first thing one notes is that the observed intensity maxima are at a lower kinetic energy than the calculated maxima. This can be explained by the fact that the electrons have a higher kinetic energy in the solid than outside due to an “inner potential”. This difference in energy is related to the bandwidth of the material (which gives a new possible lowest energy) and the workfunction. The value of the inner potential is about 10-15 eV, the sum of the bandwidth and the workfunction (see section 7.1). The inner potential is also responsible for a refraction effect of the electrons at the surface. The electron beam which leaves the crystal will be refracted away from the surface normal as it passes through the surface (see Fig. 7.10).

Another point worth noticing is the large width of the peaks in Fig. 6.14 which is due to small penetration depth of the electrons: a finite penetration depth means an effective localization in the first layers, corresponding to a

broad k and energy interval. This is intuitively clear from what we have discussed above. In the case of zero penetration, equivalent to a purely two dimensional lattice, the peaks would be infinitely broad and the third Laue condition would be unimportant. In a real crystal, however, the electrons do penetrate but their penetration depth is limited for two reasons. The first is that the peaks actually correspond to a Bragg back-reflection and therefore the penetration can not be very deep. The second is the limited electron mean free path .

The last thing one notices in Fig. 6.14 is the presence of additional peaks apart from the shifted Bragg peaks. This is due to the multiple scattering of the electrons in the solid. Indeed, intensity curves such as Fig. 6.14 can not be described by single-scattering (kinematic theory) like for the interaction of x-rays with matter. A sophisticated multiple-scattering formalism is needed to quantitatively describe the I-V curves. We will come back to this in a later section.

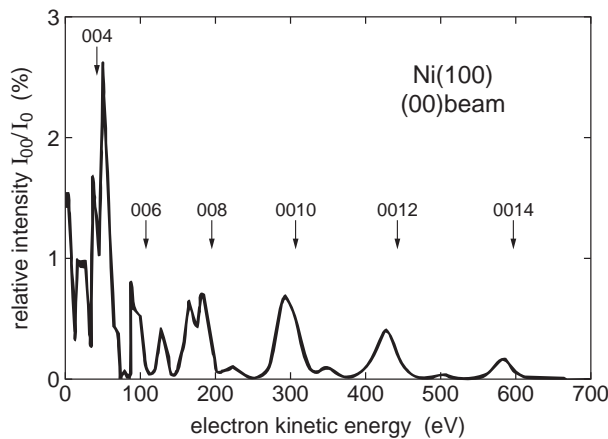


Figure 6.14: Intensity of the (0,0) spot from Ni(100) as a function of electron kinetic energy. The arrows indicate the positions where maxima would be expected if the third Laue condition would be valid. After Ref. [29].

Another new point when going from a two-dimensional lattice to a surface is the possibility of overlayer structures, i.e. we may have an overlayer (or a reconstructed layer) on the surface with a reciprocal lattice which is different from that of the substrate. What will the LEED pattern look like? One would guess that the LEED pattern is just the sum of the two reciprocal lattices but this is only partly true: due to multiple scattering one does not only get the spots of both reciprocal lattices (truncated bulk and surface/overlayer) but also all possible combinations between them. If we adopt the point of

view that the lattice of the surface is made up by the adsorbate and the first few layers of the substrate, these additional spots enter in a natural way into the reciprocal lattice. This is illustrated in Fig.6.15.

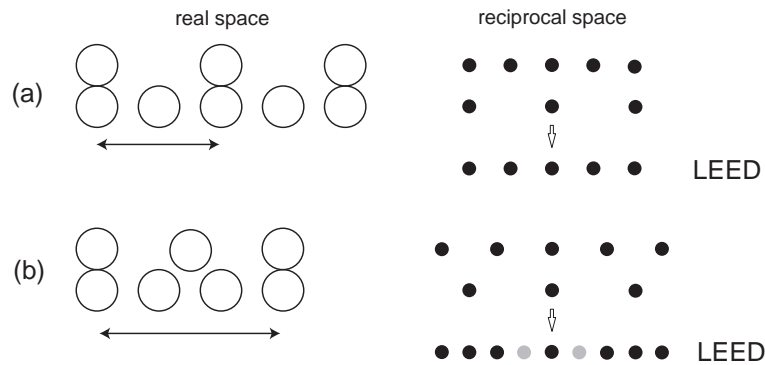


Figure 6.15: The LEED pattern shows the sum of the reciprocal lattices from substrate and overlayer plus all possible combinations between them. For a simple overlayer structure as in (a), this combination does not lead to any new spots. For a coincidence structure (b) it does (grey spots). The arrows indicate the size of the surface unit cell as a whole. When this unit cell is taken to calculate the reciprocal lattice, the “extra” spots appear in a natural way.

6.3.3 Interpretation of LEED patterns

A lot about the surface structure can be learned simply by the inspection of the LEED pattern without considering the quantitative I-V behaviour of the spots. Basically, we see the reciprocal lattice of the surface and from this we can construct models for the real lattice. There are, however, several effects complicating this analysis.

The first question which arises when inspecting a LEED pattern of a clean surface is if the surface is reconstructed or not. This can be found out by comparing the position of the spots to the positions one would expect for the (1x1) unreconstructed surface. The simplest way is to estimate the energy at which the (1x1) spots would first appear on the fluorescent screen and compare this to the measured energies. Once the (1x1) spots are identified one can describe any overstructure referring to them.

Now consider the LEED patterns of simple overlayer structures and coincidence structures. Since we know which spots are the original (1x1) sub-

strate spots we can now deduce the reciprocal lattice of the overstructure from the LEED pattern. Fig.6.16 gives a few examples.

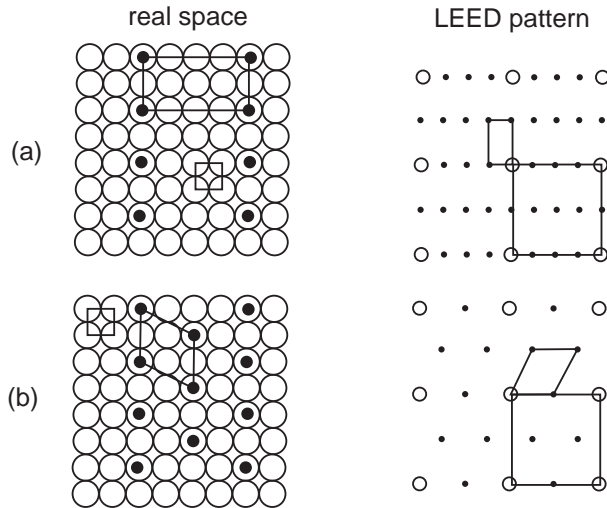


Figure 6.16: Three examples for overlayer structures and the LEED patterns produced by them. (a) a (4×2) structure, (b) a $c(4 \times 2)$ structure. In the LEED patterns the open circles are the (1×1) spots. The (1×1) unit cell in reciprocal space is also given.

From such LEED patterns the surface periodicity and the point-group of the surface may be deduced.

There is, however, one essential problem which is the existence of domains. Consider for example the structures shown in Fig 6.16. For (a) and (b) there are completely equivalent structures rotated by 90° . It is very likely that an almost equal number of both types of domains exists in the (huge) area which is sampled by the electron beam. If we neglect the coherent interference between electrons scattered from different domains then we will just have to sum up the LEED patterns from the two possible domains incoherently. Fig. 6.17 shows the incoherent sum from the two possible domains in Fig.6.16. It is obvious that the existence of domains gives the LEED pattern a four-fold symmetry while the local symmetry of the adsorbate structure is only two-fold.

The last point which we only mention very briefly is that there are also lots of imperfections on the surface. The electrons do not scatter from a perfect periodic structure but from a “real” surface at finite temperature, with steps, point defects and “dirt” in form of unwanted adsorbates. These imperfections cause an intensity loss and a broadening of the diffraction spots

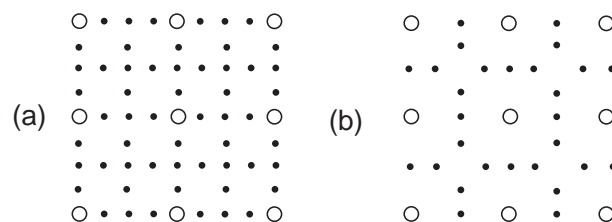


Figure 6.17: LEED patterns resulting from two different domains of the structures shown in Fig. 6.16.

and an increase of the background in between the spots. One can turn this problem into an advantage and use the spot profile of the diffraction maxima in order to learn something about the surface imperfections. This technique is called spot profile analysis LEED (SPA-LEED).

6.3.4 Quantitative structure determination

As we have seen, the inspection of the LEED pattern gives information about the surface periodicities and to some degree also about the surface symmetry. But there are still many important things one would like to know. One is the site of the adsorbed atoms. Consider again Fig. 6.16. If we shift the whole overlayer such that the atoms adsorb in bridge sites instead of on-top sites the diffraction pattern will be unchanged. Also, one could put more adsorbate atoms into the same unit cell and still keep the pattern the same. Clearly, a more quantitative analysis of LEED is needed.

This is achieved by analysing the I-V curves. The I-V curves for a particular model structure can be calculated by a computer program. Then they are compared to the measured I-V curves. If the agreement is not good, the model structure is changed and the structure is re-calculated. This process is repeated until eventually a good agreement between experiment and theory is achieved. The degree of agreement is quantified by a so-called reliability or R-factor. The lower the R-factor, the better the agreement.

In a LEED calculation the crystal is described by a so-called muffin-tin potential. This consists of spherical potentials for the ion cores and a constant potential everywhere else. The spherical potentials are characteristic for the element of the scatterer and depend somewhat also on its environment (but not very much). They can be described by a set of scattering phase shifts. This choice of potential has the advantage that reduces the problem basically to scattering from spherical potentials which can be treated very efficiently. The program must now explicitly solve the Schrödinger equation

in the muffin-tin potential including all possibilities of multiple scattering.

There are two additional effects which also have to be taken into consideration by the program. The first is the inelastic scattering of the electrons. This is handled by making the constant part of the potential in the solid complex. The imaginary part corresponds to the energy-dependent mean free path of the electrons and takes care of the inelastic scattering. The other effect is finite temperature. It reduces the scattering coherence in otherwise periodic structures and thereby reduces the intensity in the I-V curves. Finite temperature is taken into account by temperature-dependent scattering phase shifts .

The level of agreement which can be obtained between experiment and theory is remarkable, at least for many metal surfaces, and gives a high confidence into the LEED technique. Fig. 6.18 gives an example.

The possibility of high-quality calculations also means that the structural parameters are determined very precisely by LEED. The atomic positions are given within a tenth of an Angstrom or even better. But there are also some problems associated with the analysis approach employed for LEED. The success depends on the researcher's ability to come up with the right structural model which can then be refined in a trial and error iterative analysis. This is not too difficult for unreconstructed metal surfaces where the truncated bulk can be taken as a starting model. But it is a major problem for semiconductor surfaces where reconstructions with large surface unit cells are possible as we shall see below. Such large unit cells have the further disadvantage that they are extremely expensive in terms of computer time needed for the calculations. Many atoms in the unit cell mean many structural parameters which one has to get all right in order to obtain satisfactory agreement. A great danger is that there are cases where the agreement between theory and experiment is rather good but the model structure is not the right one. If one wants to have confidence in the result, it is important to have a very good agreement, or, in other words, one has to get everything right before one knows that one has anything right.

6.4 Some examples from LEED structure determination

6.4.1 Metal surfaces

As we have already discussed above, most metal surfaces do not reconstruct. The only change in the geometry upon the creation of the surface are relaxations of the layer distances. In most cases, the first to second layer

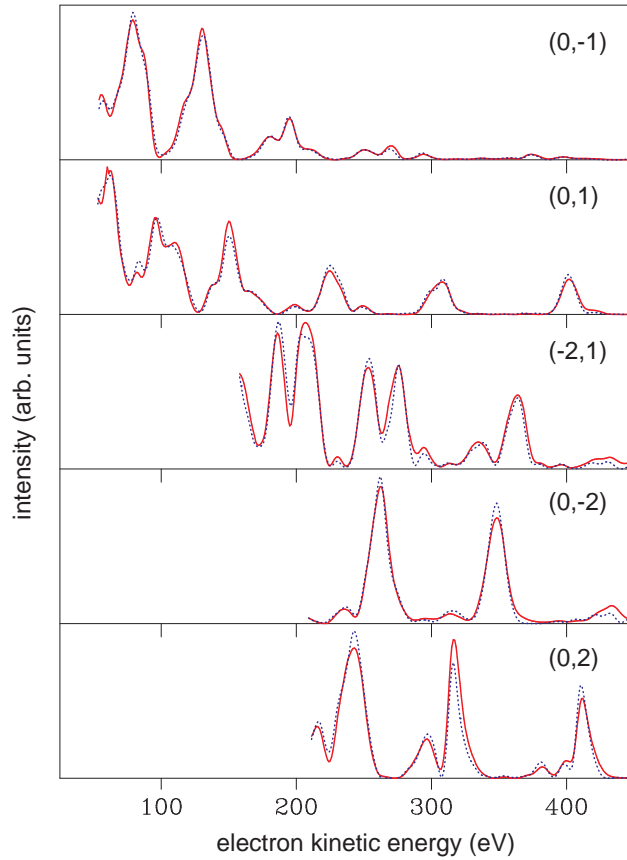


Figure 6.18: Agreement between measured and calculated LEED I-V data for different spots in case of the Al(111) surface. The full line is experimental data, the dashed line calculation [32].

distance contracts like in the simple Finnis and Heine model . The charge-smoothing effect which leads to this relaxation should be more important for more “open” surfaces (like fcc(110)) and less for “closed” surfaces (like fcc(111)). This is indeed the case. Fig. 6.19 shows the change in the first layer distance as a function of the bulk value of this distance (both normalized to the nearest neighbour distance in the bulk). The bulk value of the layer distance is a measure for the openness of the surface. Closed packed surfaces are to the right side of the plot, open surfaces to the left. The plot does not only show the experimental values for the distances (which were obtained using quantitative LEED) but also the result from modern first-principles calculations. The agreement between experiment and theory is rather good. We further note that all the points lie more or less on one

line, the “universal curve” for the interlayer distance of simple metals. The only remaining problem is that the qualitative Finnis-Heine model gets into trouble for the closed packed surfaces. They relax into the other direction! The first layer distance at the surface is even bigger than that in the bulk.

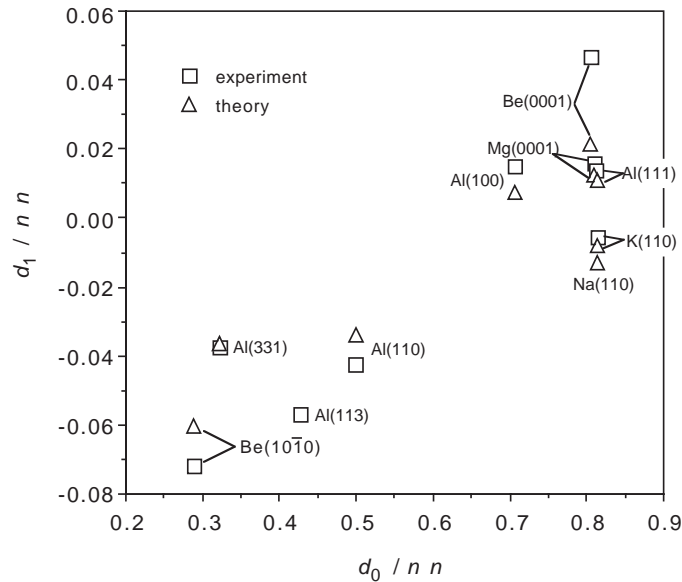


Figure 6.19: Distance between first and second layer of simple metal surfaces as a function of bulk interlayer distance (both normalized by the nearest neighbour distance in the bulk). After Ref. [30].

Very many ordered adsorbate systems have been solved using LEED. Actually, it is quite fortunate that so many adsorbates form ordered structures such that they can be studied by this technique! We give just two examples here.

Alkali atoms have always been of great interest as particularly simple adsorbate systems. We have already looked at alkalis in the lecture about adsorption. Basically, the picture is very simple: the alkali s level broadens when the atom gets close to the surface and gets more or less emptied upon adsorption. The result is a fairly ionic bond. If the substrate for alkali adsorption is a stable, closed packed surface of a simple metal one would expect simple adsorption sites for the alkali atoms without a severe perturbation of the substrate, let alone a reconstruction. A recent LEED investigation of K adsorbed on Al(111) has shown that this simple picture is not necessarily correct. [31]. K forms a $(\sqrt{3} \times \sqrt{3})R30^\circ$ for adsorption at low temperature and at room temperature. At low temperature the K atoms are adsorbed

in on-top sites on the substrate. However, when adsorbed at (or heated to) room temperature they lead to a severe reconstruction of the surface and are found in substitutional sites (see Fig. 6.20).

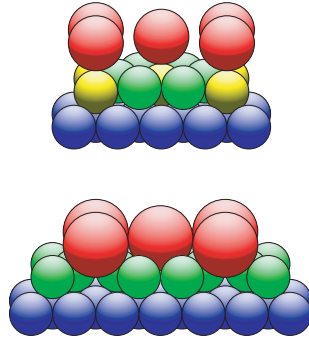


Figure 6.20: Adsorption geometry for K on Al(111) at 100 K (top) and 300 K (bottom). Both structures give rise to a $(\sqrt{3} \times \sqrt{3})R30^\circ$ LEED pattern. After Ref. [31].

Another example for an adsorbate-induced reconstruction is the (2x1) oxygen structure found on Cu(110) at half a monolayer coverage. This structure is shown in Fig. 6.21. It consists of oxygen-copper chains in the [001] direction. Evidently, half a monolayer of the top copper atoms has to be removed or added to form such a structure but LEED can not give information about the actual mechanism.

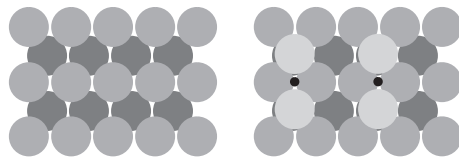


Figure 6.21: Adsorption geometry for (2x1)-O on Cu(110). Left: top view of the clean surface, Right: top view of the reconstruction. After Ref. [33].

6.4.2 Semiconductor surfaces

As mentioned above, semiconductor surfaces tend to reconstruct, sometimes in rather complicated ways. These reconstructions are very closely related to bonding in semiconductors and thus to the electronic structure. We will come back to this in a later lecture. The reconstructions present a major

problem to the LEED analysis because of the complicated structure and the large unit cell. Apart from the reconstructions there is the general feeling that the present LEED theory does not work as good for semiconductors as it does for metals. Why this is so is a tricky questions and definitely beyond the scope of these lectures. Anyway, the LEED structure determination of semiconductor surfaces is an important present research area.

We just want to show two examples of semiconductor reconstructions in order to illustrate how complicated they can be. The first is the famous (7x7) reconstruction of Si(111). When Si is cleaved in the (111) plane several reconstructions can be obtained depending on the temperature at which the cleaving is performed: (1x1), (2x1) and (7x7). Annealing the cleaved surface to high temperature always results in the formation of the (7x7) structure which remains also when cooling the crystal down again. Therefore, it is thought that this reconstruction is the one with the lowest total energy. Several structural models have been proposed for the (7x7) reconstruction. The model which is thought to be the right one is shown in Fig. 6.22. It has to be pointed out, though, that this structure has not been found by LEED.

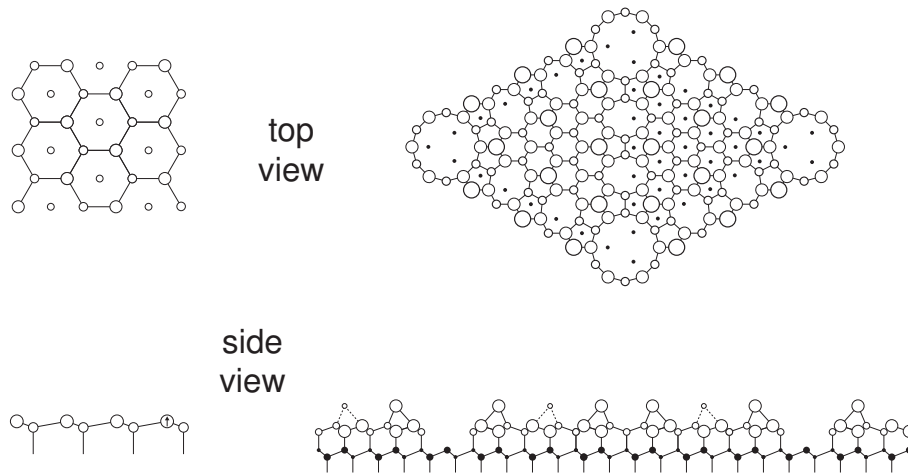


Figure 6.22: Left: ideal Si(111) surface. Right: the Takayanagi model for the Si(111) (7x7) reconstruction. After Ref. [34].

Another example is the (2x1) reconstruction of the technologically important Si(100) surface. This surface has been studied with a variety of techniques including quantitative LEED. The model favoured at present is that of a dimer reconstruction of the surface as shown in Fig 6.23. There is, however, still a considerable dispute about the details of the reconstruction,

in particular on the question if the dimer is symmetric or not.

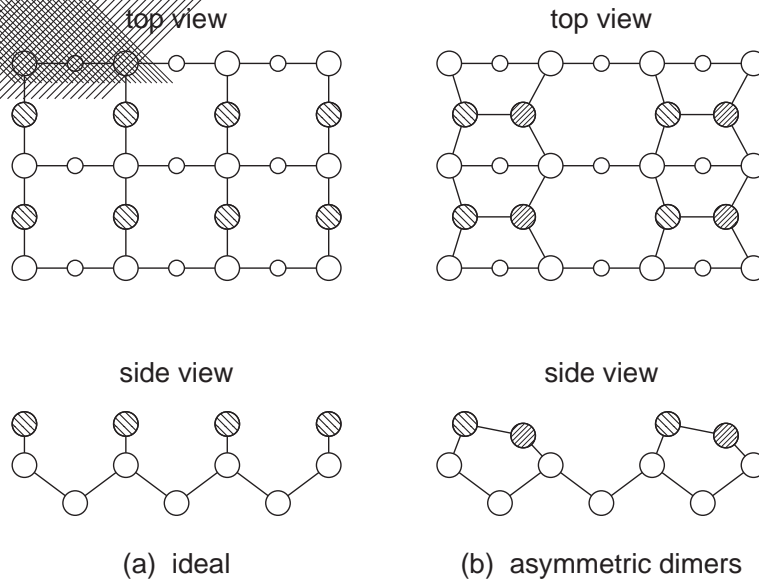


Figure 6.23: The unreconstructed Si(100) surface and the asymmetric dimer model.

6.4.3 Insulator surfaces

Studying insulator surfaces with electron spectroscopy immediately brings up the problem that the surface charges up when it is bombarded with electrons or when it emits electrons. No meaningful experiment can be done. If we want to look at insulators with LEED we have to overcome this problem somehow. There are two main strategies to do this. The first is to have a sufficient number of defects in the insulator which provide carriers such that a small conductivity results. In the case of insulating oxides this is mostly done by heating the sample in vacuum which results in oxygen vacancies. The disadvantage is that one studies a modified version of the oxide. The other possibility is to prepare a thin film of the oxide on a metallic substrate. This also gives enough conductivity to do electron spectroscopy but one has to worry about the fact that one may not really study the surface properties of the real bulk material.

Oxides surfaces were used a lot in the early days of surface science because some are so inert that they can be studied for several days even under rather poor vacuum conditions. An example for an early LEED investigation

of an insulator is the (001) surface of NiO . NiO has a rock-salt structure shown in Fig. 6.24. It is a prototype material for a highly correlated electron system. The electronic configuration of the Ni²⁺ ions is $3d^8$ and this partially filled band would correspond to a metallic ground state in a band structure picture. Yet, the strong on-site $d-d$ electron repulsion causes the material to be an insulator with a band gap of more than 4 eV! The LEED pattern from NiO(001) was found to be (1x1). For this surface there are two possibilities of structural changes consistent with such a LEED pattern: an interlayer relaxation as we know from metal surfaces and a buckling in the surface layer (i.e. a structural change where the Ni ions and the oxygen ions are not in the same plane any more). The latter geometry change is not possible with only one atom per unit cell. The LEED result is that the surface shows a small inward relaxation but no buckling.

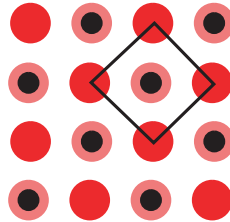


Figure 6.24: Structure and surface unit cell of NiO (top view). Top-layer Ni ions are red, second layer Ni ions are pink, oxygen ions are black.

6.5 Other scattering techniques

There are a couple of other techniques which we should mention. The first one is x-ray scattering from surface . This technique is very similar to bulk x-ray scattering with the major advantage over LEED that the theory is purely kinematic. The problem of the long mean free path of the x-rays is overcome by using a grazing incidence angle. In such a geometry total external reflection occurs because the refractive index for x-rays is smaller than one. It is, however, only very little smaller than one (in the order of 10^{-5} such that the incidence angle below which total reflection occurs is very small, a few tenth of a degree. Therefore, surface x-ray scattering requires a highly collimated x-ray beam which can only be produced at a synchrotron radiation source delivering high-brilliance light.

It is interesting to compare the advantages and disadvantages of LEED and surface x-ray scattering. One is that the momentum transfer, and hence

the sensitivity to structural parameters, is nearly perpendicular to the surface in case of LEED and nearly parallel to the surface in the case of x-ray scattering. The penetration depth is a little higher for x-ray scattering but it has the same order of magnitude as for LEED.

There are several interesting experiments involving the scattering of atoms and ions but we are not going to discuss them here (apart from He scattering in the section about vibrational properties, section 9.4). If you are interested in these techniques, consult the book by Woodruff and Delchar, section 1.3.

Two techniques based on electron scattering are discussed here in further detail: (S)EXAFS and photoelectron diffraction. Both do not rely on long-range order on the surface (like LEED). Instead, they can be used to determine the structure locally around an atom of interest. This is achieved by using specific atoms as “electron sources” instead of an external source like in LEED.

6.5.1 Extended X-ray Absorption Fine Structure (EXAFS and Surface EXAFS (SEXAFS))

The techniques of EXAFS and SEXAFS have been made possible by the construction of synchrotron radiation (SR) sources. SR has a continuous energy spectrum. In combination with a monochromator it provides a tunable x-ray source. The (S)EXAFS measurements involve scanning the photon energy around the absorption edges of the atoms in a material or on a surface. The fine structure in the absorption cross section gives information about the neighbours of the emitting atoms. The main advantages of these x-ray absorption techniques are that they work for materials where long-range order is not present and that at least the nearest neighbour distances can be obtained with rather high precision.

6.5.2 EXAFS

Fig. 6.25 shows an example for an EXAFS spectrum. Such a spectrum can be taken by exposing a thin film of material to x-rays and simply measuring the transmission through the film. The x-ray absorption of Cu is plotted vs the photon energy. As the energy reaches the K-edge the absorption increases steeply because of the possibility to excite the K-electrons. Above the edge the absorption shows a slow decrease due to the matrix element. On this slow decrease rapid oscillations in the cross section are superimposed. These are the EXAFS oscillations. The physical origin of these oscillations is quite easy to understand. The absorption cross section is given by Fermi's

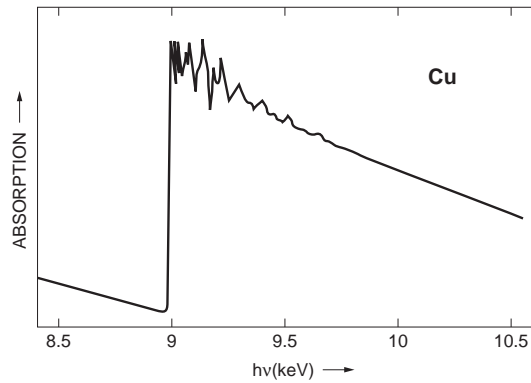


Figure 6.25: X-ray absorption of Cu in the vicinity of the K-edge.

golden rule and thus by a matrix element of the type $\langle f | \vec{H}' | i \rangle$. The initial state is simply the localized core state. The final state is the extended state of the outgoing electron wave, including all the multiple scattering processes. One can now think about the EXAFS oscillations in the following way. At low kinetic energies, from zero to a few hundred electron volts, the cross section for the back-scattering of the electrons from the neighbour atoms is rather high. These back-scattered waves have to be added coherently to the outgoing wave and this directly influences the final state at the emitter and thus the matrix element. The interference from outgoing and back-scattered waves changes with a periodicity given by the nearest neighbour distance. The effect is illustrated in Fig. 6.26.

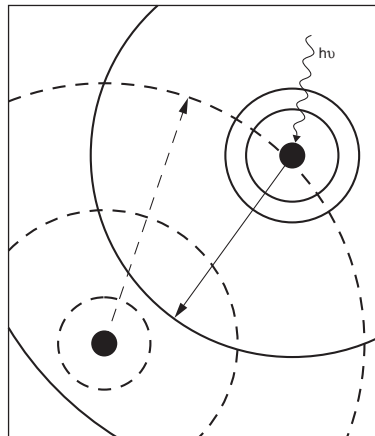


Figure 6.26: Schematic illustration of the interference leading to the EXAFS oscillations

This simple picture works only for electron energies which are not too close to the edge. Below kinetic energies of 50eV or so the oscillations contain resonant absorption from the valence states.

It is convenient to extract the EXAFS oscillations from the slowly varying background. This is done by the definition of a “fine structure function” χ

$$\chi(k) = \frac{\sigma(k) - \sigma_0(k)}{\sigma_0(k)}. \quad (6.16)$$

where σ is the measured absorption and σ_0 is the absorption due to the free atom.

If we consider a simple single-scattering picture the fine structure function is given by

$$\chi(k) = -k^{-1} \sum_i A_i(k) \sin[2kR_i + \phi_i(180^\circ, k)]. \quad (6.17)$$

where k is the electron wave number, A_i is an amplitude function defined below and ϕ_i is a phase shift. The sum runs over different “shells” of neighbours, a shell being defined as a set of neighbours having the same distance from the emitter, R_i . In principle, the desired values for R_i can be extracted from χ by a Fourier transformation. The phase shift would not be a problem in such an analysis but its energy dependence is one. It leads to wrong values for R_i . Thus the phase shifts have to be included in the analysis. One can use calculated phase shifts or one can, in contrast to LEED and Photoelectron Diffraction, use “experimental” phase shifts. The reason is that only the phase shift for 180° back scattering is of interest, not the phase shifts for all the other scattering angles. The 180° phase shift can be obtained from a material which contains the scatterer of interest and has a known structure, e.g. a single crystal.

Let’s look again at the amplitude function for the different shells. It is given by

$$A_i(k) = (N_i/R_i^2) |f_i(180^\circ, k)| W(T, K) \exp(-2R_i/\lambda). \quad (6.18)$$

N_i is the number of atoms in the shell. The $1/R_i^2$ factor leads to an effective localization of EXAFS explaining the success of a single-scattering treatment. It is caused by the fact that both emitter and scatterer are point sources. The next factor is the modulus of the scattering amplitude. $W(T, K)$ is a Debye-Waller factor which takes the thermal vibrations into account and the last factor describes the inelastic scattering of the electrons in the solid. As mentioned above, the single scattering approach works quite well, at least in order to determine the distance of the nearest neighbour shell.

6.5.3 SEXAFS

The surface version of EXAFS is called SEXAFS. One can for example use the technique for determining the bond distances of adsorbate atoms to the substrate. However, what one actually wants to know is the adsorption site and this is difficult to get from just the bondlength. Help could come from considering the absolute amplitude of the modulations because this should give the number of nearest neighbours (equation 6.17). But due to experimental difficulties (see below) it is very dangerous to use the absolute modulation strength. One can also play the following trick. The synchrotron radiation one uses for the experiment is polarized. This means that the electrons from a core level will have a certain angular distribution, depending on the direction of the polarization vector. One can take SEXAFS data for different directions of the polarization vector such that different possible neighbours would be “hit” by a high intensity of photoelectrons. Comparing the different SEXAFS spectra one can work out where the nearest neighbours are.

One has to add a few words of caution, though. SEXAFS is a very difficult experiment. The first problem is what to measure in order to get the absorption of a particular atomic species on the surface. One possibility is the intensity of the Auger signal which is emitted by the decay of the core electron one creates. Such Auger peaks are usually positioned on a high background of inelastically scattered electrons, leading to a bad signal-to-noise ration. To make matters worse, the SEXAFS modulations are only a tiny fraction of the absorption cross section (one percent or so) and there are only a few adsorbate atoms compared to a bulk EXAFS experiment.

We just give one example here which demonstrates how powerful SEXAFS is as a technique for structural investigations. SEXAFS has been used to determine the structure of the co-adsorption system $\text{SO}_2 + \text{O}$ on $\text{Cu}(111)$ which is formed upon SO_2 adsorption [36]. Fig. 6.27 shows data taken at the oxygen K-edge for two different polarizations of the incident photons. The spectra are quite different, illustrating the usefulness of the “trick” mentioned above. The Fourier transforms of the data are shown together with the result of a simulation for a particular geometry. The agreement for the closer distances is very good.

Fig. 6.28 shows the final result of this structural determination showing the position of the adsorbates and a very complex surface reconstruction.

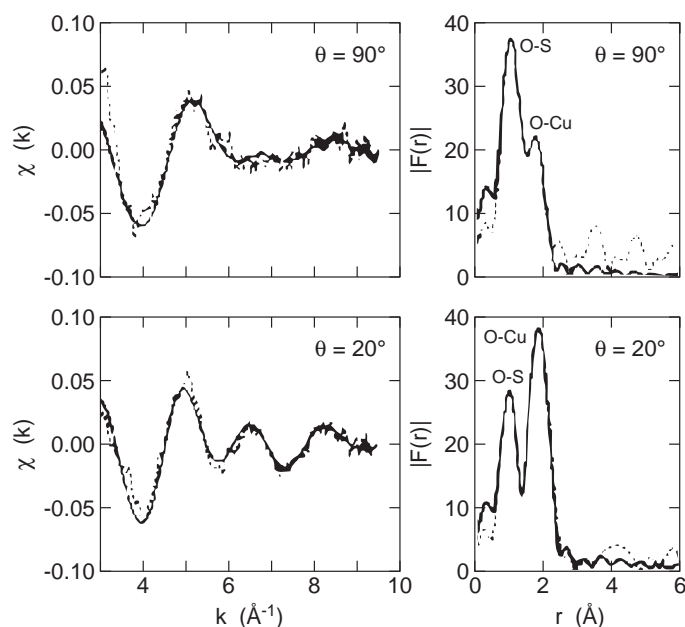


Figure 6.27: SEXAFS data from the oxygen K-edge of the co-adsorption system $\text{SO}_2 + \text{O}$ on $\text{Cu}(111)$. After ref. [36].

6.6 Photoelectron diffraction (PhD, PED)

6.6.1 Introduction

The principle in photoelectron diffraction is given in the Fig. 6.29. One measures the intensity of a core level line as a function of energy and emission angle. The electron can reach the detector on a direct path or it can be scattered at the atoms surrounding the emitter and then reach the detector. The final state is given by interference between the direct and the scattered components. This interference depends on the path-length difference and on the scattering phase shifts. This, in turn, depends on the electron wavelength / kinetic energy, on the position of the detector and on the position of the emitter with respect to the scatterers.

By varying the position of the detector or the kinetic energy of the emitted electrons the interference conditions are changed. Normally the photoemission intensity is recorded as a function of kinetic energy or emission angle. The modulation in the intensity which results from the change in the interference conditions can be used to extract geometrical information.

The technique is related to SEXAFS and LEED. SEXAFS is similar to

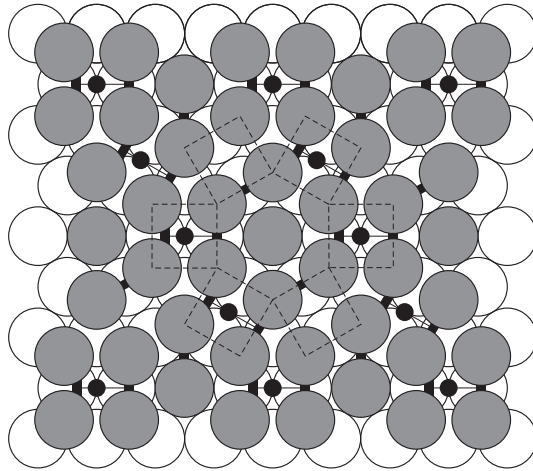


Figure 6.28: Structure $\text{SO}_2 + \text{O}$ on $\text{Cu}(111)$ as determined by SEXAFS. After ref. [36].

PhD in that the electron source is also a core level from an atom at the surface. Here the interference between the outgoing and the 180° backscattered waves is of major importance. The backscattering changes the final state intensity at the core and this in turn changes the absorption cross section. SEXAFS is very similar to PhD with the difference that the emitter itself is the detector. In a simple picture, it can be viewed as an angle-integrated PhD experiment. The PhD modulations do, of course, also contain the SEXAFS part, i.e. the modulations in the absolute cross section. This is, however, not a problem because the SEXAFS modulations are much weaker (1-3%) than the PhD modulations (30-50%).

The big difference between these two techniques and LEED is that the electron source in the latter is not in the system itself but in the far-field. It is not possible to pick an atom in the adsorbate layer and make it special by considering just the core-level intensity from that atom. All the atoms are of equal importance as scatterers. The information about the adsorbate layer relative to the substrate is only contained in the wave-part scattered by the adsorbate and its interference with the wave-part scattered by the substrate. In PhD and SEXAFS the position of the adsorbate relative to the substrate is contained in ALL scattering pathways. A further difference is that LEED is a true diffraction technique which relies on the long-range order in the adsorbate layer. PhD and SEXAFS only probe the local structure around the adsorbate. This is a great advantage for disordered systems. Multiple scattering is very important in LEED, less important in PhD and

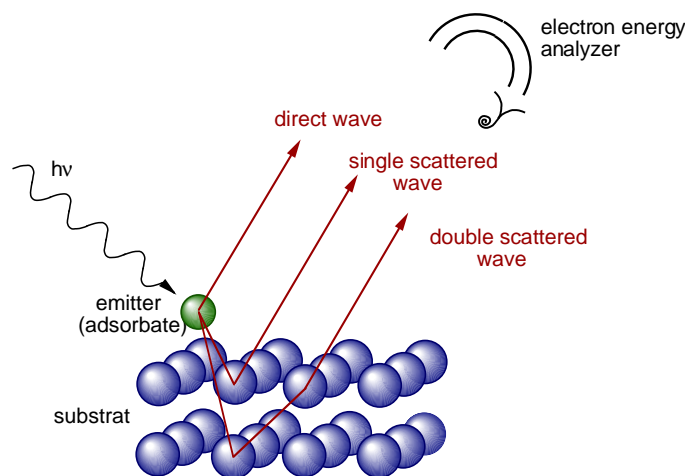


Figure 6.29: Principle of photoelectron diffraction

least important in SEXAFS. The reason is the $1/r$ fall-off of the spherical wave from the electron source and, in SEXAFS, also from the electron scatterer. PhD contains the $1/r$ effect once, SEXAFS twice. Finally, SEXAFS and PhD have chemical sensitivity: it is possible to pick out on specific atom in the adsorbate. Indeed, if there are two, say, carbon atoms in a different chemical environment it is even possible to pick one of them as an emitter because of the chemical shift in the XPS lines (only in PhD, see below).

6.6.2 Simple Theory

The basis of the theory is the scattering of electrons by ion cores. For the simple case of plane-wave scattering this can be described in terms of a scattering amplitude and a phase shift. Both are angle and energy dependent. Fig. 6.30 shows the modulus of the scattering factor.

The strongest scattering always occurs in the forward scattering direction, i.e. for a scattering angle of 0° , especially for high electron energies. At low energies there is also some scattering in the back scattering direction. For LEED the back scattering direction is of particular importance (scattering angles between 90° and 180°). For SEXAFS only 180° scattering is relevant. In photoelectron diffraction both back scattering and forward scattering has to be considered.

The most important point in the theory is to realise that the intensity at the detector is the coherent sum of the direct wave and all the waves reaching

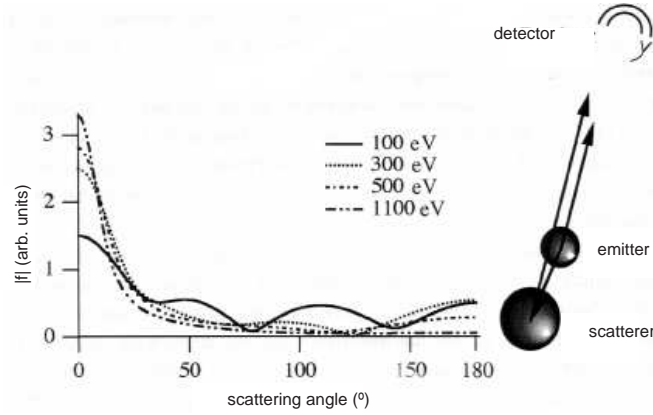


Figure 6.30: Modulus of the electron scattering factor.

the detector on however complicated scattering paths:

$$I(k, \Theta, \phi) \propto |\Psi_0 + \sum_j \Psi_{s_j}|^2 \quad (6.19)$$

The Ψ 's describe the amplitude of the different components of the wave field. Ψ_0 is reaching the detector directly. The Ψ_s are the amplitudes after several scattering processes.

The first question is how the wave function of the outgoing electron can be described without any scatters. The standard optical selection rules apply for the angular distribution, i.e.

$$l' = l \pm 1 \quad \text{and} \quad m' = m, m \pm 1. \quad (6.20)$$

The intensity can be written as an intuitive formula when the following assumptions are made:

1. single scattering
2. the wave at the scatterer is approximated as a plane wave
3. the initial state is an s core level

The result for the intensity looks like this (see also Fig. 6.31):

$$I(\vec{k}) \propto \left| \cos \Theta_k + \sum_j \frac{\cos \Theta_r}{r_j} |f(\Theta_j, k)| \exp(ikr_j(1 - \cos \Theta_j) + \phi(\Theta_j, k)) \right|^2 \quad (6.21)$$

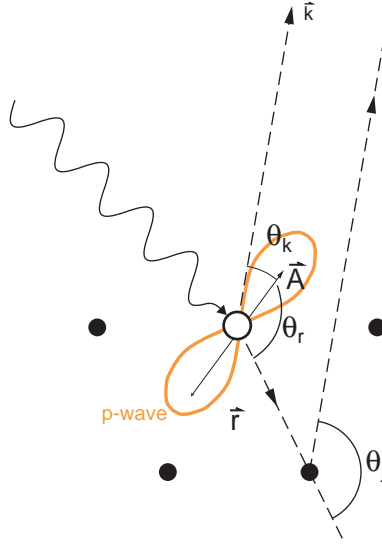


Figure 6.31: Symbols in single scattering theory.

The first term corresponds to the direct wave. The sum is over all relevant scatterers. The first term in the sum describes the intensity which arrives at the scatterer. f is the complex scattering factor. Its magnitude describes how much of this intensity is scattered in the direction of the detector. Its phase $\phi(\Theta_j, k)$ describes the scattering phase shift. The exponential term describes the pathlength difference with the direct wave.

There are two very important ingredients missing in the above formula. The inelastic scattering of the electrons attenuates the propagation of the waves in the crystal. It also makes the calculation easier because it reduces the number of important scatterers. It can be taken into account via the usual mean-free path concept. The finite temperature of the crystal makes the atoms vibrate. This means that the pathlength differences are modulated. This effect tends to wash out the photoelectron diffraction modulations. It can be taken into account via a Debye-Waller factor like in x-ray scattering. Adding this to the above formula gives:

$$I(\vec{k}) \propto [\cos \Theta_k + \sum_j \frac{\cos \Theta_r}{r_j} |f(\Theta_j, k)| W(\Theta_j, k) \exp(-L_j/\lambda(k)) \exp(ikr_j(1 - \cos \Theta_j) + \phi(\Theta_j, k))]^2 \quad (6.22)$$

Note that the inelastic mean free path λ is twice as big as the value normally taken in electron spectroscopy since it is an amplitude attenuation factor and not an intensity attenuation factor.

6.6.3 Structure determination: experimental results

Angle-scan photoelectron diffraction: forward scattering

In the angle-scan mode of PhD the core level intensity is measured as a function of emission angle keeping the photon energy fixed. An obvious advantage of this approach is that a laboratory x-ray source can be used instead of a synchrotron radiation facility.

Although such an experiment is dominated by high-energy forward scattering, it can be used to learn something about adsorbates. The intensity from an adsorbate core level can be observed at grazing emission (see Fig. 6.32). The intensity can be expected to be strongest for directions where substrate atoms lie close to the emitter. One can learn something about the symmetry of the adsorption site.

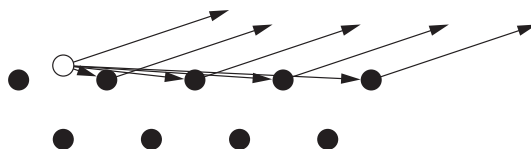


Figure 6.32: A grazing emission forwards scattering experiment.

Angle-scan photoelectron diffraction can also be used to determine the orientation of molecules on the surfaces. The intensity of the atom closer to the surface is measured. At a certain angle a forward scattering condition is met where another atom of the molecule is between the detector and the emitter. There the intensity will be increased. This allows the determination of the molecular axis orientation. Note that at high energies only a very small fraction from the core level electrons from an adsorbate will be scattered back by the substrate.

Fig. 6.33 shows the situation for a CO molecule adsorbed on a surface. Consider the emission from the carbon 1s core level (we know that the carbon atom is going to the chemical link to the surface) [37].

At high energies forward scattering dominates and the only important scattering process is along the molecular axis. Moving the analyser over the surface (in angle) will give the right tilt angle of the molecule. Fig. 6.34 shows the result of such angular scans for CO adsorbed on Ni(100). Evidently at higher coverage tilted CO species can be found.

Note: this simple interpretation is not only based on the assumption of strong forward scattering but also on a small scattering phase shift. Otherwise the interference in the direction of the molecular bond might turn out

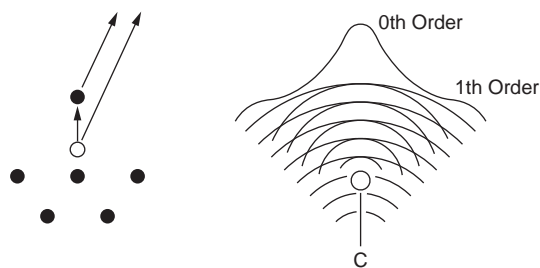


Figure 6.33: A forward scattering experiment to determine molecular orientation.

to be destructive. This has led to some confusion and has been wrongly termed "shadowing".

Scanned-energy mode photoelectron diffraction: backscattering

In scanned energy mode photoelectron diffraction the intensity at the detector is measured as a function of photoelectron kinetic energy in a fixed emission direction. Since the binding energy of the core level under consideration is constant, synchrotron radiation has to be used to vary the kinetic energy of the photoelectron. This mode of PhD is particularly interesting and it has close ties to both LEED and SEXAFS.

To illustrate this consider a typical XPS spectrum of a clean and adsorbate-covered (C_2H_2) Ni(111) surface (Fig. 6.35). As the photon energy is changed the kinetic energy of all the XPS peaks also changes. Fig. 6.36 shows a group plot of very many XPS spectra taken around the O 1s region for the system CO on Cu(110). One of the peaks is magnified. Already in this raw data plot a clear modulation of the intensity is visible. The function $I(E)$ describes now the integrated intensity of each peak. Like in SEXAFS a modulation function is defined by $I(E)$ and the slowly varying part $I_0(E)$

$$\chi(E) = \frac{I(E) - I_0(E)}{I_0(E)}. \quad (6.23)$$

The integrated $I(E)$ and the modulation function for the system above are shown in Fig. 6.37. The modulation functions for various emission directions can be viewed as the analogue to the LEED I/V beams. The interpretation of the modulation functions is not as obvious as in the angle-scan case. Multiple scattering is far more important and this also means that there is more structural information. The various modulation functions for different emission directions have to be compared to theory to obtain structural information.

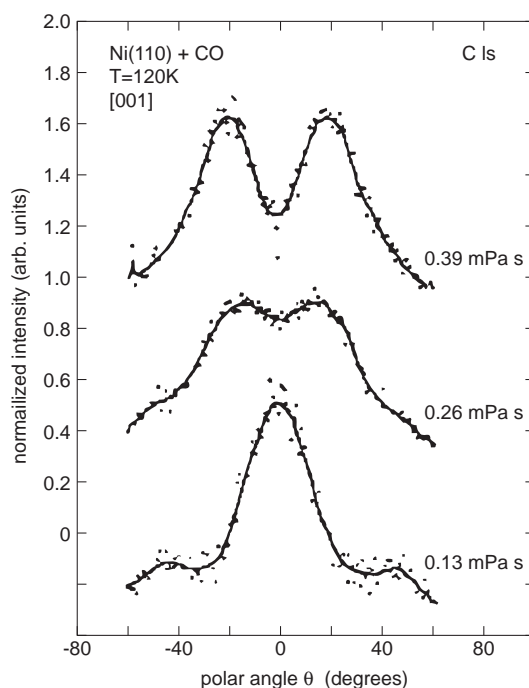


Figure 6.34: A forward scattering experiment to determine molecular orientation of CO on Ni(100). After Ref. [37].

Let us illustrate this by a simple example, the adsorption of the acetate species on Cu(110) [38]. A O 1s diffraction spectrum is compared to theoretical calculations for different adsorption sites and distances from the surfaces. The best agreement is found for a bridge site (see Fig. 6.38). The big advantage of PhD with respect to LEED lies in the dependence of local order only. However, if a molecule is adsorbed on more than one site at the same time more information is needed to obtain the right structural parameters. In such a case many modulation functions are measured and compared to theory.

A further advantage of PhD is its chemical sensitivity. The positions of O and C in the above example can be determined separately considering the O 1s and C 1s emission. Moreover, the two C atoms are in a chemically different environment. This means that the binding energies are also different (chemical shift, see 4.3.4). Hence the PhD from both C atoms can be measured independently and the modulations are quite different. This is illustrated in Fig. 6.39.

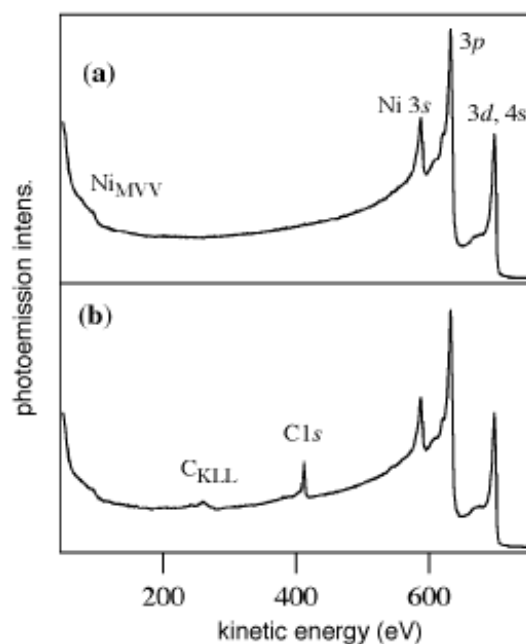


Figure 6.35: XPS spectra of clean and C₂H₂ covered Ni(111).

6.6.4 Suggested reading

D. P. Woodruff in *Angle-Resolved Photoemission, Theory and Current Applications* (eds. S. D. Kevan) Elsevier, Amsterdam (1992).

A. M. Bradshaw and D. P. Woodruff in *Applications of Synchrotron Radiation: High Resolution Studies of Molecules and Molecular Adsorbates on Surfaces* (eds. W. Eberhardt) Springer, Berlin

6.7 Scanning Tunnelling Microscopy

It is clearly desirable to have a real-space microscopic technique which can image the structure of surfaces on a truly atomic scale. Field emission microscopy is a possibility with a rather limited range of possible applications. First the advent of scanning tunnelling microscopy has made a real space atomic scale view on most surfaces possible. But the section should start with a clear warning. STM does *not* measure the structure of surfaces but, as we shall see below, the electronic structure. It is essential to keep this in mind, in particular when working with semiconductors and insulators.

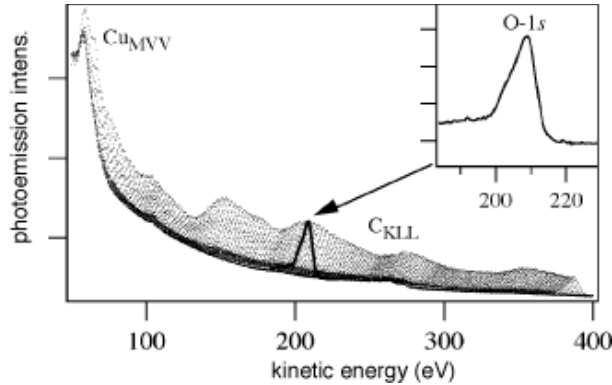


Figure 6.36: Group plot of many XPS spectra of the O 1s peak from CO on Cu(110). All the spectra are taken with different photon energies. One spectrum is magnified.

6.7.1 Basic principle and experimental setup

Scanning tunnelling microscopy is based on the quantum mechanical effect of tunnelling illustrated in Fig. 6.40. The wavefunctions at the Fermi level exponentially leak out of the metal with an inverse decay length of

$$\kappa = \hbar^{-1}(2m\phi)^{1/2} \quad (6.24)$$

where m is the mass and ϕ is the local workfunction. If now two metals are brought in close contact and a small voltage is applied between them, a tunnelling current can be measured which is

$$I_t \propto \exp -2\kappa d \quad (6.25)$$

where d is the distance between the conductors. The important message here, and the reason why STM works, is the exponential dependence of the tunnelling current on the distance between the conductors. We will come back to this several times in the following.

Fig. 6.41 shows the principle setup for an STM. It consists of a sharp tip, very close to the sample, which can be moved with high precision using three mutually orthogonal piezoelectric transducers (PET). A small voltage is applied between the tip and the sample and the current is measured. Typical values for the tunnelling voltage are from a few mV to several V or so and for the current from 0.5 to 5 nA. The tip-sample distance is a few Angstrom. The tunnelling current depends very strongly on this distance. A change of 1 Å causes a change in the tunnelling current by a factor of ten.

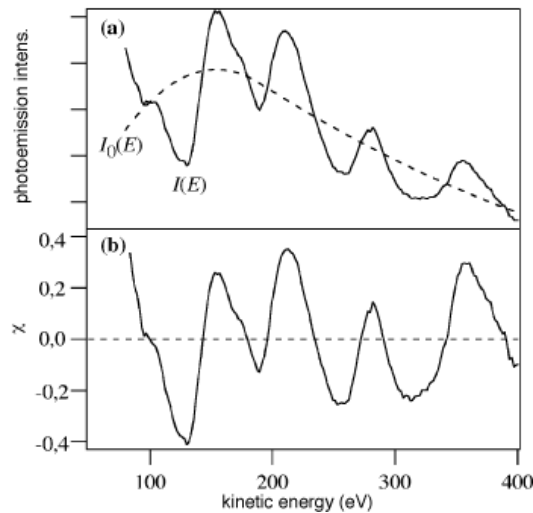


Figure 6.37: $I(E)$ and the modulation function for the O $1s$ peak from CO on Cu(110).

Most STM topography studies are performed in the so-called constant current mode. The tip is scanned across the surface by the X and Y PETs. The Z PET is in a feedback loop which applies a correction voltage to the Z voltage in order to maintain a constant tunnelling current as the XY position of the tip is changed. Since the piezo extension is proportional to the applied voltage, this correction voltage is a direct measure for the change in Z the tip has to perform in order to follow the contours of the sample and it can be used as an “image” of the sample when displayed as a function of X and Y voltages. The exponential decay of the tunnelling current with distance from the sample is crucial for this operation: even if we can only keep the current stable by 10 percent or so, this will still mean that we have a very high precision in the Z measurement because a small uncertainty in the current means virtually no uncertainty in the distance.

While the principle of STM operation is simple, its practical realization faces some formidable difficulties. The first is that the tip has to be brought at a distance of a few Angstrom from the surface and has to be stabilized there with sub-Angstrom stability. This process has to be performed in the presence of mechanical vibrations and thermal drift. The vibrational problem is solved by vibrational insulation, like suspensions by springs or the use of a support frame which has a resonance frequency very different from the usual noise frequencies of the environment. The only way to get completely rid of the thermal drift problem is to stabilize the whole microscope and sample

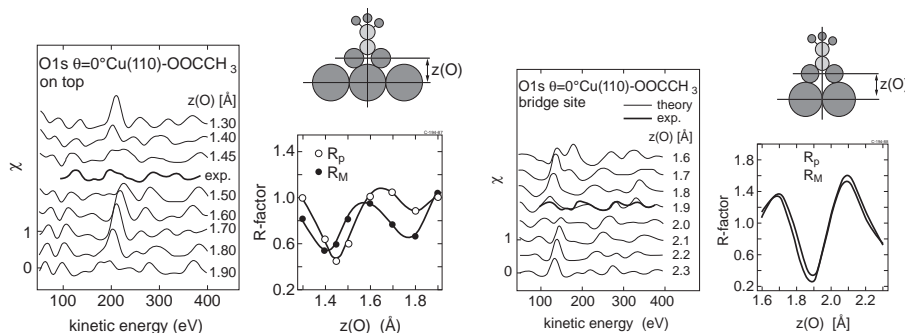


Figure 6.38: O 1s diffraction data to determine the adsorption site of the acetate species on Cu(110). After Ref. [38]. The R-factor has the same meaning as in a quantitative LEED analysis.

at the same (low) temperature. The most stable STMs today are working in a UHV vessel which is placed inside a dewar filled with liquid Helium. The next practical problem is to make an atomically sharp tip. Different techniques are used like cutting and etching and most tips are made off W or Ir. Again, the exponential decay of the tunnelling current helps: one can hope that there is one single atom sticking out a little further than all the others on an otherwise rather blunt tip. Then most of the tunnelling will happen through this atom and it will be possible to obtain images with atomic resolution. Unfortunately, it is not possible to prepare a tip a controlled and reproducible way. In particular, one has no control about the chemical nature of the outermost atom of the tip but the images depend a lot on this.

6.7.2 Theory of operation

The calculation of STM images is very difficult. For the sample one can make reasonable total energy calculations for a perfect surface. For the tip such calculations are not so easy because of the unknown shape. Even if one could calculate the wavefunctions for each system, sample and tip, separately bringing them together would render the problem hopelessly complicated because now one has a new system which totally lacks the translational invariance which was needed to solve the surface problem. The last hurdle is circumvented by Bardeen's suggestion to basically use the unperturbed wavefunctions of tip and sample and to consider just the tunnelling between them. Tersoff and Hamann have developed a simple and useful STM theory based on this approximation. They furthermore assume that the tip can be approximated by an s -wave state (i.e. that its end has spherical symmetry)

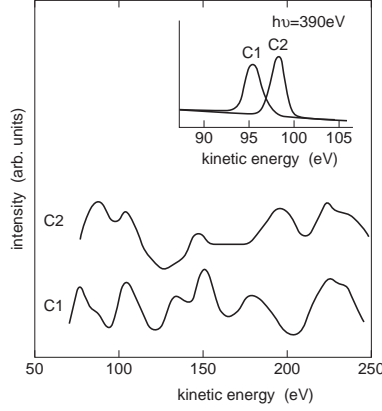


Figure 6.39: Modulation functions for the two chemically different C atoms in the acetate species on Cu(110). After Ref. [38].

and that temperature and tunnelling voltage are very low. This results in

$$\frac{I_t}{V_t} \propto D_{tip} R^2 \exp(-2\kappa R) \rho_{samp}(\vec{r}_{tip}, E_F) \quad (6.26)$$

where R is the radius of the tip, D_{tip} is the tip density of states at the Fermi level, \vec{r}_{tip} is the centre position of the tip and

$$\rho_{samp}(\vec{r}_{tip}, E_F) = \sum_{\nu} |\Psi(\vec{r}_{tip})|^2 \delta(E_{\nu} - E_F) \quad (6.27)$$

is the local density of sample states at the Fermi level. The only z dependence in these equations is in the wavefunctions of 6.27 such that we recover our exponential decay into the vacuum, as we must. These equations give a simple interpretation for constant-current mode STM images. If we scan across the surface at constant current or, more precisely, at constant $\frac{I_t}{V_t}$, adjusting just the distance of the tip over the surface, we basically follow the contours of sample density of states at the Fermi-level. Note, however, that this statement is only correct if we assume that there are no lateral changes in the workfunction of the sample.

We add an additional rather crude approximation. We write $\rho_{samp}(\vec{r}_{tip}, E_F)$ as a superposition of charge densities of the free atoms

$$\rho_{samp}(\vec{r}) = \sum_{\vec{R}} |\phi(\vec{r} - \vec{R})|^2. \quad (6.28)$$

where the sum extends over all the atoms making up the solid. Then we say that the interesting density of states at the Fermi level is just a fraction of the total charge

$$\rho_{samp}(\vec{r}_{tip}, E_F) = \rho_{samp}(\vec{r}) / E_0. \quad (6.29)$$

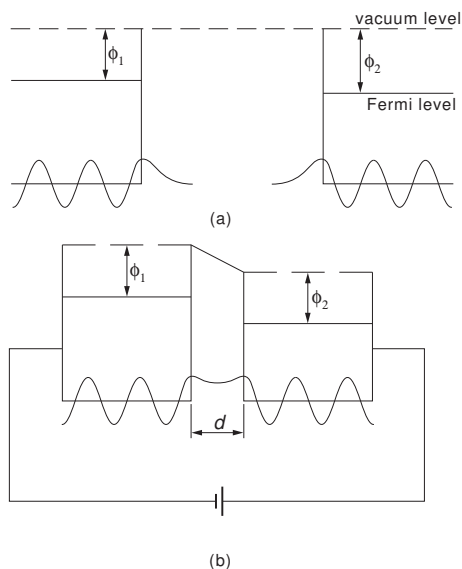


Figure 6.40: (a) Exponential leakage of the wavefunctions from a conductor into the vacuum. (b) Application of a voltage and tunnelling between two conductors because of the overlap of the wavefunction tails. Φ is the workfunction which is discussed in section 7.1.

This approximation clearly ignores the fact that there is any bonding in the solid. While the approximation of no bonding at all obviously is not a good one, we may expect it to work best for delocalized bonding because this does at least avoid the presence of strongly oriented bonds which might show up as structure in the STM images. It is evident that in this approximation the STM sees “atoms” but we have to be aware of the limits of this view!

In practice, the tunnelling voltage is not always very small. Especially for semiconducting materials a small tunnelling voltage can be impossible because there are no carriers in the gap which can be involved in the tunnelling. The tunnelling voltage can be chosen to be both negative or positive. This means that STM can look at both, occupied and unoccupied states of the sample depending on the bias voltage.

6.7.3 Clean metal surfaces

Taking STM data with atomic resolution on metal surfaces is much harder and historically later than on semiconductor surfaces. The reason is the small electronic corrugation of metal surfaces. We have already encountered this phenomenon as Smoluchowski effect / Finnis-Heine model for the metal re-

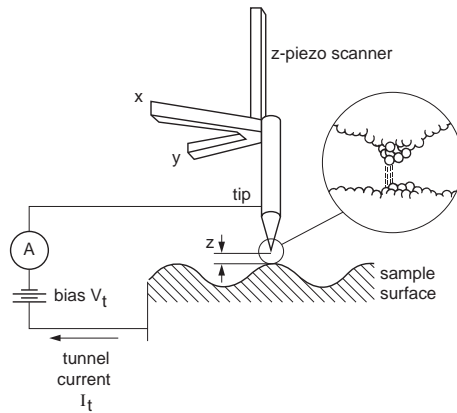


Figure 6.41: Schematic construction principle of an STM.

laxation. Nevertheless, STM investigations of metal surfaces are now possible and we give two examples.

The first is the (1×2) missing row reconstruction on the (110) surface of the fcc metal Au. Fig. 6.42. In the large scale image we can clearly see the remaining rows as well as several terraces. In the small-scale image we can again see the rows and even the atomic corrugation parallel to the rows.

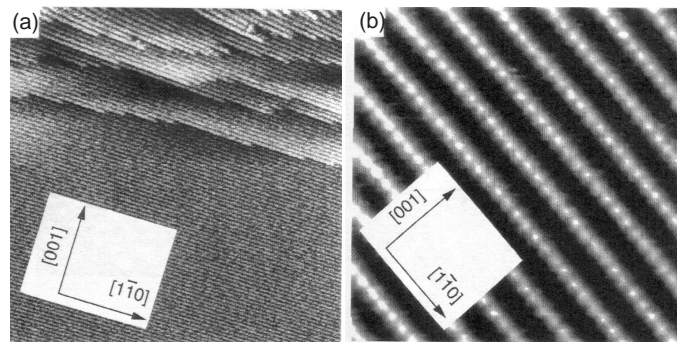


Figure 6.42: STM topographs of the (1×2) missing row reconstruction on Au(110). (a) $(800 \times 800) \text{ \AA}^2$ with the presence of atomic steps in the upper part of the image [39] and (b) $(84 \times 84) \text{ \AA}^2$ with atomic resolution even along the rows. After [40].

Au(111) shows a more complicated reconstruction. The unit cell of the reconstructed surface is much bigger than the (1×1) unit cell, as observed by LEED. In fact, a correct description of the overlayer structure is $\begin{pmatrix} 22 & 0 \\ -1 & 2 \end{pmatrix}$.

The reconstruction is caused by a denser layer of Au atoms in the first layer than in all other layers. The first layer contains 4.5 percent more atoms. The reconstruction is a compression of a hexagonal layer to accommodate these atoms. It was suggested that the atoms in the top layer are arranged such that there are regions of fcc stacking sequence (ABCABC... , like in the bulk) and hcp stacking sequence (ABAB...). These regions have to be separated by transition regions where the atoms are in less symmetric sites. It is impossible to solve such a structure quantitatively by LEED. It was just clear that the unit cell is very large but the position of the atoms in the unit cell were not known. STM was able to shed light on the reconstruction. The images in Fig. 6.43 show the reconstructed surface on different scales. Fig. 6.43 (a) shows a pattern of parwise bright lines which are due to the reconstruction. The dark area between a pair of stripes was identified as the region of hcp stacking and the area between two stripe pairs as fcc stacking. This means that there is a higher area of fcc stacking which also makes sense energetically. It is consistent with intuition, that the transition regions should appear brighter. The first-layer atoms are not placed in hollow sites and stick out further than the three-fold hollow site atoms. An atomically resolved image (b) allows to identify the unit cell and to state that the reconstruction is caused by a uniform contraction in the [110] direction. In (c), finally, a bigger overview is given which shows rotational domains of the reconstruction and transitions between them. The accommodation of more atoms in the first layer than in the other combined with the uniaxial contraction causes an elastic strain which leads to a long range “herringbone” pattern formed by the reconstruction.

6.7.4 Adsorbates on metal surfaces

How do adsorbates show up in STM images? According to our theory section the appearance of adsorbates will depend on the change they induce in the local density of states at the Fermi level. If they increase this LDOS, they will appear as protrusion, if they decrease it, they will appear as hole in the images, if they do not change the LDOS we will not be able to see them at all! Consider for example the case of Li, Si and Cl shown in Fig. 5.5. Si atoms would be well visible on jellium , Li less and Cl not at all. In a real STM experiment, however, there is still the possibility to work at a higher tunnelling voltage to improve things.

Unfortunately, it is not possible to chemically identify individual adsorbates by the appearance in the STM images. Conclusions about the chemical identity can only be drawn rather indirectly. One can, for example dose some gas on a surface which was clean before. If one can then see adsorbates, these

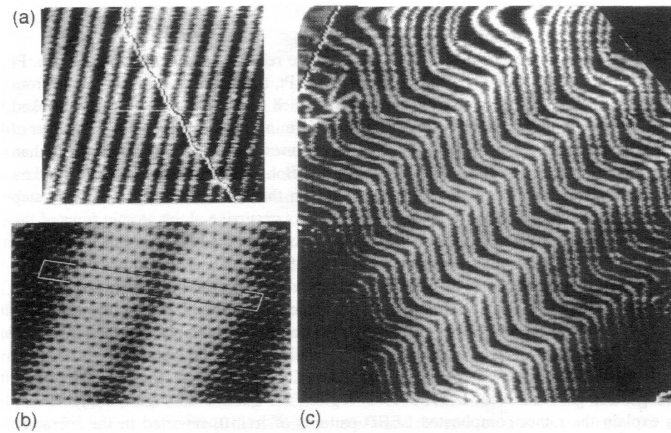


Figure 6.43: STM topographs of the reconstruction on Au(111). (a) (360 x 420), (b) (57 x 89) Å² and (b) (1230 x 1280) Å². Reprinted figure with permission from [41]. Copyright (1990) by the American Physical Society.

must be related to the gas. In the case of a monoatomic gas, the adsorbates can be identified as the gas atoms. For a molecular adsorbate one might identify the whole molecules or the fragments. Information about possible dissociation products can be taken from some other technique. There is a very recent development in STM spectroscopy which could lead to some chemical sensitivity. We will discuss this in the lecture on surface vibrations, section 9.5.

Suppose we know the chemical nature of the adsorbate. Can we then learn something about the adsorption geometry, or at least about the adsorption site? This is sometimes possible and done in the following way. Suppose we have a small adsorbate like an atom or a diatomic molecule. In the case of a small coverage we might be able to image the adsorbates and the substrate lattice at the same time. Then one can infer the adsorption site by comparing the adsorbate's position to those of the substrate atoms. Fig. 6.44 illustrates this idea. It is an STM images taken from the adsorption system S on Ni(100). One can clearly identify the lattice and the adsorbates and one would guess that the carbon atoms are adsorbed in a four-fold hollow site. However, one has to be careful since this strategy can go wrong very easily: suppose the Ni(100) surface is imaged such that the holes and not the bright spots correspond to the Ni atoms. Then carbon would be adsorbed in an on-top or even in a substitutional site.

Yet another aspect of adsorbates is the high sensitivity of STM towards surface contamination and defects. Note that a low contamination level of 1

percent, almost invisible in AES and XPS, at least for certain atoms, would show up rather drastically in an STM image if you take into account that it would mean one adsorbate atom in 10x10 substrate atoms.

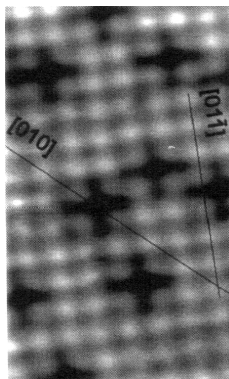


Figure 6.44: STM image of S adsorbed on Ni(100). Reprinted figure with permission from [42]. Copyright (1993) by the American Physical Society.

6.7.5 Adsorbate induced reconstruction of metal surfaces

STM can contribute a lot to the understanding of adsorbate induced reconstructions. Consider our example of the adsorbate system (2x1) oxygen on Cu(110). LEED has shown that this reconstruction consists of copper-oxygen chains in the first layer (see Fig. 6.21). STM can also reveal how the transport of substrate atoms needed for the reconstruction takes place. Fig. 6.45 shows a series of STM images taken as the reconstruction proceeds.

6.7.6 Semiconductor surfaces

Atomic resolution is much easier to get on semiconductor than on metal surfaces. The reason is the higher corrugation of the latter. STM can also be helpful to get some starting ideas about the complex structures in semiconductor reconstructions which can then be refined by a “real” structural analysis like LEED or surface x-ray diffraction. On the other hand, the more directional bonding in semiconductors should make the interpretation of STM images as pure atomic structure even more problematic than on metal surfaces. We give two examples with which we come back to the two Si structures discussed in connection with LEED.

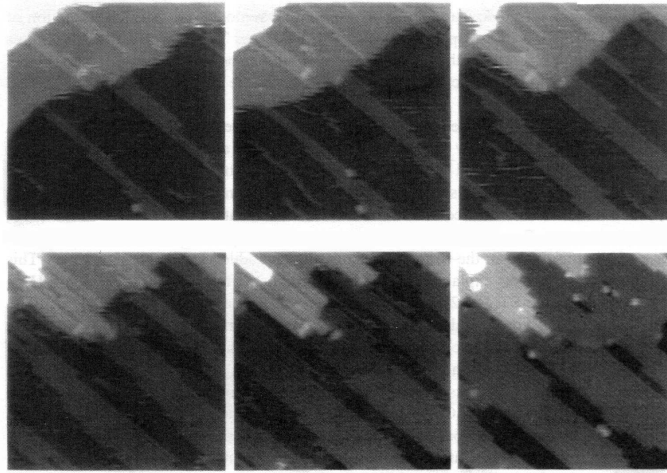


Figure 6.45: STM images taken during the oxygen adsorption on Cu(110). On the upper left corner of the first image two steps are seen. The grey lines perpendicular to the steps are due to the reconstruction. As more and more oxygen is adsorbed the reconstructed area increases but the steps are “eaten” away. This is clear evidence for the fact the the reconstruction is of added-row type with copper atoms stemming from the steps [43].

The Si(111)(7x7) reconstruction was among the first surfaces studied with STM. STM has contributed a lot to the understanding of this structure. Fig. 6.46 shows calculated STM images based on the superposition of atomic charges (equ. 6.28) together with the experimental data. Despite of all the shortcomings of this approximation it gives an almost quantitative agreement with Takayanagi’s model of the reconstruction.

A similar insight was gained for the (2x1) reconstruction of Si(100). First, it was found that the reconstruction consists of rows of dimers like in Fig. 6.21. Later, it was established that the dimers are buckled but this buckling might disappear at sufficiently high temperature. Fig. 6.47 shows an example of the atomically-resolved Si(100)-(2x1) structure. The asymmetry of the dimers is clearly evident. Unfortunately, the authors of the paper did not mention the temperature at which the experiment was done!

6.7.7 Insulator surfaces

It is obvious that STM is not the right tool to study the surfaces of insulators. A tunnelling current through the sample is not possible and the tip crashes into the sample upon approach. Like in all electron spectroscopy techniques,

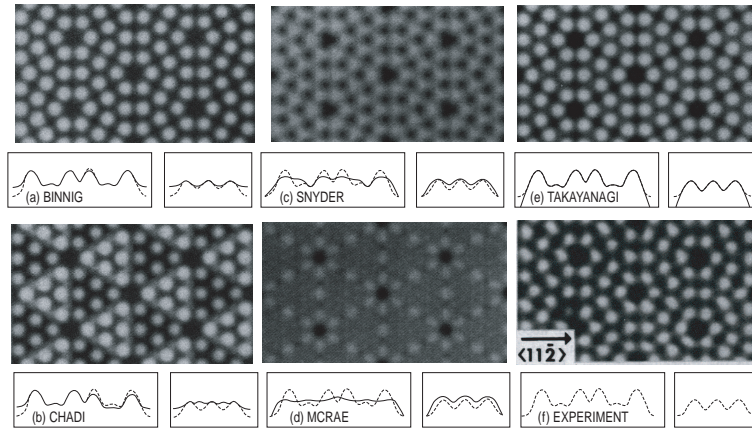


Figure 6.46: Calculated STM images for various models of the Si(111)(7x7) reconstruction and comparison to the experimental data. Images and two linescans through the images. Solid lines are calculations, dashed lines the data. Reprinted figure with permission from [44]. Copyright (1986) by the American Physical Society.

it helps to heat the sample in order to have (thermally activated) carriers. If a sufficient density of carriers is present in the bulk, one still has to choose the tunnelling voltage such that one can either tunnel into unoccupied states above the gap or out of occupied states below the gap. As an example, we discuss an STM investigation of the NiO(100) surface[46]. The sample was heated to about 200°C during the measurements, at room temperature no imaging was possible¹. Fig. 6.48 (a) shows an atomically-resolved empty state image of the NiO(100) surface, i.e. an image obtained with a positive bias voltage on the sample. It was argued, that the bright spots on the image correspond to the Ni ions. Fig. 6.48 (b) also shows an empty state image with a point defect in the middle. The previous Ni ions are still barely visible. A mesh is laid above the Ni ions. It permits the defect to be localized on a Ni site. The defect changes the contrast in the Ni ions surrounding it. This change is strong in the next-nearest neighbours, not in the nearest neighbours. This view is consistent with the present picture of covalent bonding in NiO shown in Fig. 6.48 (c). The bonding between the d states of the Ni atoms is achieved only through the p orbitals of the oxygen atoms in between. Since the p states on each oxygen atom are orthogonal, two simple cubic sub-lattices are formed which are displayed in different

¹Note that this temperature would not be sufficient to excite a reasonable of electrons over the 4 eV band gap in NiO. There must be more to the heating than just this.

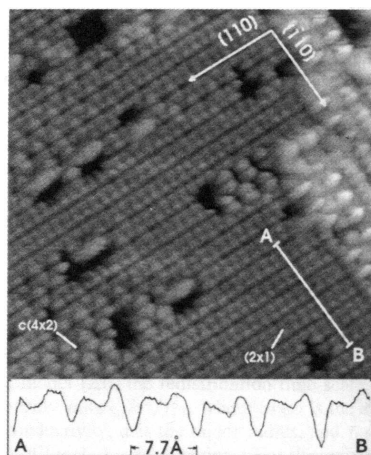


Figure 6.47: STM image of the Si(100)-(2x1) structure. The dimer rows are found along the (110) structure. A linescan across the dimers in the bottom of the figure shows their asymmetry. Reprinted figure with permission from [45]. Copyright (1995) by the American Physical Society.

shades in the figure. If a defect on a Ni site is created, it is obvious that the nearest neighbour Ni ions will not notice this very much but the next-nearest neighbours will. The STM image therefore confirms this picture of bonding in NiO.

6.7.8 Other applications and further instrumental development

STM can be applied to many other problems which can not be treated in this context. In interesting field is the dynamics of surfaces. One can learn a lot about diffusion and similar phenomena. With a fast STM, “movies” of changes on the surface can be taken.

A possible problem in the interpretation of STM images is the strong tip surface interaction due to the high electric field. One has to keep in mind that one does not necessarily observe the surface but the surface in presence of the tip. This disadvantage can also be turned into an advantage: one can use the tip to manipulate surface and/or adsorbate atoms and build artificial structures on the nanometre scale . One can for example write letters with the STM tip or create patterns of atoms to store information. It is, however, rather questionable if such techniques will ever be applied to something really useful because it simply takes too much time to build such structures.

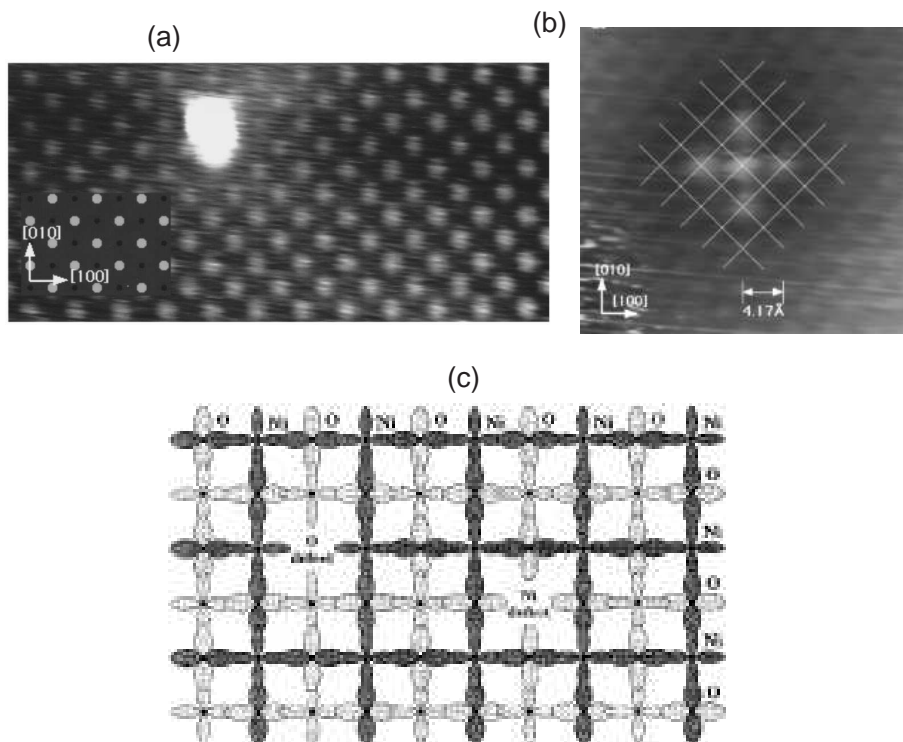


Figure 6.48: STM images taken on NiO(100). (a) atomically-resolved empty state image (b) atomically-resolved empty state image with a defect (c) sketch of the bonding in NiO. Reprinted figure with permission from [46]. Copyright (1997) by the American Physical Society.

Another field which has taken off considerably in the last few years is the use of scanning tunnelling spectroscopy (STS) where the tip is parked over a particular point on the surface and basically the tunnelling current is measured as a function of voltage. This opens the possibility to measure electronic effects on a very small scale but it is also difficult, since the STM has to be very stable. In addition to this, one *really* has to worry about the electronic structure of the tip when doing such an experiment. We will come back to STS in the lectures about surface electronic structure and surface vibrations.

Last but not least, there are interesting technical improvements. One is the development of scanning force microscopy . A scanning force microscope does not rely on a tunnelling current and can therefore also be used on insulators. Fig. 6.49 shows a sketch of such an instrument. The tip of the microscope is mounted on the end of a cantilever. As the tip is brought into

close contact with the sample, a force is exerted on the tip which leads to a small deflection of the cantilever. This deflection can be measured as a function of x and y coordinates in the same way as for the STM. Recent progress in this technique has yielded measurements with truly atomic resolution on some surfaces.

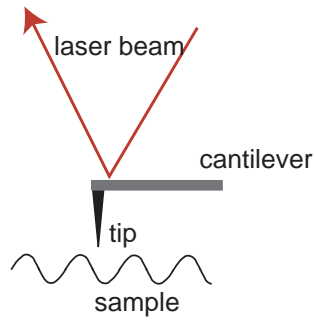


Figure 6.49: Principle of the scanning force microscope.

6.8 Further reading

For a discussion of surface thermodynamics, consult [3]. The basics of surface structure is discussed in [2]. A detailed discussion on LEED can be found in the same book but for more detailed information see [47][49][48]. A good review of photoelectron diffraction is [50]. There are many books about scanning tunnelling probe techniques by now. See for example [51]

Chapter 7

The electronic structure of surfaces

7.1 Work function

For all the following considerations, it will be relevant that materials have a work function, i.e. that one has to pay some energy in order to extract an electron from a solid. In a photoemission process, for example, the electrons lose kinetic energy as they cross the surface. Let's examine this a little further.

The workfunction of a metal is defined as the smallest energy needed to extract an electron at 0 K. Formally, this definition is made for an infinitely large crystal plane. One takes an electron from infinitely deep inside the crystal and brings it through the surface, infinitely far away into the vacuum. In practice, one wishes to avoid external fields and fields set up by the edges of the crystal. The definition is modified such that one brings the electron far away from the surface compared to atomic dimensions but not far compared to crystal dimensions. The energetics involved in this is displayed in Fig. 7.1. There are two potentials displayed. The first is the electrostatic potential $\phi(z)$. This potential changes a little when going into the crystal. The change is due to the surface dipole layer which is caused by the spill-out of the conduction electrons (see Fig. 2.5). The potential difference between inside and outside the crystal is called $\Delta\phi$. The other potential is the full one-electron potential $\nu_{eff}(z)$. This is obtained from the electrostatic potential by adding the exchange-correlation potential μ_{xc} . $\nu_{eff}(z)$ shows that the electron reaches a much lower total potential energy inside the crystal than that caused by the electrostatic part. This must be so, because the exchange and correlation will cause the electrons to go out of each others way and

therefore their potential energy will decrease. A lowering of potential energy goes along with an increase of kinetic energy. The zero for the kinetic energy if the bulk is different from the zero outside. The difference is the so-called inner potential $V_0 = \mu + \Phi$, i.e. the occupied band width plus the work function.

The chemical potential can now be referenced to the $\nu_{eff}(z)$ or to $\phi(z)$. It is called μ or $\bar{\mu}$, respectively. The workfunction, finally, is the difference between the Fermi level and the vacuum level. It is called Φ . We can write down an expression for the workfunction:

$$\Phi = \phi(+\infty) - \mu = \Delta\phi - \bar{\mu}. \quad (7.1)$$

The right hand side of this equation now allows us to think about the workfunction as being made of two parts. A surface-part $\Delta\phi$ and a bulk-part $\bar{\mu}$. Workfunctions of metals have values between about 1.5 eV and 5.5 eV.

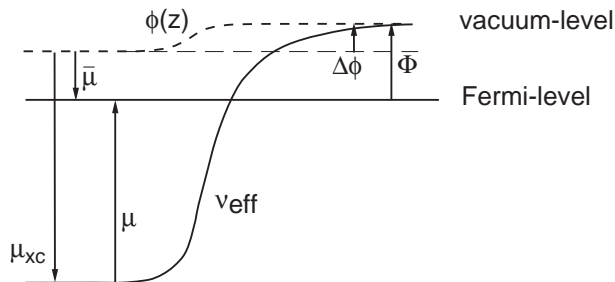


Figure 7.1: Definition of the energies contributing to the workfunction.

The surface part of the workfunction is of interest here because any change of the surface in terms of morphology or adsorption will be changing the workfunction. The workfunction (change) can be used as a fingerprint of the state the surface is in. Workfunction changes upon adsorption can be in the range of 100 meV to 1.5 eV for a full monolayer. One can measure workfunction changes within about 1 meV, so that this technique is very sensitive towards the state of the surface. We do not want to describe the technical methods used for measuring workfunctions here. We just give two examples for workfunction changes.

First we illustrate how the workfunction for a specific material depends on the surface orientation. Consider a closed packed and an “open” surface of some material. On the open surface we find the Smoluchowski effect of charge smoothing [28]. This smoothing leads to a dipole moment which opposes the dipole created by the flow-out of the electrons (see Fig. 7.2 and also Fig.

6.5). Hence, the work function of a closed packed surface will be higher than that of an open surface. This is illustrated in Fig. 7.3 for a number of W surfaces. The closed packed (110) surface has the highest workfunction.

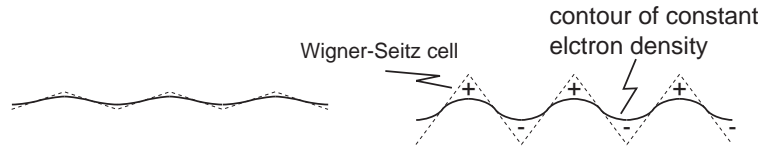


Figure 7.2: Charge distribution at a closed packed (left) and at an open (right) surface.

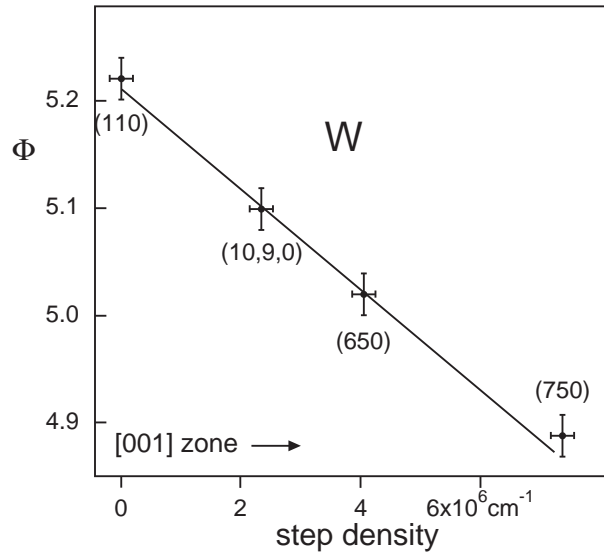


Figure 7.3: Workfunction of W for different surface orientations. After Ref. [52].

Another important example is the change of the workfunction upon adsorption. A famous case is the adsorption of alkali metals which drastically lowers the workfunction. We can immediately see why, considering the charge distribution of an alkali atom on a jellium surface (see Fig. 5.6). In very simple terms, the bond is ionic and the alkali metal gives an electron to the surface. This does also lead to a dipole moment which also opposes the spill-out of the electrons and reduces the workfunction. At low coverage, the dipole-dipole interaction between the alkali atoms will keep them far apart

and the workfunction decreases linearly as a function of coverage. At high coverage, the same interaction causes a depolarization of the dipoles and leads to a metallic bond. This increases the workfunction again by a small amount. Fig. 7.4 shows the workfunction change upon the adsorption of potassium on tungsten.

The workfunction change upon alkali metal adsorption can be very useful to calibrate the coverage. In the real world, adsorption can also be used to lower the workfunction of tungsten filaments such that they do not have to be heated so much to produce the same amount of electrons and therefore live longer.

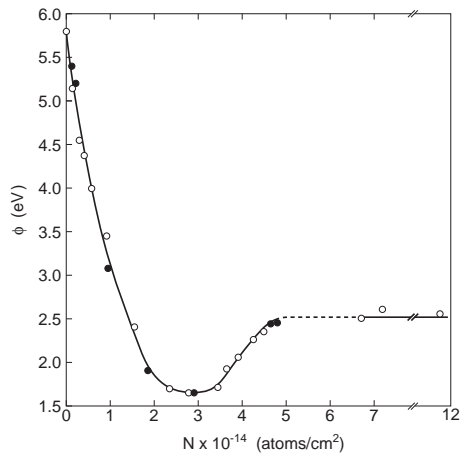


Figure 7.4: Workfunction change upon the adsorption of K on W(110). After Ref. [53].

7.2 Electronic surface states: basic ideas

In section 2.3.6 we have seen that one can obtain new solutions to the Schrödinger equation caused by the introduction of the surface. Inside the crystal they have the form

$$\psi_{\vec{k}}^-(\vec{r}) = u_{\vec{k}_{\parallel}}^-(\vec{r}_{\parallel}) e^{i\vec{k}_{\parallel}\vec{r}_{\parallel}} e^{-\kappa r_{\perp}} \quad (7.2)$$

with a complex wave-vector κ perpendicular to the surface. The new solutions decay exponentially both into the vacuum and into the bulk and are thus located at the surface and called surface states. They are characterized by the quantum number \vec{k}_{\parallel} and an energy $E(\vec{k}_{\parallel})$. k_{\perp} is not a good quantum

number any more because of the broken periodicity in the direction perpendicular to the surface. If we wish to relate surface states to bulk states in the reciprocal space we can think about the k_{\perp} of the surface state as a rod like in the Ewald construction known from LEED (Fig. 6.11).

It is important to realize that a true surface state can not be degenerate with any bulk state. By this we mean the following: For a true surface state with \vec{k}_{\parallel} and $E(\vec{k}_{\parallel})$ there can not be any bulk state with the same energy and \vec{k}_{\parallel} for any value of k_{\perp} , i.e. on the whole k_{\perp} -rod of the surface state. If there was such a state, the surface state could couple to it and penetrate infinitely into the bulk. It would not be a surface state any more.

This requirement gives a necessary condition for the existence of a surface state. We can illustrate it by introducing the concept of the projected bulk band structure. Fig. 7.5 shows the structure and Brillouin zone of the hcp metal Be and the surface Brillouin zone for the closed packed Be(0001) surface. Every point in the surface Brillouin zone is characterized by a \vec{k}_{\parallel} . For every point we can ask: at which binding energies are there bulk electronic states with this particular \vec{k}_{\parallel} and an arbitrary k_{\perp} somewhere in the bulk Brillouin zone. The answer to this question for many points along high-symmetry lines of the surface Brillouin zone is the so-called projected band structure. For Be(0001), it is shown in Fig. 7.6.

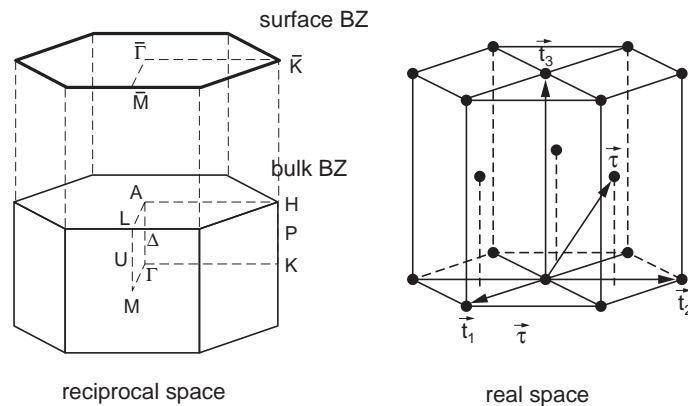


Figure 7.5: Real space structure and Brillouin zone of Be. The Be(0001) surface is the closed packed surface on top of the real-space hexagon. The surface Brillouin zone of Be(0001) is also shown. It is the projection of the bulk Brillouin zone in the (0001) direction.

In order to illustrate again how the projected band structure is formed, we calculate it for just one point, $\vec{k}_{\parallel} = (0, 0) = \bar{\Gamma}$, i.e. the centre of the

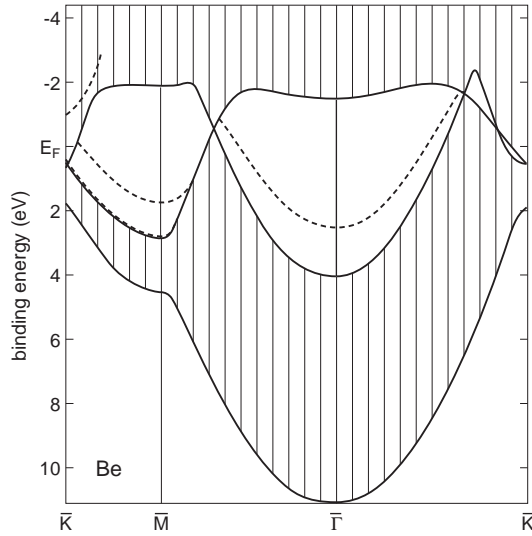


Figure 7.6: Projected bulk band structure and electronic surface states for Be(0001). For the shaded areas there are bulk states with the same \vec{k}_{\parallel} and energy for a k_{\perp} somewhere in the bulk Brillouin zone. After Ref. [54].

surface Brillouin zone. For this point we have to consider all the k-points in the bulk Brillouin zone with the same \vec{k}_{\parallel} . These points lie all along the $\Gamma - A$ direction of the bulk Brillouin zone. Now let us look at the bulk band structure in this direction in Fig. 7.7. There is a free-electron like band going from Γ to A , being folded back to Γ . For all energies between the bottom of the valence band and a binding energy of about 4 eV it is possible to find a value of k_{\perp} such that there is a bulk state with $\vec{k}_{\parallel} = (0, 0)$ and that energy. So there can not be any surface states. This energy range is also shaded for the $\bar{\Gamma}$ point, i.e. for $\vec{k}_{\parallel} = (0, 0)$ in Fig. 7.6. At higher energies, up to the Fermi level, there are no bulk states in the $\Gamma - A$ direction. There is a gap in the projected bulk band structure where a surface state could “live”. Fig. 7.6 does indeed show one as a dashed line.

A close inspection of Fig. 7.6 shows that there are also dashed lines (meaning surface states) which do go into the projected bulk band continuum, in contrast to what we have said above. These are bulk states with a high amplitude at the surface. They are called surface resonances .

There is also a completely different type of surface states which we should mention in a few words. Consider an electron in front of a metal surface. The screening properties of the metal can be described by a positive image charge in the metal which has an attractive interaction with the electron. One can

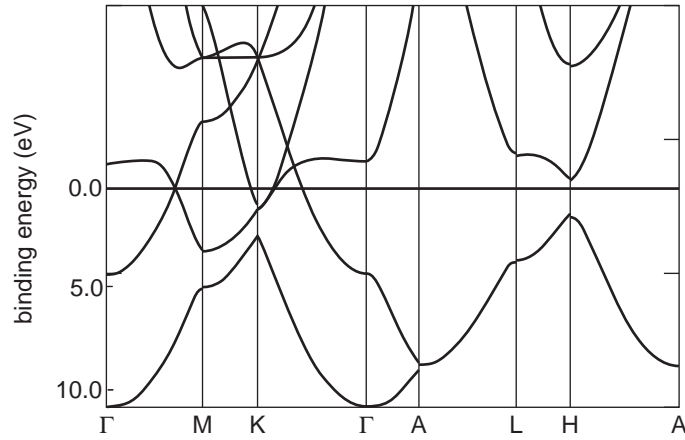


Figure 7.7: Bulk band structure of Beryllium. After [55].

describe this as if the electron moves inside an attractive Coulomb potential in front of the surface. Such a potential can actually support unoccupied bound states, so-called image potential states. These states lie above the Fermi energy of the solid but below the vacuum energy. This means that image potential states can be populated but the electrons in these states can not leave the solid.

7.3 Measuring the electronic structure of surfaces with angle-resolved photoemission

7.3.1 Introduction

In angle-resolved photoemission spectroscopy (ARPES) one illuminates a surface with UV light and detects the photoemitted electrons. The spectrometer is designed such that it accepts just a small solid angle and analyses the energy-distribution of the electrons emitted in that solid angle. As we shall see below, angle-resolved photoemission is *the* technique for the determination of surface (and bulk) band structures. It was developed in the mid 70s. Before, the photoelectron distribution from a sample was only measured in an angle-integrated way, i.e. $I(E_{kin}, h\nu)$. It was then that people realized that angle-resolved photoelectron spectroscopy $I(E_{kin}, h\nu, \Theta, \Phi)$ could be used to determine the occupied band structure of a crystal. The basic idea is very simple: one determines the energy and (all three components) of the \vec{k} vector of the emitted electrons. From this one tries to infer $E(\vec{k})$

inside the solid, i.e. the occupied band structure.

A necessary ingredient for the success of ARPES was the development of synchrotron radiation. As we shall see later, the ability to change the photon energy continuously is of high importance.

It is trivial but worth mentioning that photoelectron spectroscopy can only be used to study the occupied electronic states of the sample up to the Fermi level. The unoccupied states can be measured by a technique called inverse photoemission which is based on shooting electrons at a surface and detecting the emitted photons. This technique is not discussed in any detail here.

7.3.2 The photoemission process

Theory

In photoemission we are concerned with transitions from (occupied) initial states to free final states. The transition rate is given by Fermi's golden rule:

$$\frac{d\omega}{dt} = |\langle \Psi_f | \mathbf{H}' | \Psi_i \rangle|^2 \delta(E_f - E_i - h\nu), \quad (7.3)$$

where \mathbf{H}' is the perturbation Hamiltonian. For a system irradiated by light \mathbf{H}' can be written down by replacing \mathbf{P} in the original Hamiltonian \mathbf{H}_0 by $\mathbf{P} + (e/c)\mathbf{A}$ and adding the electrostatic energy due to the scalar potential. So the full Hamiltonian is

$$\mathbf{H} = \mathbf{H}_0 + \frac{e}{2mc}(\mathbf{A}\mathbf{P} + \mathbf{P}\mathbf{A}) - e\Phi + \frac{e^2}{2mc^2}|A|^2. \quad (7.4)$$

The last term is always small and can be neglected. Furthermore, one can always find a gauge where the scalar potential vanishes. So the differential photoionization cross section can be written as:

$$\frac{d\sigma}{d\Omega} \propto |\langle \Psi_f | \mathbf{A}\mathbf{P} + \mathbf{P}\mathbf{A} | \Psi_i \rangle|^2 \delta(E_f - E_i - h\nu), \quad (7.5)$$

or, using the commutator $[\mathbf{P}, \mathbf{A}] = -i\hbar\nabla\mathbf{A}$,

$$\frac{d\sigma}{d\Omega} \propto |\langle \Psi_f | 2\mathbf{A}\mathbf{P} - i\hbar\nabla\mathbf{A} | \Psi_i \rangle|^2 \delta(E_f - E_i - h\nu). \quad (7.6)$$

For not too high energies (< 1 keV or so), we can assume that $\nabla\mathbf{A}$ is small and can be neglected. This is true in the crystal and in free space but not necessarily at the surface. If we neglect this surface contribution for the moment, we can make the so-called *dipole-approximation* and use a constant

vector potential \mathbf{A}_0 . Using commutation relations the transition rate can be written:

$$\frac{d\sigma}{d\Omega} \propto | \langle \Psi_f | \mathbf{A}_0 \mathbf{P} | \Psi_i \rangle |^2 \delta(E_f - E_i - h\nu), \quad (7.7)$$

$$\frac{d\sigma}{d\Omega} \propto | \langle \Psi_f | \mathbf{A}_0 | \mathbf{r} | \Psi_i \rangle |^2 \delta(E_f - E_i - h\nu), \quad (7.8)$$

$$\frac{d\sigma}{d\Omega} \propto | \langle \Psi_f | \mathbf{A}_0 \nabla V | \Psi_i \rangle |^2 \delta(E_f - E_i - h\nu), \quad (7.9)$$

where V is the potential in the original Hamiltonian \mathbf{H}_0 . From the last equation it can already be seen that for a constant potential (free space, for instance) there is not photoemission. This is also obvious when we think about the requirement to conserve energy and momentum at the same time.

So far, we did not talk about the nature of the wave functions in the transition rate. They should be the exact many body wave functions of the system but it is more convenient to work in a single- particle picture. Let us write the ground state many particle wave-function as

$$\Psi_0^N = \phi_i \Psi_i^{N-1}, \quad (7.10)$$

where ϕ_i is the single-particle wave-function of the electron to be removed and Ψ_i^{N-1} is the properly anti-symmetrized determinant of the remaining $N - 1$ electrons. Similarly we write the final state as

$$u_k \Phi_{i,j}^{N-1}, \quad (7.11)$$

where u_k is the wave-function of the free electron and $\Phi_{i,j}^{N-1}$ are the possible states for the ionic system, i.e. the system with one electron missing. The notation is that there is an electron missing from orbital i and the ion is in the excited state j . Now the transition matrix element can be split up into a single and many-particle part:

$$\frac{d\sigma}{d\Omega} \propto | \langle u_k | \mathbf{A} \mathbf{P} | \Phi_i \rangle \langle \Phi_{i,j} | \Psi_i \rangle |^2 \delta(E_f - E_i - h\nu). \quad (7.12)$$

This turns into the single-particle picture if $\langle \Phi_{i,j} | \Psi_i \rangle = \delta_{i,0}$, i.e. when the electrons in the ionic state just remain where they have been before in the non-ionized state. But this is not the case. So when we project Ψ_i^{N-1} onto the eigenstates of the ionic system there will not only be overlap with the ground state but also with some of the excited states with j not equal to zero. If the system is left in an excited state there will be less energy available for the photoelectron. So-called satellite or shake- up lines will appear at higher binding energy (lower kinetic energy). We have already encountered this, less formally, in the section about XPS 4.3.

Photoexcitation from molecules

Photoemission from molecules can illustrate how simple symmetry considerations can be employed to learn something about the initial states. Consider a linear diatomic molecule like CO. The molecular orbitals can be classified into σ and π orbitals by their symmetry (see Fig. 5.7). The σ orbitals are rotationally symmetric around the main axis. The π orbitals have a change sign with a 180° rotation and have a nodal plane in the molecular axis.

Fig. 7.8 shows the calculated photoemission intensity for CO for photoemission from the 4σ initial state. The polarization vector and the detector are along the axis of the molecule which means that a final state of an electron reaching the detector must also have σ symmetry. This is consistent with the plotted intensity. A π initial state would lead to a zero photoemission intensity in the geometry. This method can be used to determine the orientation of molecules on a surface. We come back to this point later.

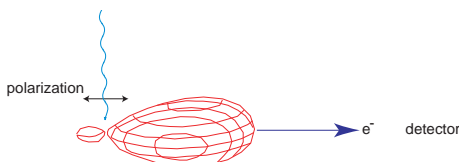


Figure 7.8: Photoemission from the CO 4σ orbital with polarized light. After Ref. [56].

Photo-excitation in a periodic potential

Let us discuss the photoemission process in the presence of a potential, like in a real crystal. We ignore the effect of the surface, i.e. the fact that the potential ends at some point.

The simplest case of a potential is a constant potential. The electronic states are free-electron like, i.e. $E = (\hbar^2 k^2 / 2m)$. The problem as illustrated in Fig. 7.9 is that energy and momentum can not be simultaneously conserved in this process because the momentum of the photons is so small ($\hbar\omega = \hbar ck$).

For a periodic potential, band gaps open at the zone boundary (extended zone scheme). Because of the periodicity in k , all the bands can be folded back into the first zone by adding a reciprocal lattice vector. In the reduced zone scheme vertical transitions are possible. Formally the momentum conservation has changed from $\vec{k}_f = \vec{k}_i$ to $\vec{k}_f = \vec{k}_i + \vec{G}$ where \vec{G} is a reciprocal

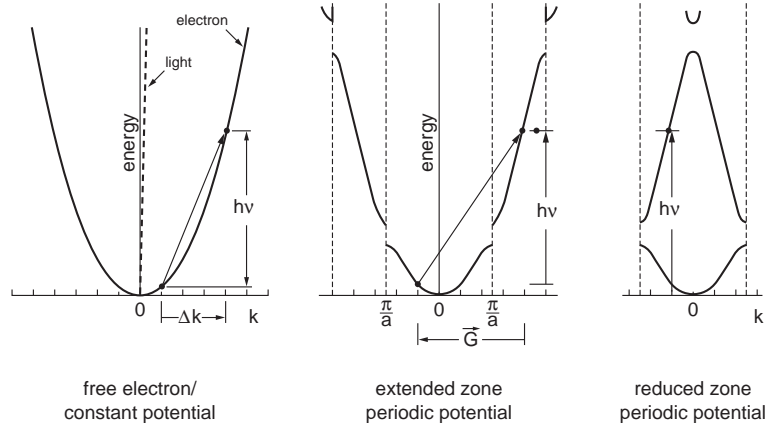


Figure 7.9: Momentum conservation in angle-resolved photoemission.

lattice vector. Note, that even the most simple vertical transitions are Umklapp processes in that they involve a reciprocal lattice vector. Formally this can be seen by putting the appropriate (Bloch) initial and final states in the photoemission matrix element:

$$| \langle \Psi_f | \nabla V | \Psi_i \rangle |^2 \delta(E_f - E_i - h\nu), \quad (7.13)$$

It is the gradient of the potential which provides the possibility of photoemission. A periodic potential has, of course, a non-vanishing gradient.

In this context it is interesting to mention the effect of the potential associated with the termination of the crystal, i.e. with the surface. In the most simple case this is a step. Then

$$\nabla V = \frac{\delta V}{\delta z} \vec{e}_z, \quad (7.14)$$

and the matrix element becomes

$$| \langle \Psi_f | \frac{\delta V}{\delta z} A_z | \Psi_i \rangle |^2 \delta(E_f - E_i - h\nu). \quad (7.15)$$

The step perpendicular to the surface chooses only the perpendicular component of \mathbf{A} . The step can provide any momentum \vec{k} in the direction perpendicular to the surface since its Fourier transform contains all possible frequencies. Therefore the \vec{k} -vector component perpendicular to the surface k_\perp is not conserved but the component parallel to the surface \vec{k}_\parallel still is.

7.3.3 Instrumentation

There are two commonly used light sources in UV photoemission. One is a gas-discharge lamp in which a noble gas discharge is taking place in a high electric field. The light is guided into the UHV chamber by a quartz-glass tube with a tiny hole (to avoid a high noble-gas pressure in the chamber). The lamp is differentially pumped. The other light source is synchrotron radiation. Its most important advantages are tunability and polarization.

The most common electron analysers are hemispherical analysers like discussed in an earlier lecture. The angular resolving capability of such analysers can be achieved by a small hole (aperture) in the entrance or by an electrostatic lens. For ARPES it is important to change the angle of emission in order to change \vec{k}_{\parallel} . This can be done by either moving the sample or the analyser. Moving the sample with the required precision is very difficult. A common way to change the angles is to mount the analyser on a goniometer in the chamber.

7.3.4 The three step model

An intuitive and often-used way to look on photoemission is the so-called three step model.

1. A photon is absorbed in the crystal by an electron. The electron is excited from an occupied initial to an unoccupied final state.
2. The excited electron is brought to the surface taking into account the direction of propagation of the final state and the mean free path.
3. The electronic wave function of the final state is matched to a free-electron wave function outside the solid.

In the last step the electron has to overcome the potential barrier at the surface. For the kinetic energy of the electron this means that it will be lower in the vacuum since the potential energy is higher.

It is important to notice that the whole system of semi-infinite solid and vacuum has a translational symmetry only parallel to the surface. Therefore the \vec{k} -vector parallel to the surface \vec{k}_{\parallel} is a good quantum number and is conserved during the photoemission process.

This is not true for the perpendicular component of \vec{k} . k_{\perp} is not determined by the photoemission experiment. The most severe change in k_{\perp} happens because of the kinetic energy change which leads to a refraction at the surface barrier (see Fig. 7.10). We have encountered this process already in our discussion about LEED. The picture may imply that k_{\perp} is merely changed during the transmission of an electron through the surface but that it is still well defined. Unfortunately, this is not the case. The symmetry

breaking normal to the surface means that k_{\perp} is not a well-defined quantity any more.

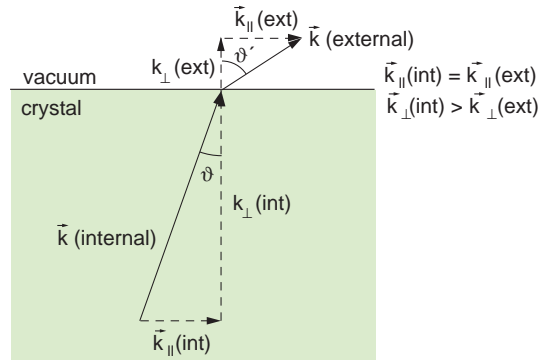


Figure 7.10: Refraction at the surface potential barrier.

7.3.5 Band mapping: 2d bands and 3d bands

How is angle resolved photoemission now used to determine band structure, i.e. to determine $E_i(\vec{k}_i)$? Let's follow the three step model.

1. An electron is excited from an initial state with energy E_i to a final state with energy E_f .

In the reduced zone scheme this excitation is vertical with $\vec{k}_f = \vec{k}_i$. In the (more appropriate) extended zone scheme we have

$$\vec{k}_f = \vec{k}_i + \vec{G} \quad (7.16)$$

2. The final state electron is transmitted through the crystal. It may get lost on the way but at this point we don't really care about those electrons which get lost.

3. The electron is transmitted through the surface. This costs kinetic energy due to the work function.

We measure \vec{k} and E_{kin} of the electron in the vacuum. If k_{\perp} was conserved then we would directly obtain the energy and \vec{k} of the initial state. This would solve the experimental task of band-structure determination. Unfortunately, we just get information about the initial state energy and the wave vector component parallel to the surface.

The problem can safely be ignored in the case of a two-dimensional sample. There, only \vec{k}_{\parallel} is of interest anyway. The most important example for this in our context is the dispersion of an electronic surface state

$E(\vec{k}_{\parallel})$. But there are also other important cases of two-dimensional or quasi two-dimensional systems, namely layered materials. The most common is graphite. Others are transition metal dichalcogenides like MoS₂. Other quasi two-dimensional materials of great current interest are transition metal perovskite oxides. The cuprate high T_C superconductors are members of this family.

A classical example for band mapping in two dimensions is the free-electron surface state on Cu(111). It exists in the necks of the bulk Fermi surfaces. Fig. 7.11 shows this surface state seen with ARPES as the angle of emission is varied. The data shown in the left-hand part of Fig. 7.11 consists of so-called energy distribution curves (EDCs). In an EDC the photoemission intensity is measured as a function of electron kinetic energy at a fixed emission direction and photon energy. The electronic states show up as peaks in an EDC. As the emission angle is varied, the binding energy of the peak changes. In the present case the binding energy decreases for higher off-normal angles. Eventually, the peak disappears because it crosses the Fermi level and turns into an empty band. On the right-hand side of 7.11 the same data is displayed as a grey-scale plot. Such plots are common today and are made possible by technical progress which permits taking large data sets with many angles.

It is easy to infer the bands structure:

$$\vec{k}_{\parallel i} = \vec{k}_{\parallel f} = \sin(\Theta) \sqrt{\frac{2m}{\hbar^2}} \sqrt{E_{kin}} = \sin(\Theta) \sqrt{\frac{2m}{\hbar^2}} \sqrt{h\nu - E_{bin} - e\Phi} \quad (7.17)$$

Θ is the emission angle as defined in Fig. 7.11. E_{bin} is the binding energy, measured with respect to the Fermi level. E_{kin} is the kinetic energy of the electrons outside the solid, measured with respect to the vacuum level. This definition of the energy zeros is of practical importance. As we shall see later, the Fermi edge shows up in many photoemission spectra such that the binding energy of a peak can be read directly from the spectrum as the difference between the peak position and the position of the Fermi edge. From this binding energy, the kinetic energy outside the solid can be calculated by simply subtracting the work function Φ (see Fig. 7.1). The work-function Φ must be obtained by some other technique (this can also be done by photoemission).

After having read the binding energy from the spectrum, equ. 7.17 can be used to calculate $\vec{k}_{\parallel i}$ and one obtains the desired dispersion $E_{bin}(\vec{k}_{\parallel i})$ which is shown in Fig. 7.12.

Let us return to the problem of determining the band-structure of a three-dimensional solid. How can we circumvent the problem with k_{\perp} ? We restrict

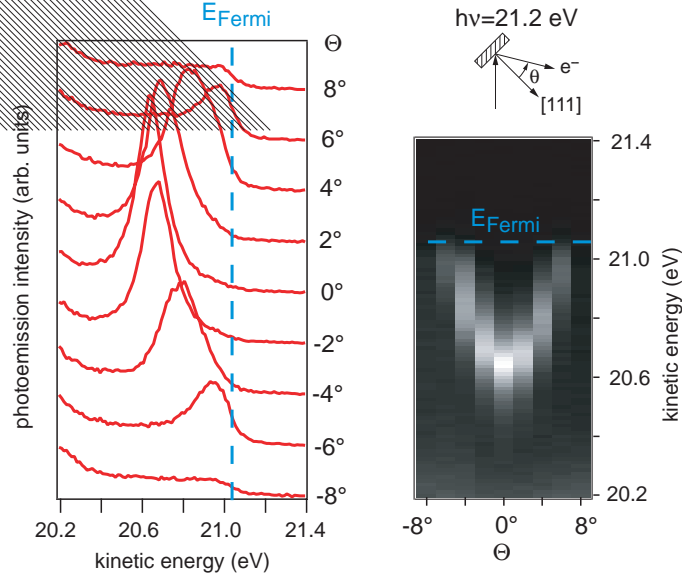


Figure 7.11: Surface state dispersion on Cu(111). Left: EDCs close to normal emission. The dispersion of the surface state is clearly evident. Right: Grey-scale image of the same data.

ourselves to normal emission geometry. This makes things easy, mainly because the component of the wave-vector parallel to the surface is 0:

$$\vec{k}_{\parallel f} \propto \sin(\Theta)\sqrt{E_{kin}}, \quad (7.18)$$

independent of the kinetic energy of the electrons. Note that if we take an EDC in any other geometry, the \vec{k}_{\parallel} -vector is different for every point in the spectrum because the kinetic energy is different but this is not so for normal emission.

Fig. 7.13 shows normal emission data from Be(0001) for various photon energies. There are two peaks. One changes its binding energy as the the photon energy is changed, the other does not. The latter is a surface state which we will discuss later. The first state is a bulk state. We do not know the exact value of k_{\perp} but we do see that the dispersion reaches two extrema, at about 33 eV and 99 eV photon energy. These extrema correspond to high-symmetry extrema in the band structure. Consider again the Brillouin zone of Be in Fig. 7.5. For normal emission from the (0001) closed packed surface the initial states lie on the $\Gamma - A - \Gamma$ rod. The moving peak has a smallest binding energy of about 5 eV at 99 eV photon energy. This

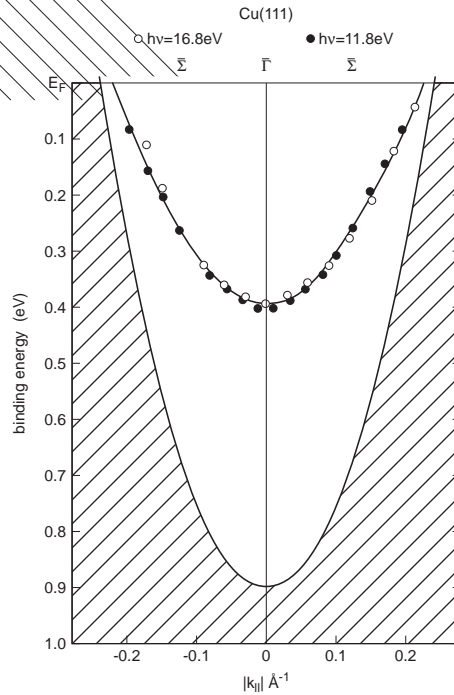


Figure 7.12: Surface state dispersion on Cu(111). After Ref. [57].

extremum corresponds to the band with the lowest binding energy at the Γ -point in the band structure of Fig. 7.7. The other extremum at 33 eV corresponds to the band with the highest binding energy, also at Γ .

This example illustrates how ARPES can be used to determine the energies of extrema in the dispersion of the three dimensional bulk band structure. If further assumptions about the final states are made, it is also possible to figure out the actual dispersion of the bands in between these extrema. We do not wish to go into the details of this here but an example is given in Fig. 7.14. It is a band structure determination of Cu in two bulk high symmetry directions. The left part is taken in normal emission from Cu(111) and the right part from Cu(110). The triangles and circles are obtained with different polarizations.

7.3.6 Some surface states investigated by ARPES

Before we start giving specific examples, here are a few important general practical considerations. Suppose we have measured an EDC from a surface and we find peaks in that spectrum. How do we know if a peak is due to a

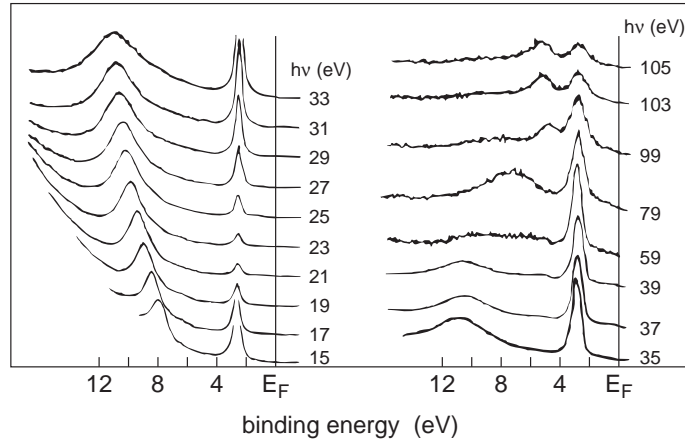


Figure 7.13: Normal emission spectra from Be(0001) taken with different photon energies. After Ref. [58].

surface state? We give some criteria and discuss them:

1. The surface state must lie in a gap of the projected bulk band structure.
2. If we take spectra with different k_{\perp} but the same \vec{k}_{\parallel} , for example by changing the photon energy in normal emission, the surface state peak has to stay at the same position in the spectrum while bulk related peaks will in general disperse. This effect is illustrated in Fig. 7.15.
3. Surface states should be sensitive to surface contamination.
4. This is not a real criterion: "Surface states tend to be sharp peaks".

The reason for (1) was that the surface state must not mix with a bulk state. Otherwise it would not be a genuine surface state. This requires some more discussion. Actually the surface state does not have to lie in a real projected bulk band gap. It is sufficient that it lies apart from states it can mix with. This subtle difference means that it can lie in a region of bulk bands with another symmetry. Sometimes strong and obviously surface-related features can be found in regions of degenerate bulk states with the same symmetry. These features could be either surface resonances, i.e. states which penetrate deeply into the bulk but have a strong amplitude at the surface, or the investigator could be misled by a band structure calculations which places the bulk band gap edges at positions which are actually not right.

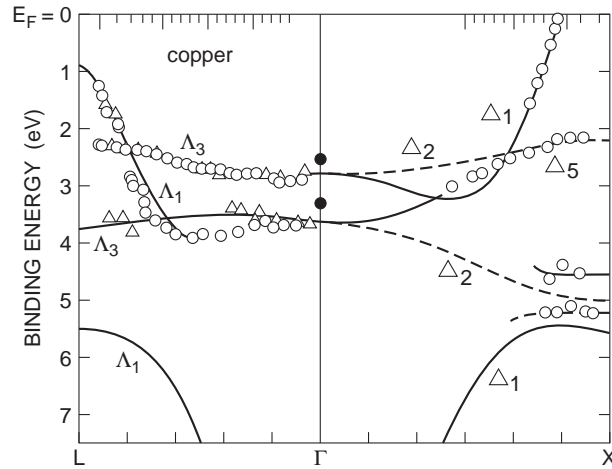


Figure 7.14: Band structure of Cu determined using photoemission and free electron final states. The lines are theory. After Ref. [59].

A nice demonstration of (2) was the set of Be(0001) spectra taken at different photon energies shown in Fig. 7.13. It is evident that the binding energy of the surface state is independent of the photon energy and k_{\perp} while the binding energy of the bulk state is not.

Point (3) is a little tricky. It should be possible to severely change the appearance of a surface state in a spectrum by putting impurities on the surface or by creating disorder. This is indeed a nice test: many surface states can be "killed" by adsorbing small amounts of contaminating atoms. However, some care is needed: A change in the surface cleanliness or order can also affect the intensity of bulk transitions. Fig. 7.16 shows an example: a Bi surface which supports a surface state is measured twice: once well-ordered and once after sputtering without annealing. The alleged surface state peaks decreases a lot in intensity. But the other peaks change, too.

The last point (4) is not a real criterion: it is often found that surface states are very sharp peaks in the photoemission spectrum. The reason is related to the fact that surface states have no dispersion with k_{\perp} . Such a dispersion, combined with the uncertainty in k_{\perp} leads to a considerable broadening of the bulk peaks which is not present in the case of surface states.

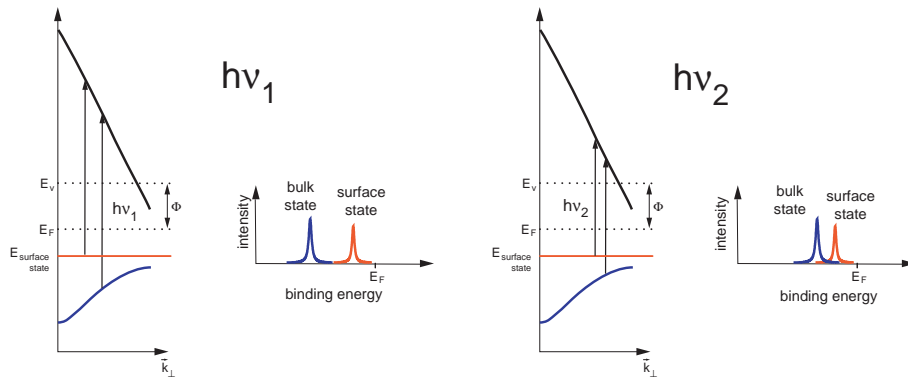


Figure 7.15: When taking a spectrum with two different photon energies but for the same \vec{k}_{\parallel} , bulk-related peaks will in general show a dispersion in the spectrum while surface state peaks stay at a fixed binding energy. One can think of the surface state as being present for all values of k_{\perp} , similar as in the Ewald construction in Fig. 6.11. See also Fig. 7.13.

Clean metal surfaces

In the foregoing discussion we have already seen three examples for surface states on metals (Be(0001), Cu(111) and Al(001)). In all three cases the surface state band was derived from the s-p band of the metal. The states are fairly delocalized and can be described in a nearly-free electron model. Historically these states are known as Shockley states. One can also, of course, approach the question of surface states from the opposite viewpoint, namely in a tight-binding picture. There the atomic orbitals which stick into the vacuum because the atoms' neighbours have been cut off, have very different electronic properties than the equivalent bulk orbitals and represent surface localized states. This kind of more localized surface state is called Tamm state. Examples of Tamm states can also be found on metals. One is a surface state which is derived from the Cu(100) *d*-band and shown in Fig. 7.17.

We should also mention that *s*–*p* surface states do not necessarily have to have a free electron like dispersion around the $\bar{\Gamma}$ point like in all our previous examples. We will discuss an example in the exercises.

Adsorbate covered metal surfaces

Angle resolved photoemission can of course also be used to probe the modification to the surface electronic structure which is induced by adsorption.

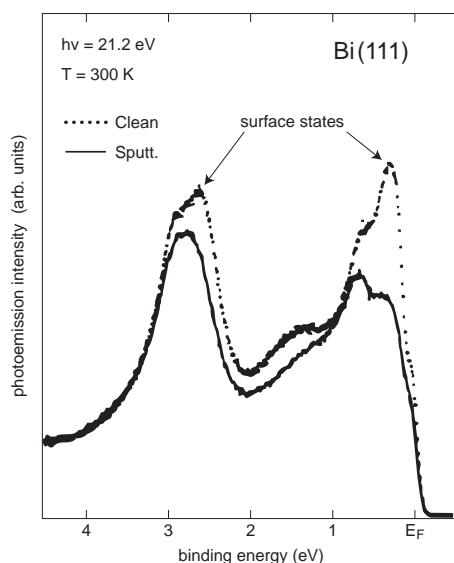


Figure 7.16: Spectra from well-ordered and sputtered Bi surface. After Ref. [60].

The electronic states of the atoms and molecules on the surface are changed from the gas phase due to the bonding. These adsorbate states may be viewed as extrinsic surface states.

Fig. 7.18 shows two spectra taken from CO on Ni(100). Both are taken in normal emission but the direction of the polarization vector is different. There are peaks found in the spectrum which are not present on the clean surface and which are related to the CO. A comparison with the energy of the peaks from the gas phase CO can be used to identify the peaks. When the polarization vector is parallel to the surface no σ peaks are found. This means that the molecular axis is perpendicular to the surface: then the light has π symmetry, the final state has σ symmetry and only π symmetry states are allowed as initial states. In this way the orientation of adsorbed molecules can be determined.

Another example involving CO adsorption illustrates what one can learn about intermolecular interactions. We have already mentioned that these interactions can (and do) often lead to ordered adsorbate structures. In an ordered structure the interactions between the molecular orbitals will lead to a two dimensional overlayer band structure which can be investigated by ARPES. A particularly interesting orbital for studying these interactions is the 4σ orbital because it often has a higher binding energy than all the electronic states in the substrate and does therefore not mix strongly with

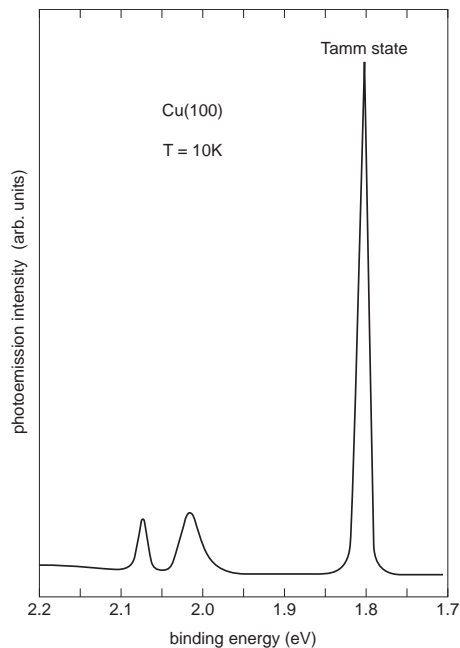


Figure 7.17: Tamm-surface state on Cu(001). After Ref. [61].

the substrate states. Fig. 7.19 shows the measured and calculated (by a tight-binding scheme) dispersion of the band derived by the 4σ state in the adsorption systems $(2\sqrt{3} \times 2\sqrt{3})R30^\circ\text{CO-Co}(0001)$ and $(\sqrt{3} \times \sqrt{3})R30^\circ\text{CO-Co}(0001)$. The sizes of the two Brillouin zones have been artificially made equal for a more convenient comparison. There is indeed a dispersion of the electronic states due to the intermolecular interaction. Furthermore, the close-packed structure shows a considerably larger bandwidth caused by the stronger interaction. Note, that the $(2\sqrt{3} \times 2\sqrt{3})R30^\circ\text{CO-Co}(0001)$ structure has a higher coverage ($\Theta = \frac{7}{12}$ ML) and thus closer intermolecular distance than the $(\sqrt{3} \times \sqrt{3})R30^\circ\text{CO-Co}(0001)$ structure ($\Theta = \frac{1}{3}$ ML).

Semiconductor surfaces

In the discussion of surface structure we have already seen that semiconductor surfaces tend to reconstruct in complicated ways rather than staying bulk terminated. This fact is very closely related to the electronic structure of the semiconductor surfaces as we shall see below. This close relation, combined with the difficulties of solving the semiconductor structures with LEED has lead to a very different aspect in the application of photoemission. Many important semiconductor structures have, in fact, been solved, at least ap-

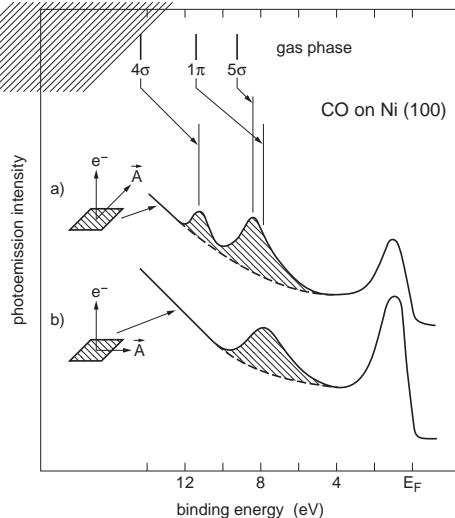


Figure 7.18: Photoemission from CO on Ni(100). After Ref. [62].

proximately, by comparing the measured dispersion of the electronic surface states to various models.

For understanding the surface states on semiconductors, let us look at the bonding in these materials first. The elemental semiconductors Si and Ge and many of the common compounds such as GaAs have a tetrahedral bonding geometry in common, i.e. each atom is bound to four neighbours with sp^3 hybrid orbitals. Although the bonding can be partly ionic in some materials, this strongly directional view is very instructive. When a surface is formed, the sp^3 hybrid bonds are cut and dangle into the vacuum. What about the electronic states derived from these dangling bonds? Suppose we have one dangling bond per unit cell. In a band structure picture we can describe the dangling bond state by a band. If the band is fully occupied it can accommodate two electrons. But the dangling bond state has only one electron and hence the band has to cross the Fermi level such that only one half of the surface Brillouin zone has occupied states due to the dangling bond. In other words, the semiconductor's surface is metallic! In the real world this does not happen very often. The dangling bonds don't like to dangle alone and the semiconductor surfaces reconstruct in complicated ways to get rid of the dangling bonds.

This concept can be illustrated nicely by the (2x1) reconstruction of Si(111). This reconstruction is obtained when Si(111) is cleaved at room temperature. It is a meta-stable structure since annealing the crystal to high temperature causes an irreversible phase transition into the (7x7) structure.

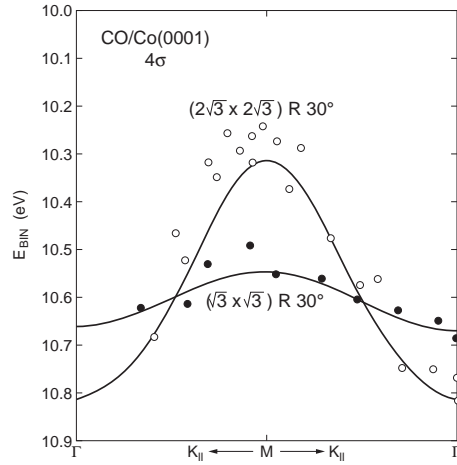


Figure 7.19: Dispersion of the CO 4σ state for $(2\sqrt{3}\times 2\sqrt{3})R30^\circ$ CO-Co(0001) and $(\sqrt{3}\times \sqrt{3})R30^\circ$ CO-Co(0001). After Ref. [63].

Let's consider the bulk terminated structure of Si(111). There is one dangling bond in the surface Brillouin zone (see Fig. 6.22) so that we have precisely the scenario discussed above, a metallic surface with an energetically unfavourable dangling bond. What happens if we introduce a (2x1) reconstruction is shown in Fig. 7.20). The larger surface unit cell leads to a surface Brillouin zone of half the original size. The new Brillouin zone boundary causes the familiar band splitting. If the original dangling bond state has a Fermi level crossing at the new boundary, the reconstruction divides the band up in one which is completely occupied and one which is completely unoccupied. It is immediately evident that energy is gained by this reconstruction because the occupied states in the vicinity of the zone boundary have lowered their kinetic energy. The surface is now semiconducting.

The actual surface geometry of the Si(111)-(2x1) reconstruction has been disputed for a long time. The model favoured now is the so-called π -bonded chain model. A previous favourite has been a buckling model. Both are shown with the calculated of surface states in Fig. 7.21. Both models lead to a semiconducting surface behaviour as expected. But there are qualitative differences. The band-width for the π -bonded chain model is larger than for the buckling model. This is consistent with intuition because the close neighbourhood of the atoms responsible for the bands should lead to a larger bandwidth. The dispute over the right model was eventually solved by ARPES. Fig. 7.22 shows the convincing agreement between experiment and theory for the π -bonded chain model.

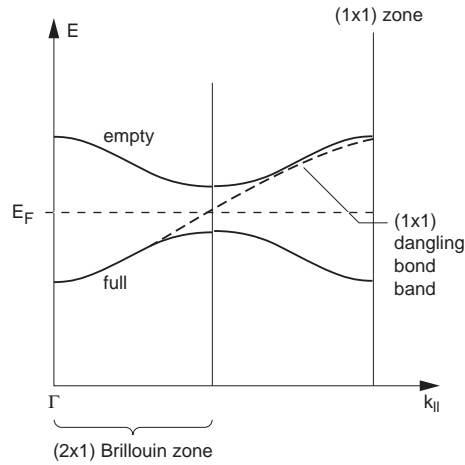


Figure 7.20: (2x1) reconstruction on Si(001).

Another interesting example of a semiconductor reconstruction is the Si(100)-(2x1) structure. Let us look at it again first with simple electron counting arguments. Si(100) has two dangling bonds per surface unit cell which are located on the same atom. In the (2x1) unit cell one would find four dangling bonds, i.e. four electrons on two atoms. These could be distributed for example in two filled electronic bands. A first result from photoemission was that a reconstruction in which two surface atoms are paired to form dimers is in better agreement with the experimental data (shown in Fig. 7.23) than other models. The disputed question is whether the dimers are symmetric or asymmetric. In a dimer-type reconstruction, two of the four electrons are used to form the dimer bond. They are in a stable configuration and give rise to the low-lying surface state band S_3 in Fig. 7.23. The question of a symmetric or asymmetric dimer mainly influences the electronic states of the remaining two electrons localized on each surface dimer. Fig. 7.24 shows that the symmetric and the asymmetric dimers lead to very different theoretical predictions. In the asymmetric dimer model, there is a considerable charge-transfer from the “down” atom to the “up” atom. The model gives rise to two well separated bands. Since we have two electrons left this corresponds to a non-metallic surface, consistent with all experimental data. The symmetric dimer also gives two bands but the bands overlap meaning that the surface has to be metallic. A detailed comparison of the measured dispersion of the S_2 state with more modern calculations shows a good agreement favouring the asymmetric dimer. However, there are still many open questions in this complicated problem for example concerning the nature of

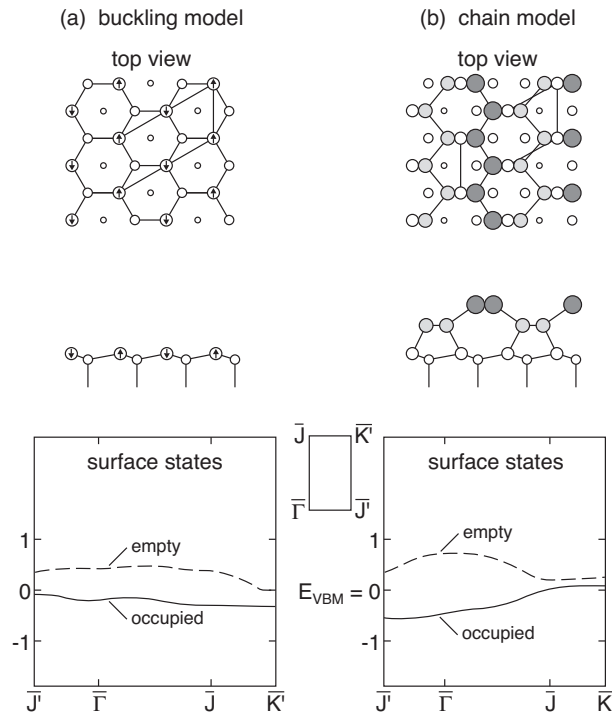


Figure 7.21: Two possible models for the (2x1) reconstruction of Si(111) and their electronic surface state dispersion. Note that the energy zero is the valence band maximum and not the Fermi energy. Both surfaces are semiconducting. After Ref. [64].

the S_1 surface state which should not appear in an asymmetric dimer model.

In the case of a doped semiconductor, the existence of surface or interface states in the gap can have a dramatic effect on the electronic structure rather far away from the surface. Consider the situation shown in Fig. 7.25 (left). We have an n-doped semiconductor which supports two surface state bands, one empty and one occupied, with the Fermi level in between. The bulk Fermi level is set such that it is close to the conduction band. The position of the surface states in the gap is such surface Fermi level lies at a much lower energy than the bulk Fermi level. This is an unstable situation because it brings bulk donors above the surface Fermi level. Electrons from the donors will flow into the previously unoccupied surface state and partially fill it. At the same time, they will leave a layer of positively charged bulk donors behind. This will go on until the energy gain by filling up the lower-lying states is equal to the energy cost for setting up an electric field in the surface

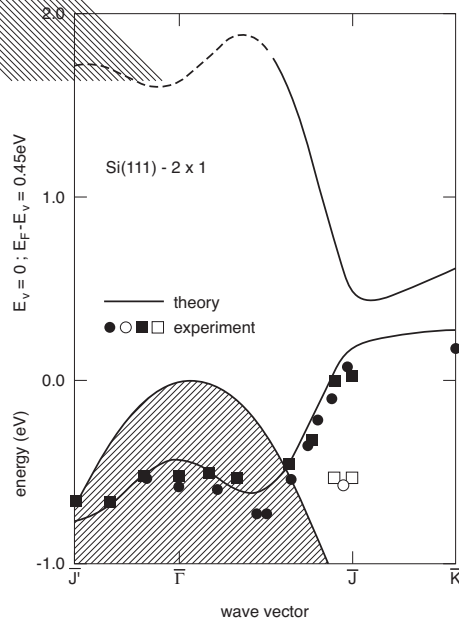


Figure 7.22: Comparison between experiment and theory for the π -bonded chain model of Si(111)-(2x1). After Ref. [65].

region. In the end, the Fermi level is constant over the whole crystal and surface like in Fig. 7.25 (right). One can also think about this effect as a band bending in the surface region of the crystal. Bulk donor levels are ionized because the electrostatic field lifts them over the Fermi level. The ionized bulk donors represent a positive space charge. This positive space layer can extend very deeply into the surface because the density of bulk dopants parallel to the surface (between 10^8 and 10^{12} cm^{-2}) is much lower than the density of surface states (about 10^{15} cm^{-2}). The layer is called a depletion layer

This effect has some interesting consequences. The first is, that one can use a heavily doped semiconductor to study states with ARPES which would be unoccupied if the semiconductor were intrinsic. Another, less pleasant, aspect is that in lightly doped semiconductors without intrinsic surface states in the gap, very small quantities of adsorbates might induce sufficient states in the gap to induce a band bending. This is a real problem because it shifts the whole spectrum with respect to the Fermi level (the reference level for the spectrometer).

A related consequence is the so-called Fermi level pinning by surface states in the gap shown in Fig. 7.26. In the bulk the Fermi level can be changed

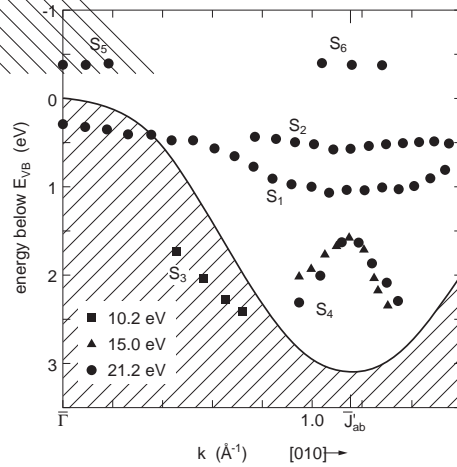


Figure 7.23: Experimental surface band structure from Si(100)-(2x1) in the $\bar{\Gamma} - \bar{J}'$ direction. After Ref. [66].

from just below the conduction band to just above the valence band by changing the doping. One would expect that the workfunction, i.e. the distance between the Fermi level and the Vacuum level would follow this change. But for certain surfaces with states in the gap this is not the case. Upon n-doping, a depletion layer is build up and the surface states are charged negatively. This dipole layer slows down the electrons from the bulk and this almost exactly compensates the gain of kinetic energy due to the higher Fermi level. In the end, the measured Fermi level is almost independent of the doping level. This effect is called Fermi level pinning.

It is clear that the forgoing discussion is only relevant for semiconductors. Space charge regions do not exist for metals because of the good screening in a metal. The conduction electrons will screen away the surface such that everything looks like bulk already after a few \AA (see Fig. 2.5).

Semimetal surfaces

We have seen that there is a big difference between the surfaces of metals and those of semiconductors. In most metals, covalent bonding is unimportant and most surfaces do not show reconstructions. On semiconductors the opposite is found. Creating the surface requires the breaking of covalent bonds and leaves so-called dangling bonds which could give rise to half-filled and therefore metallic bands. However, it turns out that on most semiconductor surfaces the atoms reconstruct such that the dangling bonds are removed and the surface is again a semiconductor, not a metal. Semimetals lie in between

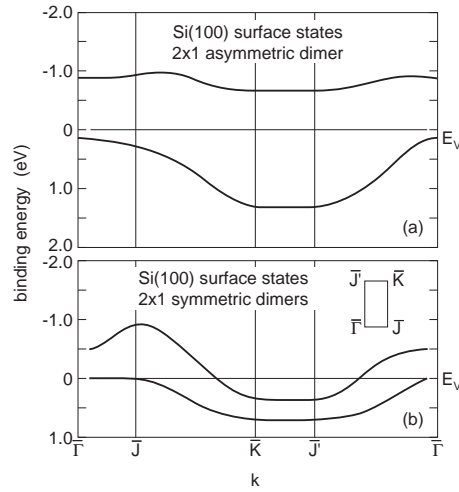


Figure 7.24: Calculated dispersion for the upper surface states of Si(100)-(2x1) for a symmetric and an asymmetric dimer configuration. After Ref. [68].

these two cases. On one hand, a semimetal is close to being a semiconductor since directional bonding is important and the valence and conduction bands are almost separated by a gap. On the other hand, a very small overlap between both bands is found at some point of the Brillouin zone such that the material is formally a metal. This delicate balance between being a metal and a semiconductor depends crucially on the structural details and is disturbed severely at the surface. A semimetal surface can be expected to turn either into a better metal or into a semiconductor. The former case is more interesting because a good metallic surface on a semimetal (or, indeed, on a semiconductor) can be taken as a model for a nearly two-dimensional metal.

The (110) surface of Bi is such a case. The truncated bulk structure is such that one dangling bond can be found in a surface unit cell containing two atoms. This relatively low density of dangling bonds is not sufficient to drive a reconstruction. Therefore the surface is a good metal, in contrast to bulk Bi. Photoemission data from Bi(110) is shown in Fig. 7.27 together with a bulk band structure projection. The data is presented in a way which is different from what we have seen so far. Very many EDCs have been taken for \vec{k}_{\parallel} points along all the high symmetry lines of the surface Brillouin zone. The plot shows the logarithm of the photoemission intensity as a function of \vec{k}_{\parallel} and binding energy. This presentation has the advantage that the dispersion is directly seen. Among other things, several surface state Fermi

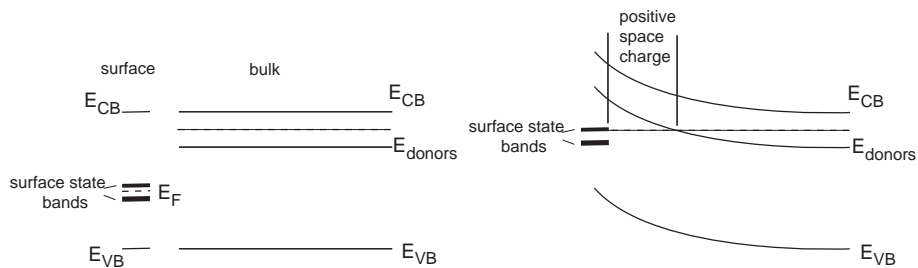


Figure 7.25: Left: Surface state bands in the bulk gap and bulk electronic structure of an n-doped semiconductor. The situation is unstable because of the non-constant Fermi level. Right: electrons from the bulk donors flow into the previously unoccupied surface states and leave a positive space charge layer behind.

level crossings are observed.

7.4 Scanning Tunnelling Spectroscopy

In the structure lecture we have only discussed the ability of the STM to provide topographic information. It is evident, however, that one can also use the STM in a spectroscopic mode in order to learn something about the density of states of the sample. This approach is called scanning tunnelling spectroscopy (STS). STS experiments are usually carried out by parking the tip at a fixed distance over the surface and measuring the tunnelling current as a function of applied voltage, an I-V spectrum. From the I-V spectrum one tries to obtain information about the sample density of states. One can also measure $dI/dV(V)$ or $d^2I/dV^2(V)$ using a small modulation voltage and a lock-in amplifier. The STS approach faces two formidable problems. The first one is of technical nature and the second lies in the data analysis.

It is difficult to measure reproducible STS data. The tip has to be at a constant height above the surface while the spectrum is taken. A small change in height will change the current much more than any spectral feature! Therefore the tip has to be held at constant height within of 0.01 Å or so. If one simultaneously wants lateral resolution one also has to keep the tip parked above the same spot on the sample although it is enough to do this within 0.1 Å. Achieving this against the thermal drift and vibrations from outside is hard. STS spectra have to be taken many times to obtain an acceptable signal to noise ration. It is desirable, that the tip does not change during these many spectra. On the other hand, it is also a good idea to take

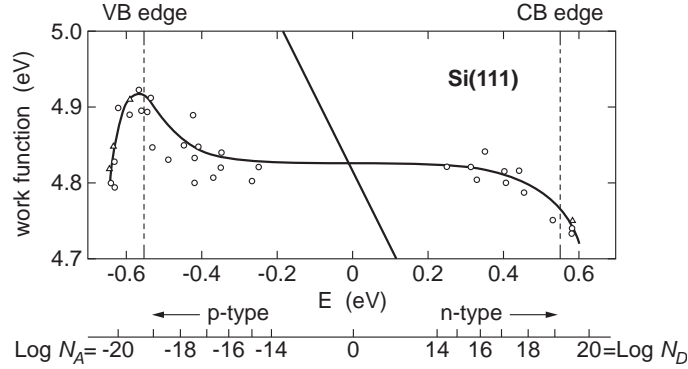


Figure 7.26: Fermi level pinning for Si(111). The measured workfunction is almost independent of the doping level. The straight line in the middle illustrates the expected behaviour due to the doping. After Ref. [69].

spectra for differently prepared tips in order to learn which spectral features are due to the tip and which are due to the sample.

So let's look at the black magic involved in analysing the spectra. We restrict ourselves to a very simplified discussion for relatively small tunnelling voltages, i.e. smaller than the workfunctions of tip and sample. We write down a simple expression for the tunnelling current.

$$I = \int_0^{eV} \rho_s(\vec{r}, E) \rho_t(\vec{r}, -eV + E) T(E, eV, \vec{r}) dE, \quad (7.19)$$

where ρ_s and ρ_t are the density of states of sample and tip, \vec{r} is the location of the tip, E is the energy measured with respect to individual Fermi levels of sample and tip, V is the tunnelling voltage and $T(E, eV, \vec{r})$ describes the tunnelling probability. We further simplify this by making the assumption that the tip density of states is constant.

$$\rho_t(E) = \text{const.} \quad (7.20)$$

A featureless tip DOS might be expected for a blunt and disordered tip. But our ideal tip for obtaining good spacial resolution will be one with just one atom at the end. So the approximation of a featureless tip might not be very good. On the other hand, one might be able to sort out the tip contribution to the $I - V$ curves because the tip DOS does not depend on the position on the sample. If we now also say that

$$T(E, eV) = \text{const.} \quad (7.21)$$

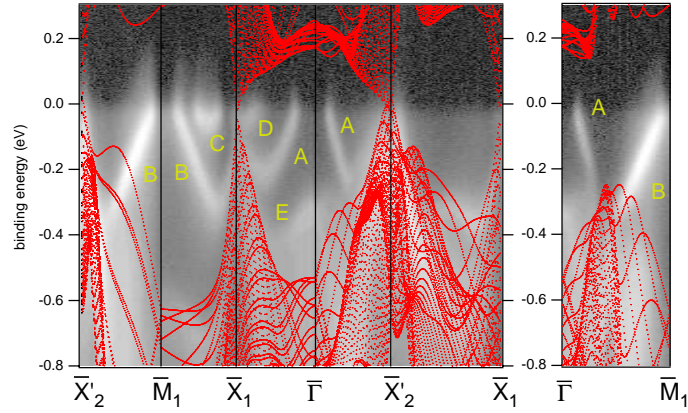


Figure 7.27: Projected band structure of Bi(110) and experimental data along several high symmetry lines of the surface Brillouin zone. The data are the logarithm of the photoemission intensity. The grey scale is defined such that black means low intensity and white high intensity. The features A,B,C,D and E are the electronic surface states. After Ref. [67].

then we can obtain the sample DOS from equ. 7.19 simply by plotting dI/dV . But a constant T is a very bad assumption. In fact, it turns out that the tunnelling probability is always highest for the states at the Fermi level. This means that if we set V such that we tunnel from the tip into the sample, most of the electrons will come from the Fermi level of the tip and we will measure the unoccupied DOS of the sample. If we reverse the sign of V most of the tunnelling electrons come from the Fermi level of the sample. We will unfortunately not learn very much about the occupied DOS of the sample. It turns out that the errors caused by 7.21 can be reduced by taking $(dI/dV)/(I/V)$ instead of simply dI/dV .

In view of all this, it is needless to say that STS results have to be treated with great care

We illustrate the capabilities of STS by going back to the (2x1) dimer reconstruction of Si(100). As we have seen above, photoemission is not quite conclusive on the question if the dimers are symmetric or not. LEED seems to favour an asymmetric dimer. STM in the topography mode has shown both symmetric and asymmetric dimers, depending on the sample temperature. The STM image shown in Fig. 6.47 clearly shows the asymmetric dimers. In the same paper, STS has been performed on the individual atoms of the dimers. The result is shown in Fig. 7.28. The STS data have been taken simultaneously with the topography data shown in the inset. In Fig. 7.28(a) the average spectrum of this surface is shown. In (b) two spectra from

the different atoms in the dimer are displayed. In the unoccupied states, a significantly higher DOS of atom 1 at about 1 eV is found. Since atom 1 is associated with the “down” atom this increase in the unoccupied DOS is consistent with the predicted charge transfer of the “down” to the “up” atom. The increase of occupied DOS in the “up” atom is not observed. This is partly due to the difficulty of obtaining spectroscopic information about occupied sample states.

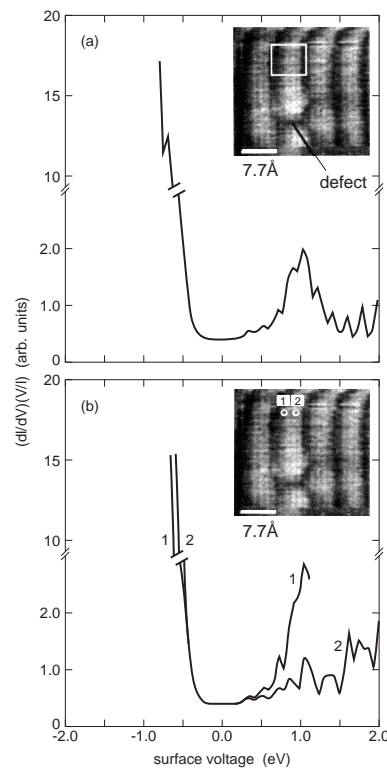


Figure 7.28: (a) Averaged tunnelling spectrum on the marked area in the inset. (b) corresponding spectra for the two positions marked in the inset. After Ref. [45].

7.5 Further Reading

For a discussion of the work function a good reference is the original paper of Lang and Kohn [70]. A good (but old) reference on angle-resolved photoemission which I have used a lot to prepare these notes is [59] but see also [71]

and [72]. The issue of work function is theoretically discussed E.W. Plummer and W. Eberhardt, *Adv. Chem. Phys.* 49, 533 (1982).

Angle-resolved photoemission, Ed. S.D. Kevan, Elsevier 1992

Chapter 8

Optical properties of surfaces

The surface optical properties, i.e. the behaviour of the electromagnetic field in the vicinity of the surface is of considerable importance in surface science. There are two main reasons: the first is the fundamental importance of the electromagnetic field for many processes, e.g. for photoemission. The other reason is the practical usefulness of light as a surface probe. Remember that most of the surface science techniques we have looked at so far are based on electron spectroscopy. This has the fundamental disadvantage that it only works in UHV. With light we have the possibility to study surface properties even in “real” environments present in heterogeneous catalysis or in semiconductor growth.

As we have seen in one of the first lectures, the main problem associated with light is the lack of surface sensitivity. The penetration depth is large such that the surface signal is relatively small. The situation is especially bad for the spectral regions where the material under investigation is “transparent”, i.e. below the fundamental adsorption edge of semiconductors and above the plasma energy of metals. Two ways have been established to do surface-sensitive spectroscopy despite this problem. The first is a difference technique. One measures the optical properties of a clean and of an adsorbate-covered surface and takes the difference between these two in order to learn something about the adsorbate. We will see an example of this in the second part of the lecture (IRAS). The other approach is to make an optical measurement which results in a 0 signal from the bulk because of *symmetry*. If this symmetry is broken at the surface, the measured signal stems from the surface region. We give two examples for this approach below.

8.1 Reflection of Light at a Surface

The classical reflection and refraction of a plane wave at a surface is described by Snell's law

$$\sin \Theta_i \tilde{n}_i = \sin \Theta_t \tilde{n}_t, \quad (8.1)$$

where Θ_i and Θ_t are the angles of incidence and refraction, respectively, and \tilde{n}_i and \tilde{n}_t are the complex refractive indices. In order to calculate the actual fields one has to consider the Maxwell equations together with the boundary condition that the tangential components of \vec{E} and \vec{H} are continuous over the interface. This leads to the famous Fresnel equations for the (amplitude) reflection coefficients

$$\tilde{r}_p = \frac{\tan(\Theta_i - \Theta_t)}{\tan(\Theta_i + \Theta_t)} \quad (8.2)$$

$$\tilde{r}_s = -\frac{\sin(\Theta_i - \Theta_t)}{\sin(\Theta_i + \Theta_t)} \quad (8.3)$$

$$\tilde{t}_p = \frac{2 \sin \Theta_i \cos \Theta_t}{\sin(\Theta_i + \Theta_t) \cos(\Theta_i + \Theta_t)} \quad (8.4)$$

$$\tilde{t}_s = \frac{2 \sin \Theta_i \cos \Theta_t}{\sin(\Theta_i + \Theta_t)} \quad (8.5)$$

These equations permit to calculate all the desired properties: Fig. 8.1 shows the reflection coefficients for light polarized parallel and perpendicular to the plane of incidence, respectively. The complex index of refraction is chosen to be $n=3$, $k=30$, representing a metal surface. Fig. 8.1 shows a highly reflecting surface with a Brewster angle near 90°

It is also interesting to calculate the electric field components at the surface for the same material. The result is shown in Fig. 8.2. It can be seen that the most important field at the surface is polarized in the plane of incidence and it is perpendicular to the surface. This field is strongly enhanced (over the initial amplitude of 1) at a grazing angle of incidence. An experiment in which we want to look at the interaction between molecules on a surface and the light should be built in such a geometry.

For the purpose of surface science, however, the Fresnel-description of the fields is insufficient. This is easily seen by looking at the \vec{D} field which has to be continuous at the surface. In a classical theory this is achieved by a delta charge-sheet right at the surface. This is of course physically meaningless in a microscopic theory. In such a theory a non-local relation between \vec{D} and \vec{E} has to be assumed and the fields have to be calculated in a self-consistent way. It turns out that such a complicated approach is essential if things like photoemission intensity from surface states are to be described.

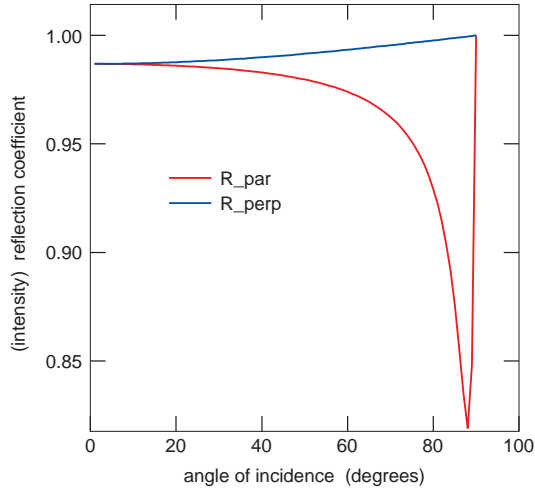


Figure 8.1: (Intensity) reflection coefficients for light polarized parallel (p) and perpendicular (s) to the plane of incidence. The complex index of refraction is $n=3, k=30$.

8.2 Polaritons

In our discussion of the surface plasmon in section 3.4.5 we have found the surface plasmon frequency to be $\omega_{sp} = \omega_P/\sqrt{2}$ and we did not consider the possibility of a surface plasmon dispersion $\omega_{sp}(q)$ which can in fact be found and measured with EELS. Whereas this dispersion is usually not very big, something rather dramatic happens when the wave vector q becomes very small, in the order of the light wave vector ω/c . For these very long wavelengths we have to consider the fact that a surface plasmon carries an electric field and it has to be treated on equal footing with an ordinary electric field, i.e. it has to fulfil the Maxwell equations. This leads to a dramatic change in the dispersion which is shown in Fig. 8.3. The surface plasmon energy is no longer constant, as it would be on this q scale, but it shows an avoided-crossing behaviour with the light dispersion line $\omega = cq_z$. The lower branch is called the surface plasmon polariton.

As a consequence of this, it is impossible to excite surface plasmons with light because energy and momentum can not be conserved simultaneously. This is easily seen from Fig. 8.3. The light dispersion line can be changed by changing the angle of incidence. For normal incidence $q_{\parallel} = 0$ and the dispersion is a vertical line in the figure. For grazing incidence $q_z = 0$ and the dispersion is $\omega = cq_{\parallel}$. For any angle in between $\omega = c(q_{\parallel}^2 + q_z^2)^{1/2}$. This means that the light dispersion and the surface plasmon polariton dispersion

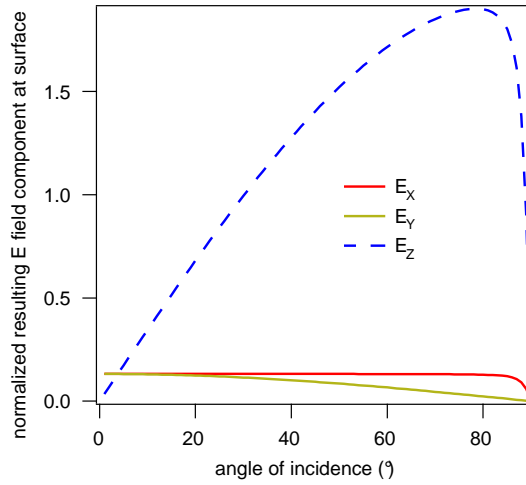


Figure 8.2: Electric field components at the surface of the material with $n=3, k=30$. The plane of incidence is the x/z plane. The z -axis is perpendicular to the surface.

never cross and hence there can not be any excitation.

In short, there are essentially two ways of circumventing this. The first is to introduce a long periodic structure, e.g. a grating, on the surface such that the surface plasmon polariton gets back-folded and this back-folded mode crosses the light dispersion lines. The same effect can be achieved by a rough surface which can be viewed as a superposition of many gratings with different periodicities. The excitation of surface plasmons via surface roughness is thought to play a role in surface-enhanced Raman scattering. The other way to achieve the coupling is to use ‘slow’ photons with an q_z which is imaginary. Then the dispersion line can be moved down, as indicated in the figure. Such light can be produced by a total reflection inside a prism mounted in a short distance over the surface. In this case, an evanescent electric field penetrates the gap between prism and surface. The field decays exponentially, i.e. it possesses an imaginary q in the z direction.

The surface plasmon is not the only mode which leads to the formation of polaritons at long wavelength. In fact, all modes of the crystal which carry an electromagnetic field have to be considered, e.g. optical phonons for materials with several atoms in the unit cell.

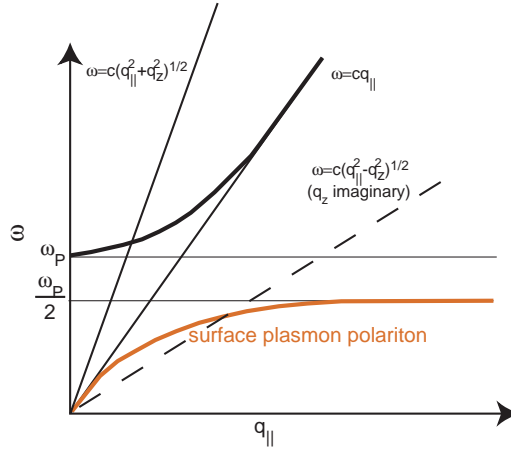


Figure 8.3: Dispersion of a surface plasmon polariton.

8.3 Reflection Anisotropy Spectroscopy (RAS)

The technique of Reflection Anisotropy Spectroscopy (RAS) is based on a symmetry-trick in order to make the optical spectroscopy surface-sensitive. The optical response of a solid is dictated by its complex dielectric tensor $\tilde{\epsilon}$ or by the complex refractive tensor \tilde{n} . In the case of a centrosymmetric material such as a cubic crystal the tensor is reduced to a complex scalar. Consequently the normal-incidence reflectivity of a cubic crystal should not depend on the azimuthal orientation of the polarization vector. This is only true, however, for the dielectric response of the bulk crystal; at the surface the inversion symmetry is broken. Any azimuthal anisotropy in the normal-incidence reflectivity of cubic crystals must therefore have its origin in the surface region. In a RAS experiment (see Fig. 8.4) one probes the difference in the normal-incidence reflectivity along two mutually perpendicular orientations of the polarization vector. Usually one or both of these directions coincide with the principal crystallographic directions in the surface.

This technique is of course rather restricted: the only possible measuring geometry is normal incidence, the bulk crystal has to have inversion symmetry and the surface must be chosen such that it has two mutually perpendicular directions which are not symmetry-equivalent (i.e. fcc(110) works but fcc(100) does not).

One important example for the usefulness of RAS is the study of surface states on metal surfaces. Fig. 8.5 shows the electronic structure in the vicinity of the \bar{Y} point of the Surface Brillouin Zone on Ag(110). Two surface states are found in the projected band gap. One state above and one state

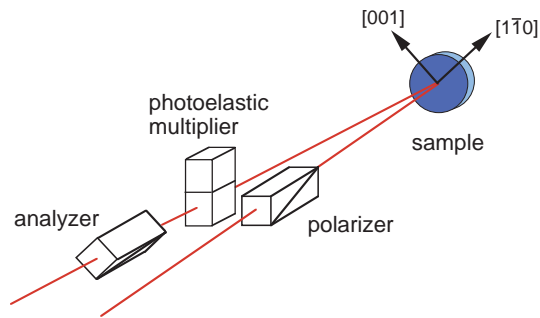


Figure 8.4: Setup for a RAS experiment. The complex difference in reflectance along two mutually perpendicular directions is measured. After Ref. [73].

below the Fermi level. Fig. 8.6 shows photoemission and RAS spectra for

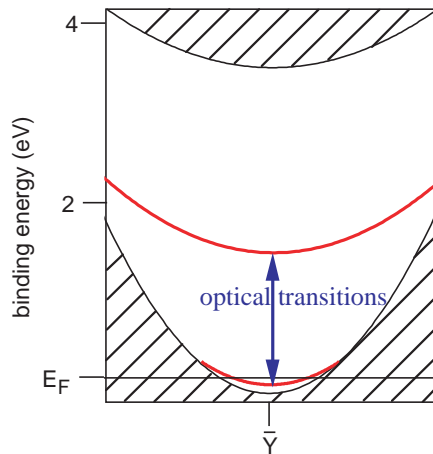


Figure 8.5: Surface electronic structure of Ag(110) in the vicinity of the \bar{Y} point of the SBZ. One occupied and one unoccupied surface state can be found.

the clean and oxygen-covered Ag(110) surface

RAS does thus allow the direct observation of surface states. This could be used to monitor chemical reactions time-resolved with a simple optical technique.

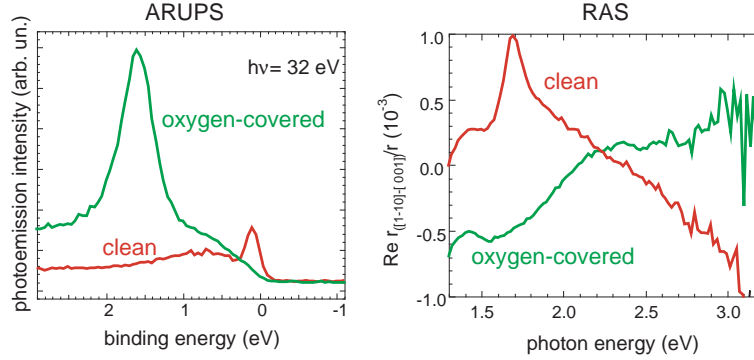


Figure 8.6: Photoemission and RAS spectra for the clean and oxygen-covered Ag(110) surface. The photoemission spectrum taken at the \bar{Y} point shows the surface state right below the Fermi level. In the RAS spectrum both surface states give rise to a peak corresponding to an interband transition between them. After [74].

8.4 Second Harmonic Generation

The non-linear technique of Second Harmonic Generation (SHG) is based on a similar idea as RAS, i.e. using optical properties which vanishes in the bulk of a centro-symmetric material. We only touch this technique very briefly here. Consider the current driven by an AC field. It can be written as

$$\vec{j} = \sigma \vec{E} + \chi : \vec{E} \vec{E} \dots \quad (8.6)$$

where χ is the third-rank tensor of second harmonic generation. In the bulk of a centrosymmetric material this tensor must vanish but at the surface it does not. Equ. 8.6 practically means that by shining light with a frequency ω on a crystal, scattered light with a frequency 2ω can be generated. This second-harmonic signal can be safely ignored for all conventional light sources, including synchrotron radiation. If one uses a laser as light source it does, however, lead to measurable intensities.

We illustrate this technique by using the same example as for RAS, the surface state on Ag(110) in Fig. 8.7. The interband transition can only be induced for one polarization direction. This leads to a different absorption of light by the surface and this, in turn, is seen in the SHG data.

SHG does have a similar disadvantages as RAS: the bulk material has to be centrosymmetric. The experimental geometry is, however, much less restricted. On the other hand, it is very difficult to tune the laser light and

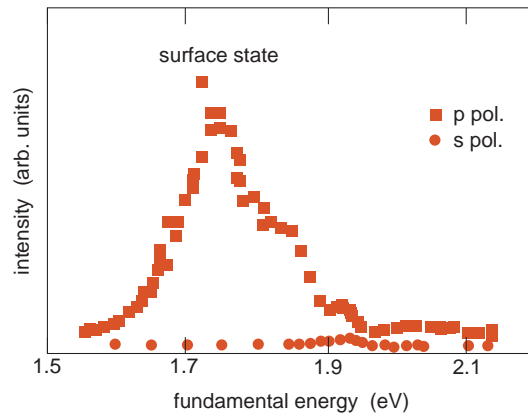


Figure 8.7: SHG spectrum from clean Ag(110) and two different polarization directions. For one polarization direction the surface state transition contributes to the SHG signal. After Ref. [75].

SHG cross section is small. This means that it takes many weeks of work to take a spectrum as in Fig. 8.7 while the corresponding RAS spectrum in Fig. 8.6 can be taken in a couple of minutes.

Chapter 9

Vibrational properties of surfaces

9.1 Introduction

The introduction of a surface gives the possibility of new vibrations which are localized at the surface. It is the same as we have already discussed for the electronic surface states but it is somewhat easier to imagine. The new states have to be again in "band-gaps" of the projected bulk phonon dispersion. This means that for the same \vec{q}_{\parallel} there is no bulk mode with the same vibrational frequency. Otherwise the surface and bulk mode would couple and the surface mode would no longer be localized at the surface. Fig. 9.1 shows the projected bulk-phonon structure for Be(0001) together with the surface phonon modes. The dashed lines are calculated surface modes based on the same force-constants which work fine for describing the phonon dispersion in bulk Be and the dots are the result of measurements. Clearly the agreement is not good. The force-constants at the surface must be different from the bulk values.

Here the force constants are not as strong as in the bulk leading to surface vibrations with a lower energy than the bulk continuum. There can of course also be surface vibrations above the bulk continuum if the force constants in the surface are stiffer.

Apart from these "intrinsic" vibrational surface states, adsorbates on the surface lead to "extrinsic" surface vibrations. In many cases these modes will lie above the bulk continuum such that they do not couple to bulk vibrations. If they lie in the bulk continuum they will couple and act a source of bulk vibrations. The "extrinsic" vibrational modes will be the modes of the adsorbate shifted in frequency due to the different chemical

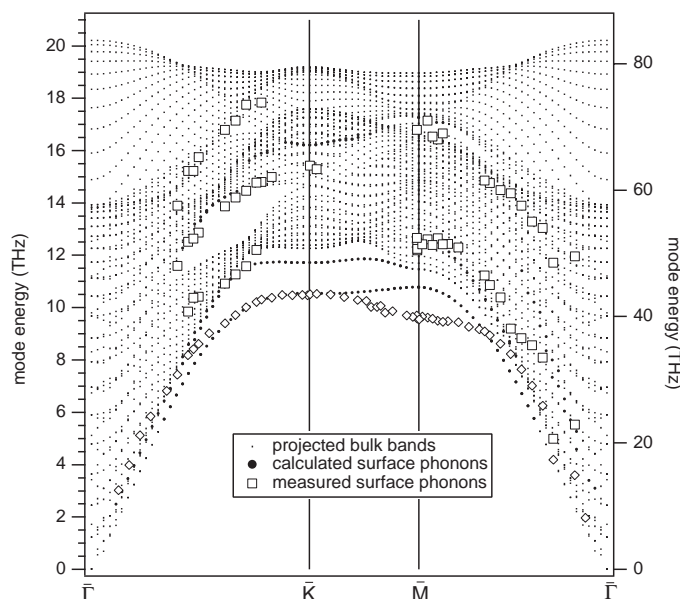


Figure 9.1: Calculated surface phonon dispersion for Be(0001) (line, from the bulk force constants) together with a measurement (markers). The continuum is the projected bulk phonon structure. After Ref. [76].

environment. But there are also new modes: the translational and rotational degrees of freedom of the free molecule will be turned into new vibrations, the so-called frustrated translations and rotation. Fig. 9.2 gives an example for the vibrational modes of a diatomic molecule on a surface. Remember that such a molecule has only one vibrational mode when it is free.

A measurement of the surface phonons requires a probe which is coupling to the vibration and which can be used with sufficiently high resolution. The substrate phonon energies lie in most cases below 50 meV. This means that the spectral resolution should be clearly better than 10 meV. Three common probes are used at present: light, electrons and atoms. As we have already discussed in the section about optical properties, light has one outstanding advantage with respect to the other probes: it can also be used under "real" working conditions of a catalyst, i.e. not in ultra-high vacuum and at elevated temperatures.

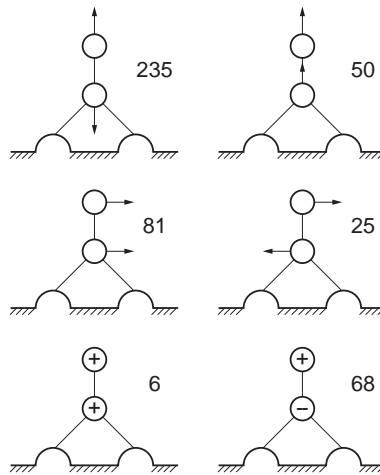


Figure 9.2: Vibrational modes and corresponding energies (in meV) for CO on a two-fold bridge site. The free molecule has only one vibrational mode, the others are frustrated rotations and translations. After Ref. [77]. The energies are only intended as an order of magnitude and are taken from Ref. [78].

9.2 Electron scattering: EELS

We know the design of an EELS or HR(high-resolution)EELS spectrometer from the lecture about electron-surface interactions. It is shown in Fig. 9.3. The instrument consists of an electron source, a double electron monochroma-

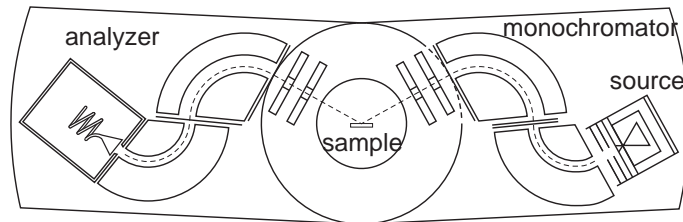


Figure 9.3: An EELS spectrometer.

tor, lenses which focus the beam on the sample, lenses which image the beam into a second double analyzer and an electron multiplier. The monochromator side of the instrument can be turned around the sample, such that different combinations of incidence / emission angles are possible. With an instrument of this design a spectral resolution of about 1 meV can be

achieved.

The most important physical aspect of the scattering is of course the conservation of energy and momentum. The impinging electrons can excite or (at not too low temperatures) destroy a phonon (see Fig. 9.4).

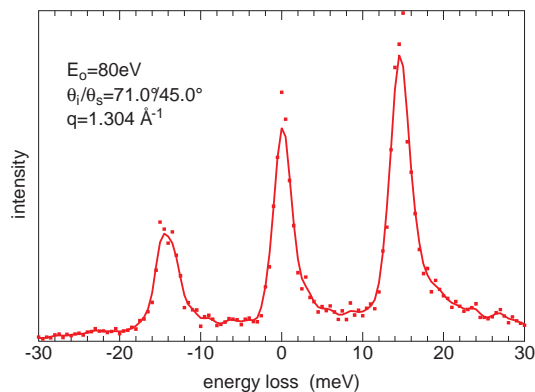


Figure 9.4: EELS spectrum from Mg(0001). There are three peaks visible: the elastic peak, a loss peak from a creating a phonon and a gain peak from destroying a phonon [79].

The energy of the phonon can be directly read from the experiment. The momentum transfer for the elastically scattered electrons is simply given by the beam energy and the scattering geometry. The momentum transfer for typical phonon losses is nearly identical to that of the elastic beam because the energy loss is so small with respect to the beam energy.

There are two important mechanisms for the interaction between the electrons and the surface (1) dipole scattering and (2) impact scattering. We want to discuss both.

Consider an electron on its way towards the surface of a metal. The electric field of the electron is screened in a classical image charge picture like illustrated in Fig. 9.5.

This means that the electron on its way above the crystal surface creates a changing electrical field perpendicular to the surface, which can couple to the surface vibrations. This mechanism has two important restrictions: only vibrations with a dipole moment perpendicular to the surface can couple to the electric field and can be excited. The interaction is of long range both perpendicular and parallel to the surface. That means that parallel to the surface all the atoms are excited in phase over a long range, hence the \vec{k} -vector parallel to the surface is small or zero and the electrons which have lost or gained a phonon are scattered again into the specular beam (the beam

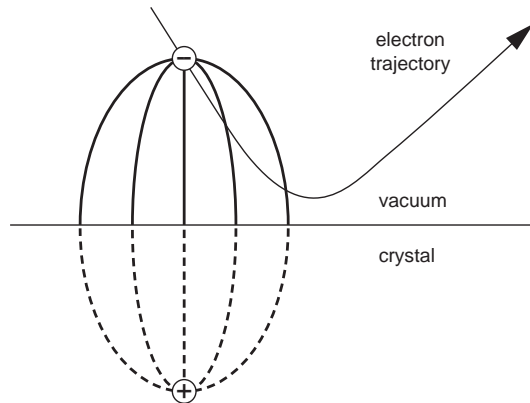


Figure 9.5: Electric field created by an electron approaching a metal surface (and its image charge).

for which $\Theta_{in} = \Theta_{out}$). The cross section for a loss is given by

$$S \propto \frac{p^2}{E_0} \quad (9.1)$$

where p is the perpendicular dipole moment and E_0 is the impact energy. In other words: dipole scattering can be observed in the specular direction, for low impact energies and of course only for vibrations with a dipole moment perpendicular to the surface.

The other and somewhat complementary scattering mechanism is called impact scattering. Here the electron interacts with the electron shell of the ions on an extremely short length scale. Therefore this type of scattering creates a broad angular distribution. The selection rules for dipole scattering (only dipoles perpendicular to the surface and only phonons near the zone centre) do not apply such that impact scattering can be used to map out phonon dispersions. The cross section for impact scattering is, however, much smaller than for dipole scattering.

The two scattering mechanisms are illustrated in Fig. 9.6. In the $\Theta_s = 0^\circ$, i.e. in the specular geometry, only the very strong loss due to the symmetric H-metal vibration can be seen. This is the only one, which is dipole active. When going away from the specular direction the other two modes can also be seen.

What can vibrational spectroscopy be used for?

A first example is the determination of chemical identity and to some extent also adsorption geometry. Fig. 9.7 shows an EELS spectrum for CO adsorbed on Pt(111) taken in the specular geometry. All the strong losses

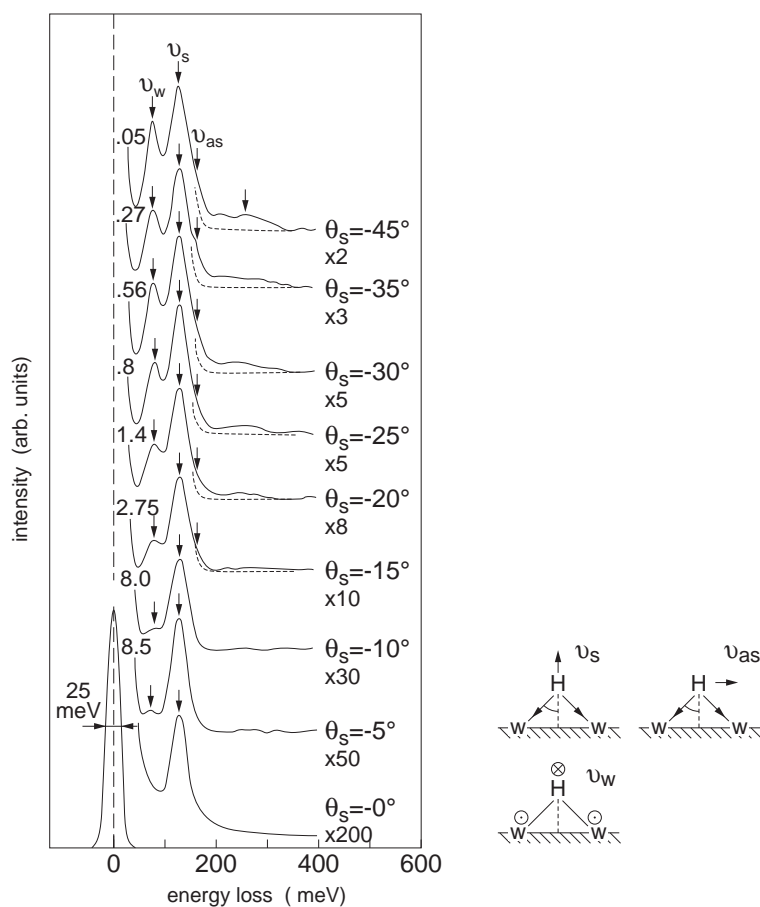


Figure 9.6: EELS spectra for H on W for different scattering geometries. After Ref. [80].

which are observed must be dipole-active. From such a spectrum a lot can be learned: Two losses can be found in the frequency range typical for the C-O stretch vibration. This means that there must be two different CO species on the surface. A comparison with metal-carbonyl complexes suggests that the higher frequency mode is the one where the CO molecule is adsorbed on top of a substrate atom and the lower frequency mode is due to a bridge site. Naive intuition is also helpful: one would argue that if the C atom has to make two bonds to the surface, then this would weaken the internal bond to the O atom. Hence the force constant would be softer and (due to $\omega = \sqrt{\frac{K}{M}}$) the mode lower in energy. One has to be careful, though, these naive pictures and even the comparison to a metal-carbonyl do sometimes lead to a wrong adsorption site.

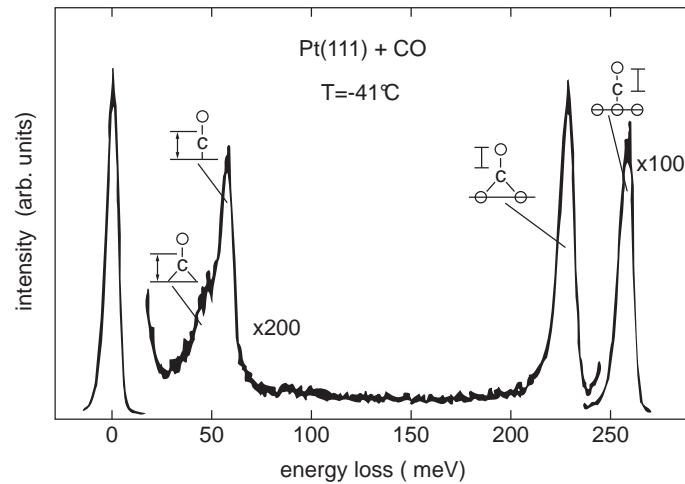


Figure 9.7: EELS spectrum of CO adsorbed on Pt(111). After Ref. [81]

One loss with an unresolved shoulder is observed in the CO-M stretch region. Again the softer vibration is associated with the bridge site for similar arguments as above.

Some losses are not observed: There should be frustrated translations and frustrated rotations of the molecule. These are not seen because they are not dipole active but also because they lie so low in energy (7 meV and 26 meV, respectively) that they could not be resolved by this particular spectrometer.

Whenever dealing with vibrations a central concept in experimental solid state physics is the isotope effect. By using different isotopes one can change the mass of the vibrating atoms without changing the force constants. The most famous example is probably that the observation of a strong isotope effect on the superconducting transition temperature has given a hint that phonons are important in BCS superconductivity. Here the isotope effect can be used to understand vibrational spectra:

Fig. 9.8 shows EELS data for acetylene and deuterated acetylene on Ni(111). The C-C stretch frequency is not really affected very much by the isotopic substitution. It shifts from 149 meV to 148 meV. But the C-H stretch frequency severely changes when going to CD: it changes from 361 to 272 meV. Interestingly the ratio of the two frequency is 1.32, not too far away from $\sqrt{2}$ which would be expected from a naive mass-difference argument.

Another application of EELS is the measurement of surface phonon dispersion curves. The problem is that for many materials the energies of the surface phonons are so low that this has only taken off in the last few years because of the technical progress in building high resolution instruments (for

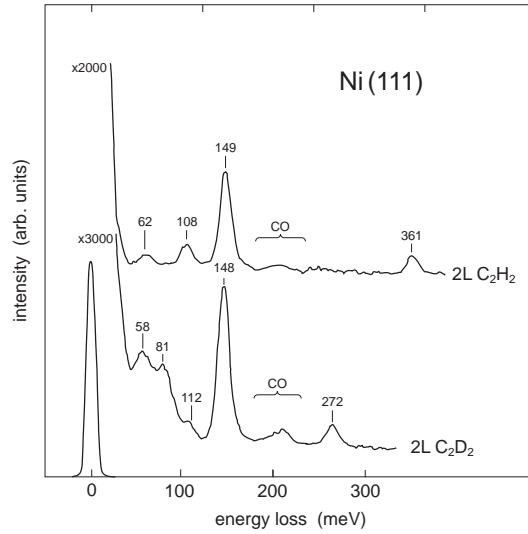


Figure 9.8: EELS spectra for C_2H_2 and C_2D_2 showing the isotope effect for acetylene on Ni(111). After Ref. [82].

very low energies one can take He atom scattering, see below). We have already seen the surface phonon dispersion for Be(0001) above. Such data is measured by changing the scattering geometry. For $\Theta_{in} = \Theta_{out}$ one probes the centre of the surface Brillouin zone. If one of the angles is changed the momentum parallel to the surface is different for the incoming and scattered electrons. In this way dispersions in the whole surface Brillouin zone can be mapped. Fig. 9.9 shows experimental data for Be(0001). This data has been used to draw the measured phonon dispersion in Fig. 9.1.

So far we have been concerned with the description of the surface in the harmonic approximation neglecting anharmonic effects. We know that anharmonicity is very important in the real world: it is needed for e.g. thermal expansion and a finite value of the thermal conductivity (it would be infinite for the harmonic solid).

Obviously anharmonicity is already important in a three dimensional solid. There is good reason to assume that it is even more important on a surface. As we have seen for Be(0001) the surface vibrations are often softer than the bulk vibrations. This is intuitively clear since the surface atoms have lost a part of their neighbours. The softer vibrations mean that the mean square amplitude of the vibrations is larger and the anharmonicity of the potential becomes more important.

Fig. 9.10 shows EELS data from Cu(110) taken in the specular geometry for temperatures between 21 K and 766 K. At low temperatures a clear

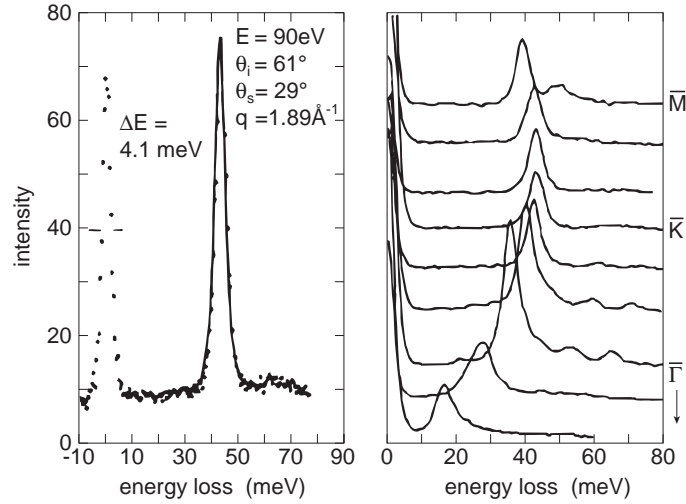


Figure 9.9: EELS spectrum showing a phonon losses from Be(0001) as a function of scattering geometry (\vec{k} -vector). After Ref. [83].

phonon loss is observed just above 20 meV. As the temperature is raised the loss broadens out and is eventually indistinguishable from the background. This is exactly what one would expect in an anharmonic solid. The phonons are no good descriptions of the anharmonic solid, remember that we have derived them in the harmonic approximation. Nevertheless, one keeps the phonon concept but one assigns a finite lifetime to the phonons. A phonon will eventually decay (this simple concept also explains the finite thermal conductivity). This is exactly what is observed in the data: for higher temperatures the lifetime gets shorter and the width of the line gets bigger.

9.3 Optical spectroscopy: IRAS

Another way of probing surface vibrations is the use of infrared radiation. The two main advantages over EELS are that light can work in a gaseous environment and that the spectral resolution is much higher (at least by a factor of 10). Disadvantages are that the spectral region is restricted, that the momentum transfer is always 0 (due to the small momentum of light) and that IR spectroscopy is not as sensitive as EELS. We restrict ourselves to an experimental configuration where the IR light is reflected from the surface and absorption due to the vibrations are observed, Infrared Reflection Absorption Spectroscopy (IRAS).

The selection rules for vibrations in IRAS are essentially the same as for

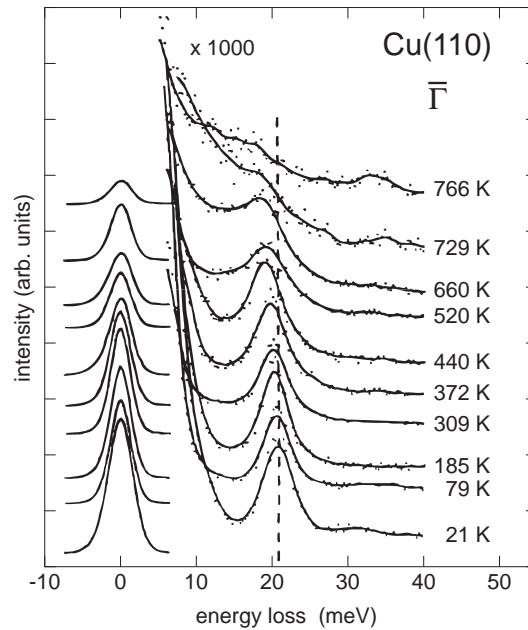


Figure 9.10: EELS data from Cu(110) in the specular geometry as a function of temperature. After Ref. [84].

dipole scattering in EELS . Consider the reflection of an infrared beam from a metal surface. The electrical field in the vicinity of the surface can be calculated using the Fresnel equations as we have seen in the first part of the lecture. For the light polarized perpendicular to the plane of incidence (*s*-polarized) the reflectivity is high for all angles of incidence (see Fig. 8.1) and the phase is reversed upon reflection. The interference of incoming and reflecting wave creates a very small field at the surface (see Fig. 8.2). For the *p*-polarized light the reflectivity is strongly dependent on the angle. At near grazing incidence a strong enhancement of the perpendicular component can be achieved while the tangential component is always small (see Fig. 8.2).

This results in the same scenario as in EELS : only the component of the electric field perpendicular to the surface can couple to the vibrations and therefore only vibrations with a dipolar moment perpendicular to the surface can be excited.

Infrared spectroscopy has really taken off since the development of Fourier transform spectrometers. They are also used for surfaces. Fig. 9.11 shows such a spectrometer: it is based on a Michelson interferometer. The light from the source is hitting a beamsplitter T. One part of the light is reflected from a fixed mirror, the other from a mirror which moves periodically in

x . The detector D measures the resulting intensity as a function of mirror displacement x (in a real experiment there would be the possibility to move a sample in front of the detector, of course). The signal $I(x)$ is averaged over many moving cycles. Then the spectral distribution $I(\lambda)$ can be calculated from $I(x)$ by a simple Fourier transform.

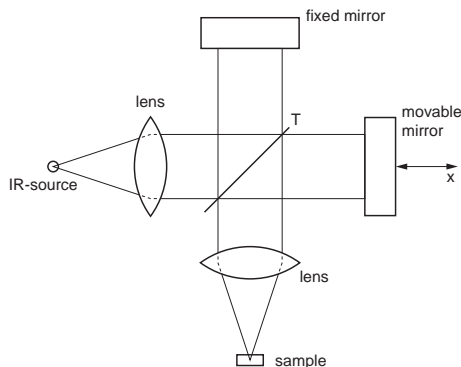


Figure 9.11: FT-IRAS spectrometer. After Ref. [85].

All one has to do is to measure the spectrum without a sample (to obtain the instrumental function) and a spectrum with sample. The spectrum with sample is then divided by the empty spectrum.

The resolution of such a set-up is given by the maximal length x . The movement can, however, not be made too long because the coherence of the light source is limited.

In reality a surface science set-up is more complicated because it involves UHV around the sample and high vacuum around the spectrometer in order to get rid of water absorption bands from the air. Such a setup is shown in Fig. 9.12. One does not measure the infrared transmission but the reflectivity

The extremely high resolution of IRAS can be used to study small effects, which are completely hidden in the broad peaks of EELS measurements, for example small energy shifts of the vibrational frequencies induced by the adsorbate-adsorbate interaction. Fig. 9.13 gives an example from a study of CO adsorption on a stepped Pt surface, Pt(533). In the beginning the CO molecules adsorb at the steps of the surface giving a characteristic vibrational C-O stretch frequency. For higher coverages, sites on the terraces are occupied as well, giving rise to a higher frequency vibration. Eventually the low frequency vibration vanishes: the coupling between the adsorbed CO molecules is so strong that the molecules at the step can not keep up their characteristic vibrational frequency.

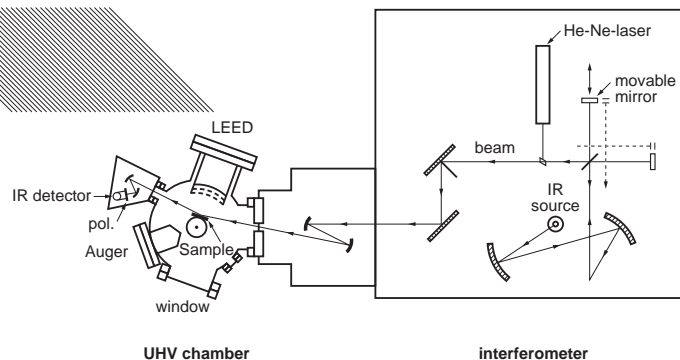


Figure 9.12: FT-IRAS spectrometer in UHV. After Ref. [86].

9.4 He Atom scattering

He atoms can also be used as a probe for detecting surface vibrations. This technique is only touched very briefly here. The use of He atoms has the advantage of very high surface sensitivity, very high sensitivity towards contamination and much higher resolution than EELS. The disadvantages are that the maximum loss energy is rather low (about 50 meV due to the energy of the He beam) and that the experiment is very complicated (see Fig. 9.14).

In He atom scattering the only interaction mechanism for the creation or destruction of phonons is impact scattering. Like in EELS, energy and momentum conservation have to be satisfied in the scattering event, but in the case of He scattering the elastic peak and the losses observed in one scattering geometry correspond to different values of the momentum transfer since the size of the loss is comparable to the energy of the beam.

In vibrational spectroscopy Helium atom scattering is somewhat complementary to EELS but the applications can be similar. Here we give just one short example. Fig. 9.15 shows the losses for the frustrated translations and vibrations of CO on Pt(111). We saw the higher energy losses already in the paragraph about EELS.

9.5 Vibrational spectroscopy with the STM

The spectroscopic mode of the STM can be used to observe vibrational excitations in just the same way like the electronic excitations discussed in section 7.4. Vibrational spectra of molecules in buried metal-oxide interfaces where already investigated in the 1960s by tunnelling spectroscopy,

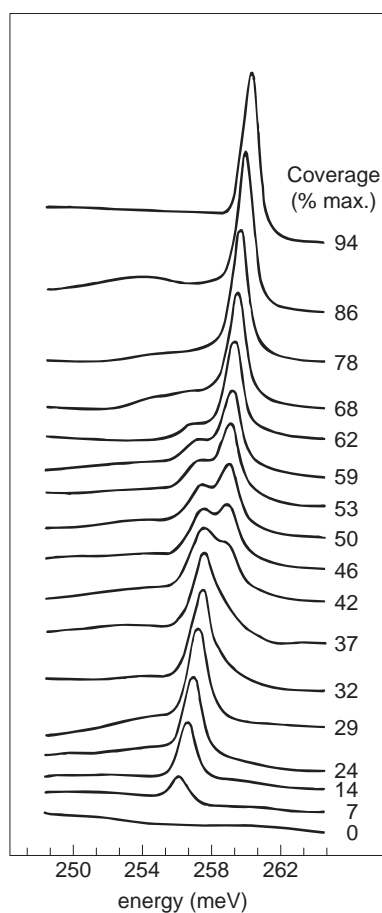


Figure 9.13: The C-O stretch frequency of CO on a stepped Pt surface as a function of coverage. After Ref. [87].

long before the invention of the STM. One observes sharp increases in the conductance dI/dV when sweeping the tunnelling voltage through the energy of a vibrational mode because above this energy a new inelastic tunnelling channel opens. The first vibrational spectra for single-molecules on a surface were measured in 1998 with the STM. Fig. 9.16 shows such spectra in the C-H stretch region of acetylene adsorbed on Cu(100). The C-H stretch peak is clearly visible in the $d^2I/dV^2(V)$ spectrum! Fig. 9.16 also illustrate the isotope shift between acetylene and deuterated acetylene.

This experiment demonstrates a major progress in STS and STM. Using vibrational spectroscopy, one can hope to gain chemical sensitivity in STM. One will also be able to study the influence of nearby adsorbates on the vibrational modes of molecules.

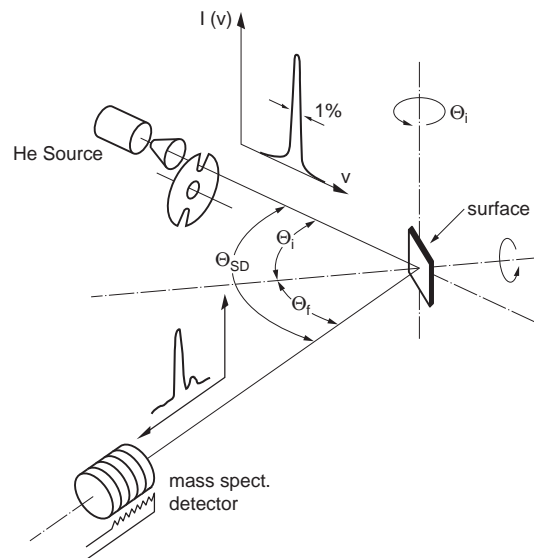


Figure 9.14: He-atom scattering apparatus. After Ref. [88].

9.6 Further reading

A good introduction about surface optical properties can be found in [3] but for all the basics like the Fresnel equations you should consult a book on optics. A good book on EELS is [77] and a good review article on IRAS is [91]. Detailed information about He scattering can be found in [2].

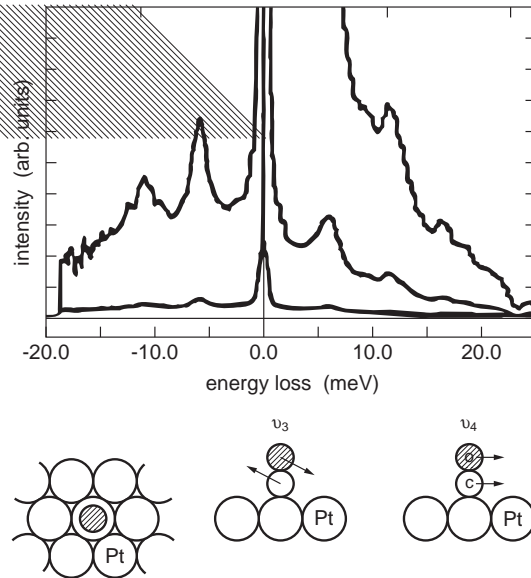


Figure 9.15: Low-energy vibrational modes for CO on Pt(111) investigated by He-scattering. After Ref. [89].

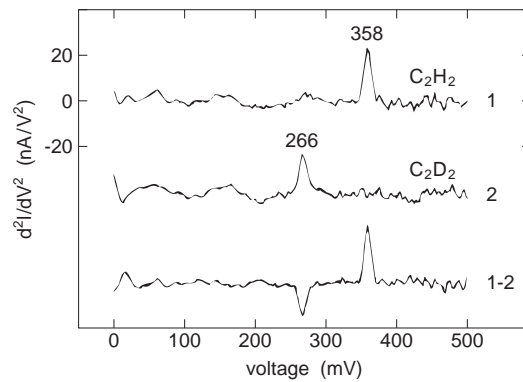


Figure 9.16: Vibrational spectra of acetylene and deuterated acetylene taken by STS from a single molecule on Cu(100). After Ref. [90].

Bibliography

- [1] H. Lüth, ‘Surfaces and Interfaces of Solid Materials’, Springer Study edition.
- [2] T. A. Delchar, and D. P. Woodruff, ‘Modern Techniques of Surface Science’, Cambridge Solid State Science Series.
- [3] A. Zangwill, ‘Physics at Surfaces’, Cambridge Univ. Press.
- [4] Martin Henzler and Wolfgang Göpel, ‘Oberflächenphysik des Festkörpers’, Teubner Verlag.
- [5] M. C. Desjonqueres, D. Spanjaard, ‘Concepts in Surface Physics’, Springer Series in Surface Sciences.
- [6] I just write down a few key-words from the very nice historical sketch found in Zangwill’s book.
- [7] A very good reference for basic technical information are usually the catalogues provided by the vacuum companies (VG, Caburn, Varian, Thermionics and so on. A book of much use for the lab is: J.T. Yates, Experimental innovations in surface science: a guide to practical laboratory methods and instruments, Springer Verlag, New York, Berlin, Heidelberg 1997.
- [8] The image is taken from the Leybold catalogue.
- [9] N. D. Lang and W. Kohn, Phys. Rev. B 1,4555 (1970).
- [10] courtesy of L. Petersen et al.
- [11] N. W. Ashcroft and N. D. Mermin, ‘Solid State Physics’
- [12] H. Ibach, ‘Solid State Physics’, Springer
- [13] Zangwill s book and references therein.

- [14] U. Fano and J.W. Cooper, *Rev. Mod. Phys.* 40, 441 (1968).
- [15] D.A. Shirley, *Adv. Chem. Phys.* 23, 85, (1973).
- [16] A. Baraldi et al., *Phys. Rev. B.* 61, 4534 (2000).
- [17] C.D. Wagner et al., “Handbook of x-ray photoelectron spectroscopy”, Perkin Elmer Corp.
- [18] “Handbook of Auger electron spectroscopy”, Perkin Elmer Corp.
- [19] E. Zaremba and W. Kohn, *Phys. Rev. B* 15, 1769 (1977).
- [20] N.D. Lang and A.R. Williams *Phys. Rev.* B**18**, 616 (1978).
- [21] E. Wimmer, C.L. Fu and A.J. Freeman, *Phys. Rev. Lett.***55**, 616 (1985).
- [22] J.E. Lennard-Jones, *Trans. Farad. Soc.* **28**, 33 (1932).
- [23] King and Wells, *Proc. Roy. Soc. London* A**339**, 245 (1974).
- [24] Tamm and Schmidt, *J. Chem. Phys.* **54**, 4775 (1971).
- [25] W.A. Brown, R. Kose and D.A. King, *Chem. Reviews* **98**, 797 (1998).
- [26] G. A. Somorjai, ‘Introduction to Surface Chemistry and Catalysis’
- [27] S. Holloway and J. Nørskov, ‘Bonding at Surfaces’, Liverpool University Press
- [28] R. Smoluchowski, *Phys. Rev.* 60, 661 (1941), M. W. Finnis and V. Heine, *J. Phys. F* 4, L37 (1974)
- [29] K. Christmann et al., *Surf. Sci.* 40, 61 (1973).
- [30] Ph. Hofmann et al., *Phys. Rev. B* 53, 13715 (1996).
- [31] K. Stampfl et al., *Phys. Rev. Lett.* 69, 1532 (1992).
- [32] David Adams, private communication.
- [33] S.R. Parkin et al., *Phys. Rev. B* 41, 5432 (1990).
- [34] Takayanagi et al., *J. Vac. Sci. Techn.* A3, 1502 (1985).
- [35] H. Over et al., *Phys. Rev. B* 55, 4731 (1997).
- [36] M. Polcik et al., *Phys. Rev. B* 57, 1868 (1998).

- [37] D.A. Wesner, F.P. Coenen and H.P. Bonzel, *Surf. Sci.* 199, L419 (1988).
- [38] K.-U. Weiss, R. Dippel, K.-M. Schindler, P. Gardner, V. Fritzsche, A.M. Bradshaw, A.L.D. Kilcoyne and D.P. Woodruff, *Phys. Rev. Lett.* 69, 3196 (1992).
- [39] J. K. Gimzewski et al., *Phys. Rev. B* 45 6844 (1992).
- [40] L. Olesen and F. Besenbacher, unpublished results.
- [41] J. V. Barth et al., *Phys. Rev. B* 42, 9307 (1990).
- [42] C. Klink et al., *Phys. Rev. Lett.* 71, 4350 (1993).
- [43] F. Besenbacher, *Rep. Prog. Phys.* 59, 1737 (1996).
- [44] R.M. Tromp et al., *Phys. Rev. B* 34, 1388 (1986).
- [45] A.W. Munz et al., *Phys. Rev. Lett.* 74, 2244 (1995).
- [46] M.R. Castell et al., *Phys. Rev. B* 55, 7859 (1997).
- [47] J. B. Pendry, 'Low energy electron diffraction'.
- [48] M. van Hove and S. Y. Tong, 'Low Energy Electron Diffraction', Springer.
- [49] G. Ertl, 'Low energy electrons and surface chemistry'
- [50] D. P. Woodruff, 'Photoelectron Diffraction' in 'Angle-resolved photoemission', ed. S. D. Kevan, Elsevier.
- [51] R. Wiesendanger, 'Scanning Probe Microscopy and Spectroscopy', Cambridge University Press.
- [52] K. Besocke, B. Kraul-Urban, H. Wagner, *Surf. Sci.* 68, 39 (1977).
- [53] R. Blaszczyszyn et al, *Surf. Sci.* 51, 396 (1975).
- [54] E.V. Chulkov, V.M. Silkin and E.N. Shirykalov, *Surf. Sci.* 188,287 (1987).
- [55] M.Y. Chou, P.K. Lam, M.L. Cohen, *Phys. Rev. B* 28,4179 (1983).
- [56] E.W. Plummer and T. Gustafsson, *Science* 198, 165 (1977).
- [57] S.D. Kevan, *Phys. Rev. Lett.* 50,526 (1983).

- [58] E. Jensen, R.A. Bartynski, T. Gustafsson, E.W. Plummer, M.Y. Chou, M.L. Cohen and G.B. Hoflund, *Phys. Rev. B* 30,5500 (1984).
- [59] E.W. Plummer and W. Eberhardt, *Adv. Chem. Phys.* 49, 533 (1982) and references therein.
- [60] F. Patthey et al., *Phys. Rev. B* 49,11293 (1994).
- [61] D. Purdie et al., *Surf. Sci.* 407,L671 (1998).
- [62] R.J. Smith et al., *Phys. Rev. Lett.*, 37, 1081 (1976).
- [63] F. Greuter, D. Heskett, E.W. Plummer and H.-J. Freund, *Phys. Rev. B* 27, 7117 (1983).
- [64] K.C. Pandey, *Phys. Rev. Lett.* 47, 1913 (1981).
- [65] F.J. Himpsel, *Appl. Phys.* A38, 205 (1985)
- [66] G.V. Hansson and R.I.G. Uhrberg in *Angle-Resolved Photoemission, Theory and Current Applications*, ed. S.D. Kevan, Elsevier 1992 and references therein.
- [67] S. Agergaard et al. *New Journal of Physics* 3, 15 (2001).
- [68] D.J. Chadi, *Phys. Rev. Lett.* 43, 43 (1979).
- [69] F.J. Allend and G.W. Gobeli, *Phys. Rev.* 127, 152 (1962).
- [70] N. D. Lang and W. Kohn, *Phys. Rev. B* 3,1215 (1970).
- [71] S. D. Kevan (ed.) ‘*Angle-Resolved Photoemission, Theory and Current Applications*’, Elsevier.
- [72] S. Hüfner, ‘*Photoelectron Spectroscopy*’, Springer
- [73] *Phil. Trans. R. Soc. Lond. A* 344,453-467 (1993).
- [74] K. Stahrenberg, T. Herrmann, N. Esser, J. Sahm, W. Richter, S.V. Hoffmann and Ph. Hofmann *Phys. Rev.* 58, R10207 (1998).
- [75] L.E. Urbach et al., *Phys. Rev. B* 45,3769 (1992).
- [76] J. Hannon et al., *Phys. Rev. B* 53,2090 (1996).
- [77] H. Ibach, D. L. Mills, “*Electron Energy Loss Spectroscopy and Surface Vibrations*”, Academic Press, New York 1982

- [78] N.V. Richardson and A.M. Bradshaw, Surf. Sci. 88, 255 (1979).
- [79] Ismail, private communication.
- [80] W. Ho et al., Phys. Rev. Lett. 40, 1463 (1978).
- [81] M. Schulze, PhD thesis, University of Hannover 1988.
- [82] S. Lehwald and H. Ibach, Surf. Sci. 89, 425 (1979).
- [83] J. B. Hannon, E. J. Mele and E. W. Plummer, Phys. Rev. B 53,2090 (1996).
- [84] A. P. Baddorf and E. W. Plummer, Phys. Rev. Lett. 66,2770 (1991).
- [85] H. Kuzmany, 'Festkörperspektroskopie', Springer 1990.
- [86] Y. Chabal et al., J. Electron Spectr. Rel. Phen., 29, 35 (1983).
- [87] B.E. Hayden et al. Surf. Sci. 149, 394 (1985).
- [88] J.P. Toennies, Physica Scripta Volume T19A, 39 (1987).
- [89] A.M. Lahee et al, Surf. Sci. 177, 147 (1986).
- [90] B.C. Stipe et al., Science, 280, 1732 (1998).
- [91] Y.J. Chabal, Surf. Sci. Rep. 8, 211 (1988).

Index

- activation energy, 65, 69–71
- active sites, 75
- activity, 75
- adsorbate-adsorbate interaction, 66
- angle-resolved photoemission, ARPES, 136
- anharmonicity, 178
- associative adsorption, 60, 62, 69
- Auger electron spectroscopy (AES), 56
- Auger transitions, 43, 45, 46, 56, 106

- Bardeen approximation, 118
- Bloch waves, 26, 29
- Bravais lattice, 20, 83

- calorimetry, 72
- channeltron, 36
- chemical shift, 53, 109, 114
- chemisorption, 61
- CO, 11, 17, 32, 45, 63, 64, 66, 74, 112, 117, 139, 149, 173, 175, 181, 182
- Cooper minimum, 51
- corrosion, 8, 9, 59
- critical points, 40
- crystal shape, 77
- cylindrical mirror analyser, 36, 56

- de Broglie wavelength, 86
- Debye-Waller factor, 105, 111
- dielectric function, 38
- dipole scattering, 174
- dipole-active transitions, 176
- dipole-approximation, 137
- dipole-selection rules, 49
- dissociative adsorption, 60, 62, 65, 67, 69
- domains, 83, 94
- Drude model, 24

- Electron Energy Loss Spectroscopy, 34, 42, 165, 173, 180
- electron mean free path, 34, 48, 86, 92, 96, 111, 141
- electron spectroscopy, 33
- electronic surface states, 10, 30, 133
- Eley-Rideal pathway, 74
- Ewald construction, 89
- EXAFS, 103
- exchange-correlation potential, 130
- exciton, 39

- Fermi level pinning, 155
- Finnis-Heine model, 81, 97, 120
- first Brillouin zone, 22
- free electron model, 25
- Fresnel equations, 164
- Friedel oscillations, 28

- He atoms scattering, 182
- heat of adsorption, 72, 73
- hemispherical analyser, 36, 141
- herringbone reconstruction on Au(111), 122
- heterogeneous catalysis, 8, 59, 62, 73, 74, 163
- high T_C superconductors, 9, 44, 143

image potential states, 136
 impact scattering, 175
 incommensurate lattices, 86
 Infrared Reflection Absorption Spectroscopy (IRAS), 179
 inner potential, 91, 131
 interband transition, 40
 ion gauge, 14–16
 ion pump, 13
 isotope effect, 177

 jellium model, 28, 63, 122, 132

 K_α radiation, 46
 Koopman's theorem, 53, 55
 Kramers-Kronig relations, 38

 Lambert's law, 39
 Langmuir model, 68, 70, 72
 Langmuir-Hinshelwood pathway, 74
 Laue conditions, 88, 91
 Lennard-Jones model, 64
 Lindemann formula, 79
 local density approximation, 63
 Low energy electron diffraction (LEED), 86

 matrix notation, 84
 Miller indices, 22, 80
 molecular mean free path, 12
 muffin-tin potential, 95
 multiple scattering, 87, 92, 104

 nano technology, 9, 127
 Newns-Anderson model, 62
 NH_3 synthesis, 59, 74
 NiO , 102, 126

 periodic potential, 26
 phonon, 32, 39
 Photoelectron diffraction (PhD, PED), 107
 photoemission process, 137

 physisorption, 60
 Pirani gauge, 14
 plasmon, 40
 poisoning of a catalyst, 75
 polariton, 165
 pressure measurement, 14
 primitive unit cell, 20
 projected band structure, 134
 promotion of a catalyst, 75

 quadrupole mass spectrometer, 17, 71

 R-factor, 95, 118
 rationally related lattices, 85
 reconstruction, 23, 44, 81, 99, 121, 125, 151, 153
 Reflection Anisotropy Spectroscopy (RAS), 167

 relaxation, 23, 81, 121
 relaxation energy in XPS, 55
 rotary vane pump, 12
 roughening transition, 77

 satellite peaks, 47, 55, 138
 scanning force microscopy, 128
 scanning tunnelling microscopy (STM), 115
 scanning tunnelling spectroscopy (STS), 158, 182
 scattering phase shifts, 95, 96, 105, 107
 second harmonic generation (SHG), 169
 selectivity, 75
 SEXAFS, 106
 Shockley states, 148
 $\text{Si}(100)$ -(2x1), 100, 125, 153, 157, 160
 $\text{Si}(111)$ -(7x7), 100, 125, 151
 simply related lattices, 85
 Smoluchowski effect, 81, 120, 131
 SPA-LEED, 95
 sputtering, 44, 45, 147

super-structures, 80
surface cleaning, 44
surface core level shifts, 54
surface melting, 77
surface resonances, 135, 146
surface sensitivity, 33, 38, 163, 182
surface tension, 29, 78
surface x-ray scattering, 102
synchrotron radiation, 48, 52, 53, 102,
103, 106, 137, 169

Tamm states, 148
Tersoff-Hamann model, 118
Thermal Desorption Spectroscopy, 71
tight binding model, 27
truncated bulk, 80
turbomolecular pump, 12

ultra high vacuum, UHV, 11
universal curve, 35

van der Waals force, 44, 60, 66
vapour pressure, 15

Woods notation, 84
work function, 130
Wulff construction, 78

X-ray photoelectron spectroscopy (XPS),
46
X-ray sources, 46
XPS binding energies, 52
XPS cross sections, 49